DOTTORATO DI RICERCA IN ENERGIA E AMBIENTE

Dipartimento di Ingegneria Astronautica, Elettrica ed Energetica

XXX Ciclo

Thermal hydraulic design of DEMO Water Cooled Lithium Lead Breeding Blanket and integration with primary system and balance of plant

Progettazione e analisi termoidrauliche, del design del Water Cooled Lithium Lead Breeding Blanket e del Primary Heat Transfer System per la realizzazione del reattore a fusione DEMO

Supervisors:

Prof. Ing. Gianfranco Caruso

Dr. Ing. Alessandro Del Nevo

Dr. Ing. Fabio Giannetti

Author:

Ing. Emanuela Martelli

Coordinator of the Ph.D. Program:

Massimo Corcione

FEBBRAIO 2018

"This page has been intentionally left blank"

Abstract

The Ph.D. work, conducted at ENEA C.R. Brasimone, is carried out in the framework of the European Power Plant and Physics Technological Programme, under the coordination of the EUROfusion Consortium, and it was co-funded by the EUROfusion Engineering Grant.

The aim of this Ph.D. thesis work is the development of the conceptual design of the Water Cooled Lithium Lead breeding blanket and its Primary Heat Transfer System, as well as their integration, demonstrating the compatibility with the DEMO requirements.
The activity is focused on the thermal-hydraulic design, the sizing and analyses of the Breeding Blanket system and of the main components of the Primary Heat Transfer System, Energy Storage System and Power Conversion System. This has been pursued through engineering approaches and the application of numerical tools, such as thermal-hydraulic system codes and CFD codes.

The conceptual design of WCLL blanket was developed starting from a review of previous designs. A preliminary layout of the coolant systems (first wall and breeding zone) and the main parameters were defined, through engineering tools, to provide input data for the development of the CAD model.

In order to verify the thermal-hydraulic performances of the WCLL blanket system, a complete three-dimensional finite volume model of the breeding blanket was set-up, using ANSYS CFXv15.0 code. The model includes solid and fluid domains, and represents, in detail, an elementary cell of the blanket (i.e. breeding unit). CFD analyses have been carried out to investigate thermal and fluid-dynamic behavior of the breeding blanket, evaluating the efficiency of the first wall and breeding zone water coolant systems, and identifying key issues and areas of improvements. Several configurations were analyzed, and it was identified a promising coolant system layout which ensures a symmetric thermal field of the breeding blanket with maximum temperature of solid structures of 430 °C.

One of the main functions of the breeding blanket is the conversion of the energy coming from the plasma in thermal energy suitable for power generation systems, ensuring an efficient power conversion. It requires large external auxiliary systems to perform its function, namely the Primary Heat Transfer System and the Power Conversion System, and it has to be integrated with them in a complete Balance of Plant, which satisfies DEMO tokomak constraints and requirements. This objective is pursued, for the WCLL breeding blanket, in the second part of the research activity, investigating the postulated operation of DEMO power plant through thermal hydraulic analyses of the Primary Heat Transfer System and Power Conversion System design solutions and components.

Moreover, considering the pulsed nature of DEMO reactor, with energy generated for 120 min (burn time) followed by the reactor dwell time (estimated to last 10-30 min), an Intermediate Heat Transfer System equipped with an Energy Storage System, is being investigated to mitigate the impact of plasma pulsing on PCS equipment (e.g. in the steam turbine) and in electrical grid.

The research activity led to the definition of the Primary Heat Transfer System and of the DEMO WCLL BB. The selected configuration relies on two separate systems connected with the breeding zone and the first wall, respectively. The Energy Storage System is foreseen, to accumulate energy during pulse time, using HITEC molten salt as fluid, and to deliver power to the Power Conversion System during dwell time. The main components (e.g. steam generators, circulators/ pumps, pipes, collectors) were sized, and the data were used to develop and integrate the CAD model into the DEMO baseline. A preliminary Gate-cycle™ analyses were carried out, presenting an average gross electrical efficiency of about 37.1%, considering both pulse and dwell phases.

In order to develop a dynamic model of the systems, an extended version of RELAP5/Mod3.3 code was set-up with the implementation of the PbLi and HITEC fluid properties. This had allowed to develop a thermal-hydraulic system model of the first wall and breeding zone primary systems. The model includes the in-vessel and ex vessel components of the primary side and the secondary side of the FW PHTS and BZ PHTS, and it will be used to perform thermal-hydraulic system analyses.

CONTENTS

Nomenclature

ACP	Activation Corrosion Product
BB	Breeding Blanket
BoP	Balance of Plant
BP	Back Plate
BSS	Back Supporting Structure
BZ	Breeding Zone
CAD	Computer Aided Design
CCFE	Culham Centre for Fusion Energy
CEA	French Atomic Energy Commission
CFD	Computational Fluid Dynamic
DCLL	Dual Cooled Lithium Lead
DEMO	Demonstration fusion power plant
DIAEE	Department of Astronautic Electric and Energetic Engineering
DIV	Divertor
DWT	Double Wall Tube
EFDA	European Fusion Development Agreement
ENEA	Italian National Agency for New Technologies, Energy and Sustainable Economic Development
ESS	Energy Storage System
EU	European Union
FEM	Finite Element Method
FW	First Wall
HC	Helical
HCLL	Helium Cooled Lithium Lead
HCPB	Helium Cooled Pebble Bed
HCSG	Helical Steam Generator
HEX	Heat Exchanger
HTC	Heat Transfer Coefficient
IB	Inboard Blanket
IHX	Intermediate Heat Exchanger
IHTS	Intermediate Heat Transfer System
ITER	International Thermonuclear Experimental Reactor
KIT	Karlsruhe Institute of Technology
LOCA	Loss of Coolant Accident
MCP	Main Coolant Pump
MHD	Magneto Hydro Dynamic
MS	Molten Salt
NWL	Neutron Wall Load
OB	Outboard Blanket
OTSG	Once Through Steam Generator

PbLi	Lithium Lead
PCS	Power Conversion System
PHTS	Primary Heat Transfer System
PPPT	Power Plant Physics & Technology
PPCS	Power Plant Conceptual Study
PR	Poloidal-Radial
PRZ	Pressurizer
PT	Poloidal-Toroidal
PWR	Pressurized Water Reactor
RELAP	Reactor Loss of Coolant Analysis Program
SEAFP	Safety and Environmental Assessment of Fusion Power
SG	Steam Generator
SYS	System
TES	Tritium Extraction System
TF	Toroidal Field
TH	Thermal-Hydraulic
TM	Thermo-Mechanic
TR	Toroidal-Radial
VV	Vacuum Vessel
WCLL	Water Cooled Lithium Lead
WP	Work Package

List of Figures

List of Tables

1 INTRODUCTION

Energy demand is expected to be more than double by 2050 [1] as the combined effect of the increase of population and energy consumption per capita in developing countries. Moreover, considering the progressive depleting of fossil fuels and the necessity of a cleaner ways to produce energy, humanity is forced to invest more and more in the research for alternative power sources that can prove their long-term sustainability and security. In this framework, nuclear fusion is becoming more and more considered as the most probable solution to the energy problem, ensuring sustainability and security of supply: fuels are widely available and virtually unlimited; no production of greenhouse gases; intrinsically safe, as no chain-reaction is possible; environmentally responsible - with a proper choice of materials for the reaction chamber, radioactivity decays in a few tens of years and at around 100 years after the reactor shutdown all the materials can be recycled in a new reactor.
In 2012 EUROfusion' s preceding organization [2], EFDA, has published a roadmap which outlines hot to supply fusion electricity by 2050. The *roadmap to the realization of fusion energy*" [1] breaks the quest for fusion energy down into eight missions, which are:

1) Demonstrate plasma regimes of operation (based on the tokamak configuration);
2) Demonstrate a heat exhaust system capable of withstanding the large load of DEMO;
3) Develop materials that withstand large 14 MeV neutron fluence without degrading their physical properties;
4) Ensure tritium self-sufficiency through technological solution for the breeding blanket; which will have to be made consistently with the choice of the components for the transformation of the high-grade heat into electricity (the so-called Balance of Plant).
5) Implement the intrinsic safety features of fusion into the design of DEMO following the experience gained with ITER;
6) Combining all the fusion technologies into an integrated DEMO design; e.g. exploiting a complete Balance of Plant (BoP) including the heat transfer and associated electrical generation systems;
7) Ensure the economic potential of fusion by reducing the DEMO capital costs and developing long-term technologies;
8) Bring the stellarator line to maturity.

For each mission, the roadmap reviews the status of research, identifies open issues, proposes a research and development plan and estimates the required resources. It points out the needs to intensify industrial involvement and to seek all opportunities for collaboration outside Europe.

1.1 Framework of the activity

The PhD research activity is conducted in the framework of a cooperation between DIAEE (Department of Astronautic, Electrical and Energetic Engineering) of University of Rome and the Experimental Engineering Division (FSN-ING) of ENEA C.R. Brasimone, under the coordination of the European Consortium for the Development of Fusion Energy (EUROfusion).

EUROfusion Consortium manages and coordinates fusion research activities funded by Euratom for the realization of DEMO reactor and in accordance with the *Roadmap to the realization of fusion energy*, in the frame of Horizon2020 programme. It was established in 2014 to succeed the European Fusion Development Agreement (EFDA). The EUROfusion consortium agreement has been signed by thirty members research organizations and universities from 26 European Union countries plus Switzerland. Italy is one of the member of EUROfusion and ENEA is the national programme' s leading actor and coordinator. Such programme involves many major universities (e.g. Sapienza University of Rome, University of Pisa, University of Palermo, University of Torino, etc.), university consortia (e.g. CREATE), research institution (e.g. INFN, CNR, etc.) and industries (e.g. Ansaldo Nucleare, CSM).

ENEA actively participates to the conceptual development of the DEMO power plant. In particular, at Experimental Engineering Division (FSN-ING) of ENEA C.R. Brasimone, R&D activities are pursued to develop the Water Cooled Lithium Lead (WCLL) design in the framework of the Breeding Blanket (WPBB) and Balance of Plant (WPBoP) Projects of the EUROfusion Power Plant Physics & Technology (PPPT) Programme.

1.2 Objectives of the research activity

The research activity is devoted to the development of the conceptual design of the WCLL breeding blanket and its PHTS, as well as their integration, demonstrating the compatibility with the PPPT DEMO requirements, focusing the attention on thermo-hydraulic aspects. The R&D activities are implemented in the EUROfusion Work Package Breeding Blanket (WPBB) and in the Work Package Balance of Plant (WPBoP) and funded by the EUROfusion Engineering Grant. A flow chart of the PhD activity is reported in Fig. 1.1.

The conceptual design of WCLL blanket was developed in the first part of the activity, starting from a review of previous designs. A preliminary thermal-hydraulic layout of the coolant systems (first wall and breeding zone) and the main parameters were defined, through engineering tools, to realize the CAD model (at CREATE).

Based on the CAD model, a complete three-dimensional finite volume model of the breeding blanket was set-up, using ANSYS CFXv15.0 code. The model includes solid and fluid domains, and represents, in detail, an elementary cell of the blanket (i.e. breeding unit). CFD analyses have been carried out to investigate thermal and fluid-dynamic behavior of the breeding blanket, to evaluate the efficiency of the FW and BZ water coolant systems, and to verify that maximum temperature of solid structures is in the allowed limits, as well as to identify key issues and areas of improvements. Then, efforts have been made to improve systems efficiency, to optimize temperature distribution, simplifying the overall system and enhancing feasibility.

The feasibility of design choices has been verified by thermo-mechanical (University of Palermo), neutronic (ENEA Frascati and CEA) and MHD analyses (University of Rome and KIT), getting the results of thermodynamic and fluid-dynamic analyses as input and providing feedbacks and indications.

The second part of the activity has the objectives of integrating the WCLL blanket system in a complete Balance of Plant and investigating the postulated operation of DEMO power plant through thermal hydraulic analyses of the Primary Heat Transfer System (PHTS) and Power Conversion System (PCS) design solutions and components. The aims of these investigations are to: evaluate the dimensions of the PHTS main components (e.g. steam generators, circulators/ pumps, pipes, collectors) and identify technical feasibility issues; understand the commercial availability of components and the potential R&D needs; establish the PHTS layout requirements and evaluate the integration implications with other systems inside the tokamak building. The technology development, design and system engineer rules are defined by industries (ANN, SRS) which support the progress of the activity.

The pulsed nature currently considered for the DEMO reactor operation imposes unique design problems on the PCS: the energy in DEMO will be generated for 120 min (burn time) followed by the reactor dwell time (estimated to last 10-30 min) mandatory in a tokamak device for recharging the transformer. An Intermediate Heat Transfer System (IHTS) equipped with an Energy Storage System (ESS) using HITEC Molten Salt (MS) as heat transfer fluid is being investigated to mitigate the impact of plasma pulsing on PCS equipment (i.e. in the steam turbine) and in electrical grid.

In order to develop a dynamic model of the systems an extended version of RELAP5/Mod3.3 code has been set-up with the implementation of the PbLi and HITEC fluid properties, as well as some relevant heat transfer correlations.

The research activity has led to the development of a complete conceptual design of WCLL breeding blanket, fully and satisfactorily integrated with the PHTS. Moreover, the configuration and main components of PHTS, including the ESS to deal with DEMO pulsed operation, and PCS are defined.

1.3 Structure of the thesis

This thesis is structured in seven sections. The first section includes the framework, motivation and objectives of the PhD research, while § 7 presents conclusions and future perspectives.

An overview of the nuclear fusion technology and the concept breeding blanket is described in § 2, highlighting the implication on DEMO reactor.

Then, § 3 describes in detail the Water Cooled Lithium Breeding Blanket concept, the main functions, the requirements and rationales, the development from 2014 to 2017 and the lesson learned and implication on design.

The thermal-hydraulic analyses of the WCLL blanket are reported in § 4. This section presents the CFD model of the breeding unit developed to perform thermal and fluid-dynamic analyses of the breeding and the thermal analyses of the Back Supporting Structure.

Then, § 5 and § 6 presents the integration of the WCLL blanket system and PHTS, and thermal-hydraulic design and analyses of the PHTS, ESS and PCS. In particular, an overview of PHTS and BoP functions and requirements is described in § 4, providing also a configuration suitable and specifically addressed to WCLL breeding blanket.

Finally, § 6 presents the thermal-hydraulic model of the FW and BZ PHTS developed with the thermal-hydraulic system code RELAP5/Mod3.3, and the main features of the nodalization, Moreover, the preliminary verifications of nodalization (i.e. evaluation of pressure drops and heat exchangers performances) are presented and discussed.

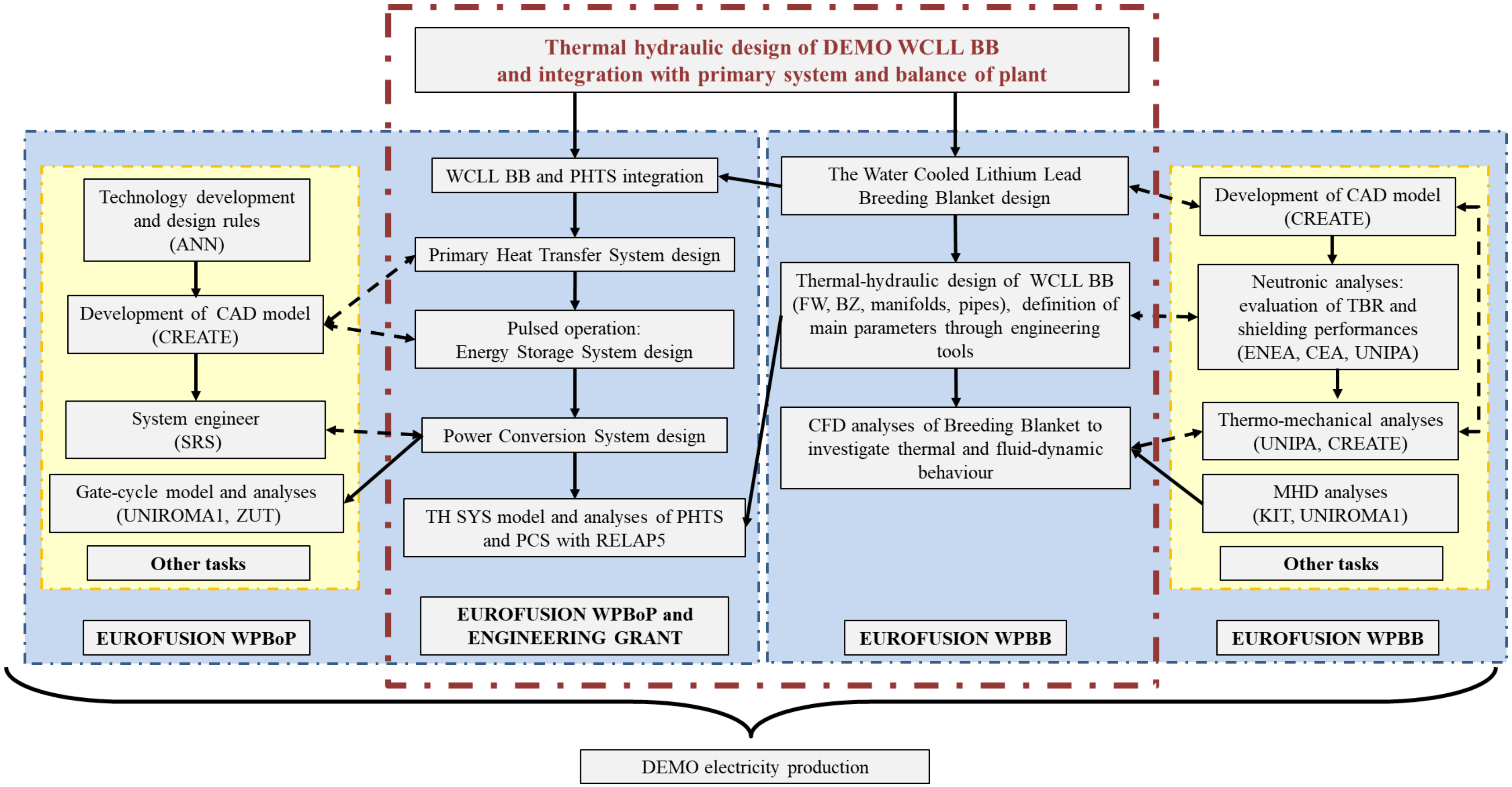

Fig. 1.1 – Flow chart of the PhD research activities.

2 BACKGROUND

2.1 Nuclear Fusion Technology

Fusion is the process that powers and drives the production of energy in stars [3]. It is a reaction in which nuclei join to form a heavier atom whose mass is less than the sum of the masses of the reactants. This reduction of mass leads to the production of large amounts of energy following the famous Einstein equation $E = mc^2$. The amount of energy released varies depending on the exact elements that are fusing. For example, the fusion of the hydrogen isotopes deuterium (D) and tritium (T) according to the reaction

$$D + T \rightarrow {}^{4}He + n \text{ (Q=17.6 MeV)}$$

produces 17.6 MeV of energy which is the kinetic energy of neutron (14 MeV) and the alpha particle (3.5 MeV).

In order for a fusion reaction to take place the two nuclei must have enough energy to overcome the repulsive Coulomb force acting between the nuclei and approach each other sufficiently close that the short-range attractive nuclear force becomes dominant.
Thus, the fusion fuel must be heated to elevated temperatures, i.e. for the D-T reaction, the gas temperature must exceed $5x10^7$ K before a significant fusion rate is feasible, at these temperatures the gas exists as a macroscopically neutral collection of ions and unbound electrons which is called plasma.

The hot fusion plasma must not touch the reactor wall, and it is therefore confined. Two main approaches have arisen to confine plasma: inertial confinement and magnetic confinement. In the former approach a small pellet of D-T fuel is bombarded by high-power laser causing it to explode, so creating high density plasma for few nanoseconds. The latter approach, which is more widespread, uses strong magnetic fields to confine the plasma within a vacuum vessel with a toroidal shape (tokamak).

2.2 Breeding blankets

The D-T reaction is the reactions on which tokamak reactors are based, being, among the known fusion reactions, the most promising one as it is a good compromise between energy produced, large cross section and, above everything, the availability of both isotopes on Earth. Deuterium exists at 0.0153 at % in sea-water and is readily extractable, thus constituting essentially infinite fuel source [3]. Tritium undergoes beta decay with half-life of 12.5 yr. Achieving Tritium self-sufficiency is a critical issue in the development of a self-sustaining fusion power plant operating with a DT fuel cycle.

A feasible option to generate Tritium in a tokamak reactor is through nuclear reactions between the high energy neutrons (14 MeV) generated in the fusion reaction with Lithium in the blanket, the region surrounding the plasma chamber.
There are two main reactions producing tritium blanket:

$$^{6}Li + n \rightarrow \ ^{4}He + T + 4.78\ MeV$$
$$^{7}Li + n \rightarrow \ ^{4}He + T + n - 2.47\ MeV$$

The first reaction has a large cross section for thermal (slow) neutrons, while the second reaction is more probable with fast neutrons. Thus, for breeding purposes, the blanket (surrounding the plasma) should contain ^{6}Li. Since natural lithium is 92.44% ^{7}Li, enrichment techniques up to 90% ^{6}Li are required. The second reaction with ^{7}Li is endothermic (threshold 2.5 MeV), the mechanism of absorption and release of a neutron opens the possibility for a self-sufficient tritium production in a fusion reactor: each neutron produced in the fusion reaction will produce at least one Tritium nucleus.
In order to feed the fusion process accordingly to the reactions involving Li and neutrons, the blanket is composed of a compound of Lithium and neutron multipliers material to enhance the breeding. An additional production of neutrons is needed because the losses due to capture and absorption reaction in structural materials and the leakage through ports and divertor lower the availability of neutrons of a 30% in respect to the total neutron population. The materials commonly used as neutron multipliers are Beryllium and Lead.

Of the energy produced by D-T fusion 80% leaves the plasma immediately in the form of kinetic energy of the 14-MeV neutrons. These neutrons transfer their energy to the blanket materials, constituting as such a volumetric heat source in the blanket, which has to convert the fusion energy into heat that can be extracted by a suitable cooling system and converted into electric power through heat exchangers and turbines. This is carried out by means of coolant fluids that circulate through the blanket structure.

The remaining 20% of the energy produced in fusion and all energy externally supplied to heat the plasma ultimately leave the plasma as energetic charged particles or atoms or as radiative energy, in any case constituting a surface heat source incident on the first material surface facing the plasma. Since the blanket is located between the plasma and the magnet, one of its functions is shielding the super-conducting magnets (and the vacuum vessel that contains the entire system).

The three above mentioned blanket functions (breeding, heat extraction and shielding) are schematically shown in Fig. 2.1.

Different classes of blanket concepts with solid or liquid breeding material have been proposed [5][6]. The combination of candidate tritium breeder (i.e. Li-containing materials), structural materials (e.g. martensitic steels, V alloys, Cr alloys, SiCf/SiC), coolants (e.g. water, helium, liquid metals such as Pb–17Li and lithium, molten salts such as FLiBe), and for neutron multipliers (i.e. Pb and Be) is done on the basis of material compatibility, operating temperature window, and safety.

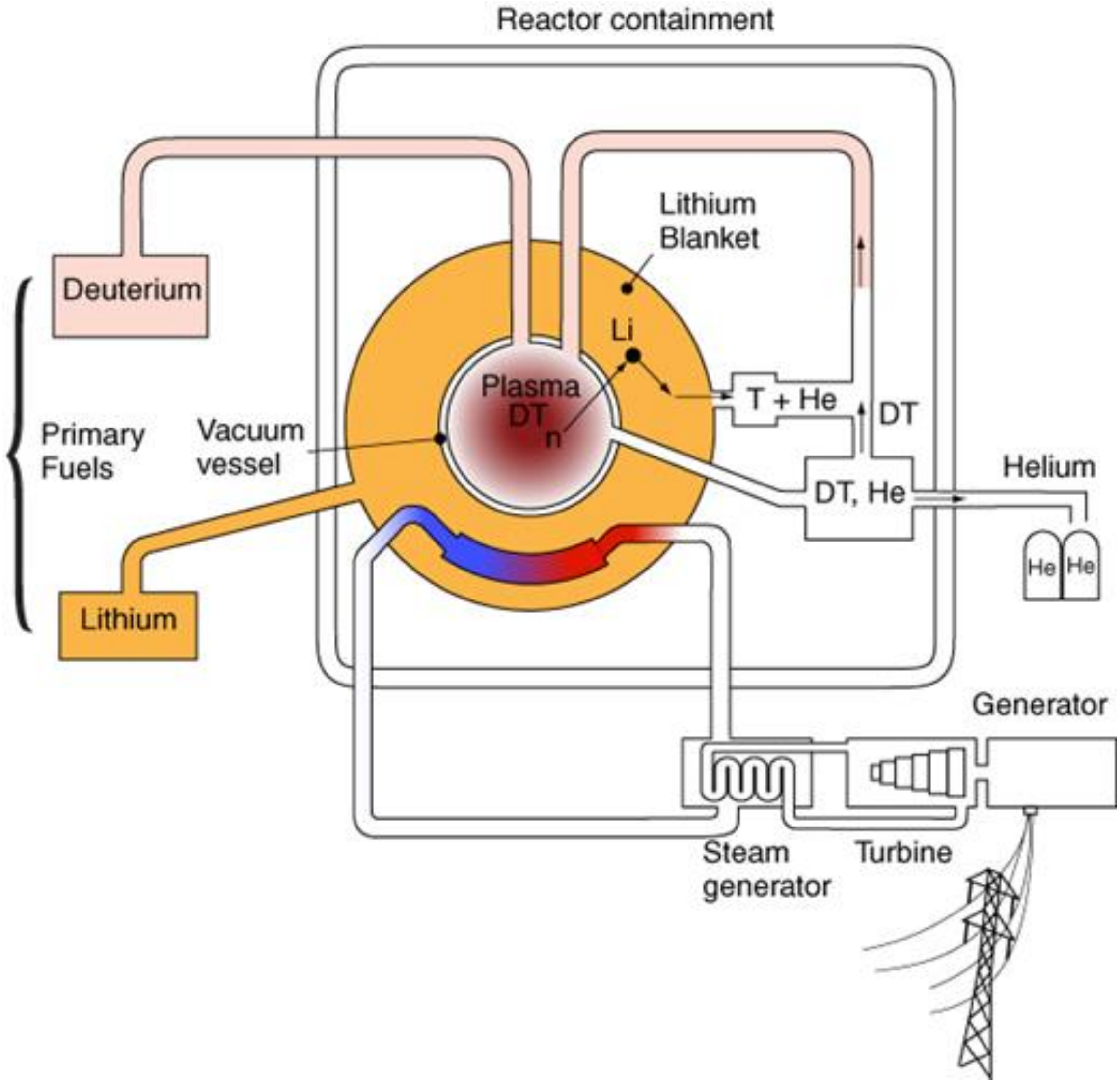

Fig. 2.1 – Schematic of a fusion reactor [4].

2.3 DEMO

The EU (European Union) fusion roadmap foresees a Demonstration Fusion Reactor (DEMO) to follow ITER as the remaining crucial step towards the exploitation of fusion power. Major requirements of the PPPT-DEMO plant [7][8] are:

1. Produce net electricity for the grid at the level of a few hundred MWs;
2. Breed the amount of tritium needed to close its fuel cycle; and
3. Demonstrate all the technologies for the construction of a commercial fusion power plant, including an adequate level of availability.

Several outstanding technology and physics integration issues must be resolved before a DEMO plant concept selection is made. Each of them has very strong interdependencies. They include the selection of: the breeding blanket concept and, in particular, the selection of blanket and coolant; the divertor concept and its configuration; the first wall design and its mechanical and hydraulic integration to the blanket, considering that the first wall might see higher heat loads than assumed in previous studies; the heating and current drive (H&CD) mix; the remote maintenance scheme and; a compatible plasma scenario.

The breeding blanket is the key component, since the choice of the breeder blanket (type of coolant, the type of breeder, the technology used for the Tritium extraction) impacts not only the design of the BB itself but also the design of the interfacing systems and because of the overall tokamak layout. The systems most impacted by the architecture and technological choices of the BB are the Primary Heat Transfer System (PHTS), the Tritium extraction and coolant purification system, the Vacuum Vessel Pressure Suppression System (VVPSS), the systems requiring in-vessel penetrations, the Remote Maintenance as well as the safety of the plant.

For these reasons the selection of the type of blanket is a strategically choice that constraints strongly the whole DEMO plant design, its safety features and economic viability.

3 EU DEMO WCLL BB

3.1 WCLL BB functions and configuration

The breeding blanket is a major system of a fusion reactor. It has to interface the plasma, to remove the heat generated in the tokamak plasma and transfer it to the PHTS, ensuring an efficient power conversion, being one of the main objective of a fusion reactor the production of electricity. Moreover, the breeding blanket shall also breed the tritium (T) used in the fusion reaction, thus ensuring the self-sufficiency of the reactor, and shield the Vacuum Vessel (VV) and superconducting coils.

The Water Cooled Lithium Lead is one of the selected breeding blanket concepts to be investigated in the EUROfusion Breeding Blanket Project (WPBB) in 2014-2020 [8], besides the Helium Cooled Lithium Lead (HCLL), the Helium Cooled Pebble Bed (HCPB) and the Dual Coolant Lithium Lead (DCLL).

The WCLL blanket is based on the use of reduced activation ferritic-martensitic steel (Eurofer) as structural material, liquid Lithium-Lead (PbLi) enriched at 90% in ^{6}Li as breeder, neutron multiplier and tritium carrier, and water at Pressurized Water Reactor (PWR) conditions as coolant (295-328 °C, 15.5 MPa).

The WCLL Blanket Systems is constituted by the following subsystems:

1. The Blanket segments, that can be further divided in:
   - The blanket segments, including the integrated First Wall (FW), the Breeding Zone (BZ), that are discussed in detail in Sects. 3.3.1 and 3.3.2.
   - The Back Supporting Structure (BSS) providing mechanical attachments and the manifold distribution system that feeds the modules and connects the PHTS outside the vacuum vessel, described in Sect. 3.3.3.
2. The PbLi loop insuring the circulation of the breeder inside the modules and outside the VV for the tritium extraction purposes. Its auxiliary systems like the PbLi purification/chemistry control system are also included.
3. The Tritium Extraction System (TES), which interfaces with the PbLi loop and with the Fuel Cycle.

3.2 Design requirements and rationale

The reference configuration for WCLL blanket design is DEMO 2015 [9]. It has 18 Toroidal Field (TF) coils, each of them corresponding to a sector (20°). One DEMO sector is composed of two inboard segments and three outboard segments, for a total of 36 and 54 segments, respectively. Each sector has an upper port and a lower port to allow the feeding and the outlet of the water coolant and the PbLi pipelines. The main geometry of

the segments is simplified to face, as much as possible, manufacturing and remote handling issues.
The operational concept is DEMO 1, which assumes nine pulses with a burn time of 2 hours per day. During the pulse mode, the thermal power calculated with PROCESS code is 2436 MW [10].

The WCLL BB design is developed on the basis of PPPT DEMO requirements [8]. The complete set of requirements on which the blanket system evolves in parallel with the design; a first version of the BB System Requirement Document (SRD) has been already produced and updated [11][12][13]. The main general requirements are [8]:

- The first blanket set has to be designed for a lifetime corresponding to neutron damages of 20 dpa, with a second set aiming to 50 dpa; this means that one scheduled replacement of the whole blanket system is necessary in the life of the reactor (which will be sum up to about 70 dpa).
- The blankets shall be adapted to a reactor maintenance system based on a remote handling vertical replacement scheme through large upper ports.
- DEMO has to produce the T necessary for the thermonuclear reaction, thus the breeder and neutron multiplier materials shall be located in proximity of the plasma flux and neutron adsorption materials shall be minimized in the breeding zone. The amount of steel that is used as structural material has to be reduced; amount of steel larger than 12-15% can degrade the tritium breeding ratio (TBR) to unacceptable levels.
- The design of cooling systems accounts for the Eurofer maximum temperature limit of 550 °C: the blanket has to ensure an effective cooling of all parts under surface and volumetric heat to cope with temperature limits of the materials.
- The structures forming the blanket have to withstand the mechanic loads coming mainly from the coolant pressure, thermal stress and electromagnetic loads. The structural assessment is performed following mainly RCC-MRx rules. Critical for the mechanical design is the assessment of the box behavior in case of in-box LOCA
- EM force constitutes another typical load challenge for the tokamak reactor; they are caused by electric currents induced by magnetic transients interacting with magnetic fields (Lorentz forces) or simply by the stationary interaction of magnetic fields with magnetic material (Maxwell forces).

3.3 Design evolution and consolidated configuration

The study started from a review of previous designs performed in 1995 [6][14] and then in the frame of PPCS programme [15], and EFDA studies done at CEA in 2012 [18], in order to identify strengths and weakness. Since 2014, ENEA and its linked third parties is in charge for the development of WCLL BB design. A scheme of the WCL blanket concept evolution from 1995 to 2017 is reported in Fig. 3.1.

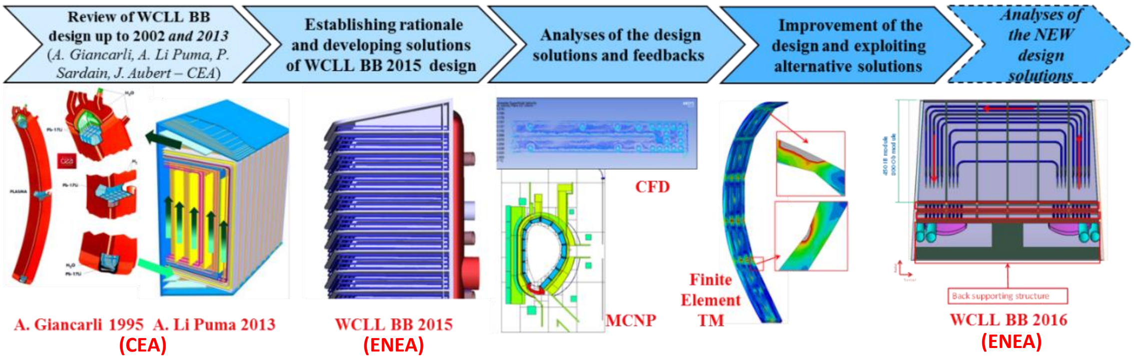

Fig. 3.1 – DEMO WCLL BB design evolution from 1995 to 2017.

Pioneering studies on Water Cooled Lithium Lead blanket concept were performed in 1995 [14], for the development of a European fusion power plant. The design was developed assuming a single module blanket type poloidal segmentation (one blanket module for inboard and one module for outboard blanket), as shown in Fig. 3.2. This configuration allowed a maintenance from the top of the whole module. As consequence, manifold and inlet/outlet collectors for both coolant and liquid breeder are located at the top of the module. The design point for an outboard segment is given in Tab. 3.1.

In 2004, in the frame of PPCS programme [15][17] further studies were performed on WCLL concept (PPCS model A). In this conceptual design the segmentation of the blanket modules was defined on the basis of remote handling specifications and assumed six modules in poloidal direction (Fig. 3.3). Each module is essentially formed by a directly cooled steel box performing the function of PbLi container and by a Double Walled C-shaped Tube (DWT) bundle, immersed in the liquid metal, in which the water coolant circulates. The module box is reinforced by radial and toroidal stiffeners to withstand the disruption-induced forces and the full water-pressure under faulted condition. The main parameters are reported in Tab. 3.2.

In 2012, in the frame of EFDA programme, CEA developed an innovative design for WCLL concept [18]. The blanket design was constituted of small modules of different sizes made with straight surfaces, attached together along the poloidal direction on a Back Supporting Structure (BSS) and fed with pipes at the rear of the modules. Along the poloidal direction each outboard segment has 8 modules and each inboard segment has 7 modules. Only the Equatorial Outboard Module (EOM) was developed in detail and is shown in Fig. 3.4. The relevant parameters of the WCLL design developed at CEA are reported in Tab. 3.3.

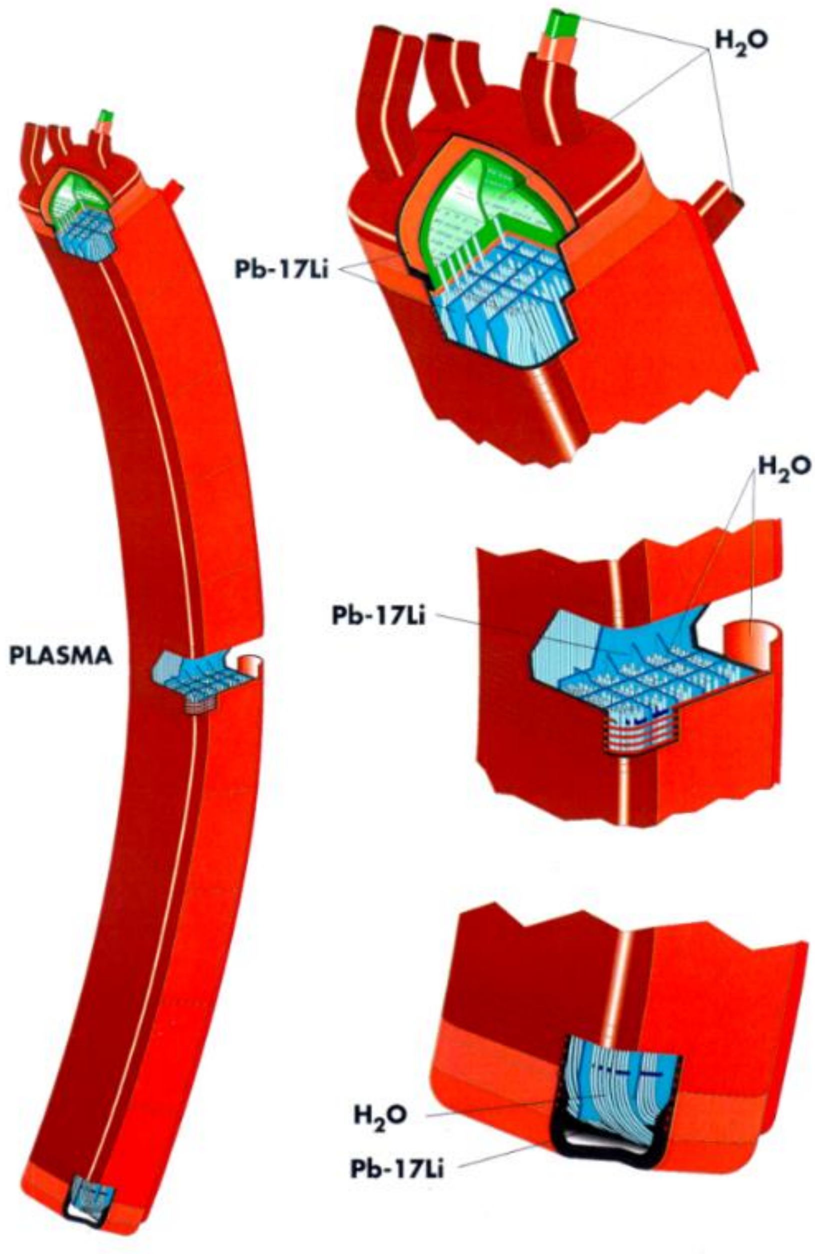

Fig. 3.2 – DEMO WCLL BB: view of the single box concept (CEA, 1995) [14].

#	**Parameter**	**Unit**	**Value**
1	Fusion Power	***MW***	3300
Pb-17Li-pool/water coolant			
2	Pressure	***MPa***	15.5
3	Inlet temperature	***°C***	265
4	Outlet temperature	***°C***	325
5	Maximum velocity	***m/s***	5.9
6	Nb. DW poloidal U-tubes	**--**	205
FW/water coolant			
7	Pressure	***MPa***	15.5
8	Inlet temperature	***°C***	300
9	Outlet temperature	***°C***	325
10	Maximum velocity	***m/s***	5.0
11	Nb. DW poloidal U-tubes	**--**	378
12	Maximum temperature of the PbLi/steel interface	***°C***	480

Tab. 3.1 – DEMO WCLL BB: design point for an OB segment (CEA, 1995) [14].

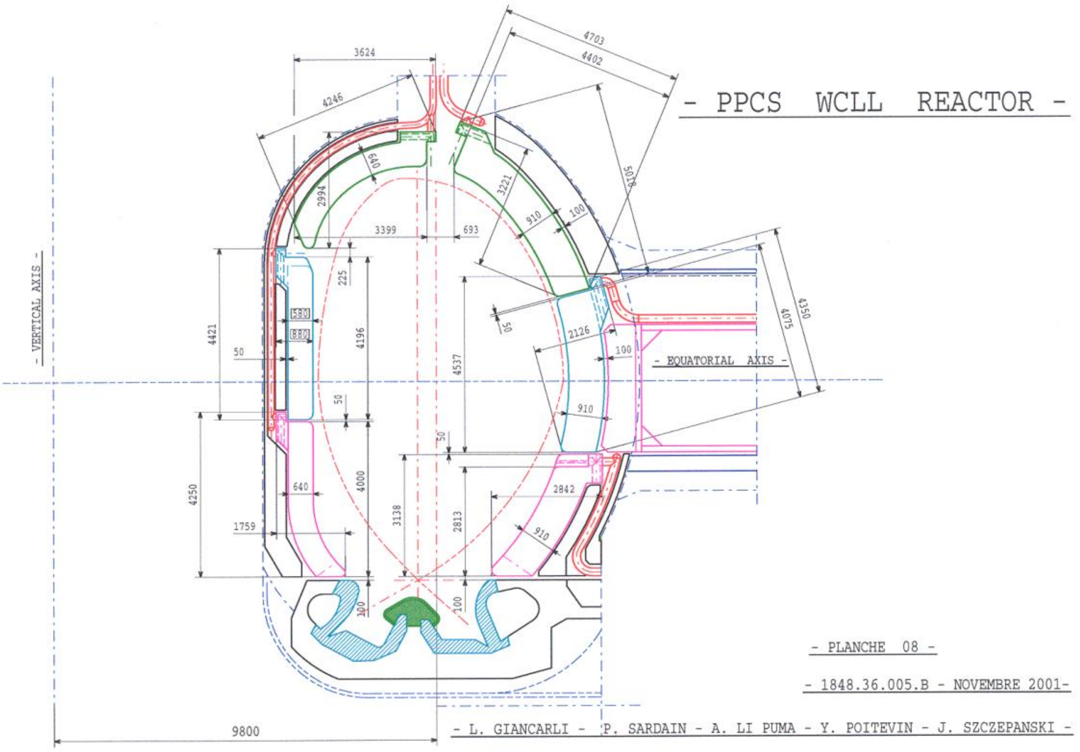

Fig. 3.3 – DEMO WCLL BB: poloidal distribution of the WCLL modules in PPC studies (PPCS studies, CEA, 2003) [15][17].

#	**Parameter**	**Unit**	**Value**
1	Fusion Power	***MW***	5000
Pb-17Li-pool/water coolant			
2	Pressure	***MPa***	15.5
3	Inlet temperature	***°C***	285
4	Outlet temperature	***°C***	325
5	Maximum velocity	***m/s***	5
6	Nb. DW C-shaped tubes (per modules)	**--**	11
FW/water coolant			
7	Pressure	***MPa***	15.5
8	Inlet temperature	***°C***	285
9	Outlet temperature	***°C***	325
10	Maximum velocity	***m/s***	5.0
11	Maximum temperature of the PbLi/steel interface	***°C***	480

Tab. 3.2 – DEMO WCLL BB: design parameters (PPCS studies, CEA, 2003) [17].

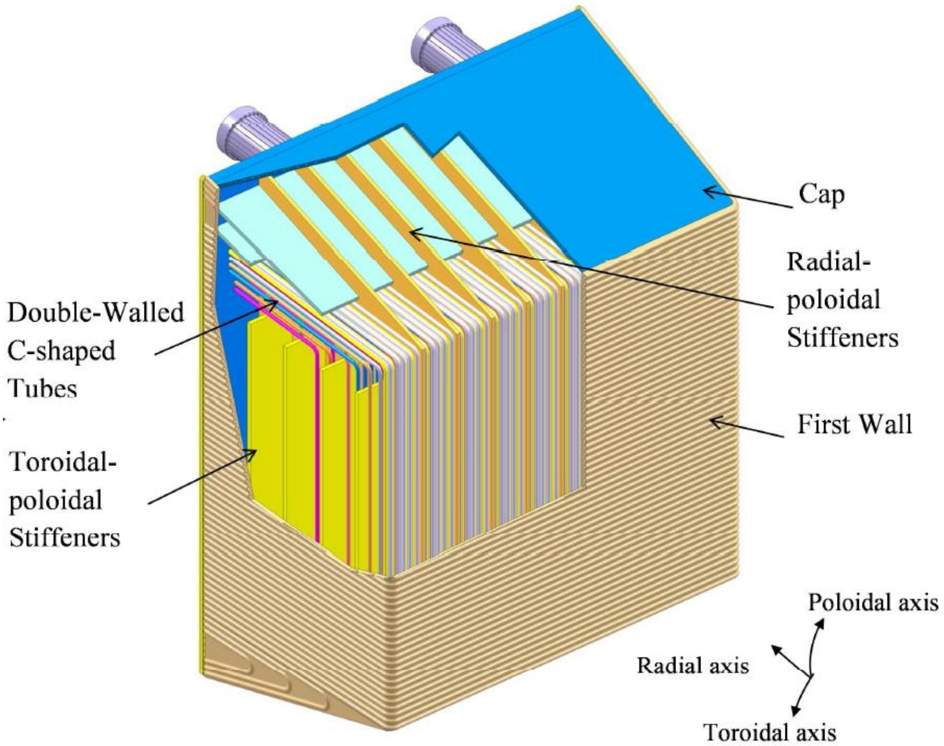

Fig. 3.4 – DEMO WCLL BB: equatorial outboard module (EFDA studies, CEA, 2013)[18].

#	**Parameter**	**Unit**	**Value**
1	Fusion Power	***MW***	1943
Pb-17Li-pool/water coolant			
2	Pressure	***MPa***	15.5
3	Inlet temperature	***°C***	285
4	Outlet temperature	***°C***	325
5	Maximum velocity	***m/s***	2.3-3
6	Nb. DW C-shaped tubes in EOM	**--**	11
FW/water coolant			
7	Pressure	***MPa***	15.5
8	Inlet temperature	***°C***	285
9	Outlet temperature	***°C***	325
10	Maximum velocity	***m/s***	3
11	Nb. channels in EOM	**--**	57
12	Maximum temperature of the PbLi/steel interface	***°C***	480

Tab. 3.3 –DEMO WCLL BB: design parameters (EFDA studies, CEA, 2013)[18].

Starting from 2014, ENEA and its linked third parties developed the new WCLL blanket concept [21]-[29]. In 2015 a deep revision of the WCLL design was proposed, establishing rationale and developing design solutions [30][31].

Maintaining the MMS approach, a new segmentation of WCLL blanket was investigated and proposed [32]. Each segment, inboard and outboard, is divided in 7 small modules of different sizes made with straight surfaces, attached together along the poloidal direction with a Back Supporting Structure (BSS) and fed with pipes routed through the BSS.

Only the central equatorial outboard module (EOM) was developed in detail [33][34] (see Fig. 3.5). It consisted of an Eurofer steel box, reinforced by an internal grid of radial-poloidal and poloidal-toroidal plates. There are 15 radial-toroidal stiffeners of 12 mm thickness that divide the module in 16 elementary cells, hereinafter called “breeding unit”, of a total height of 123 mm. Each breeding unit is divided in 6 channels in toroidal direction by 5 radial-poloidal stiffeners of 16 mm thickness.

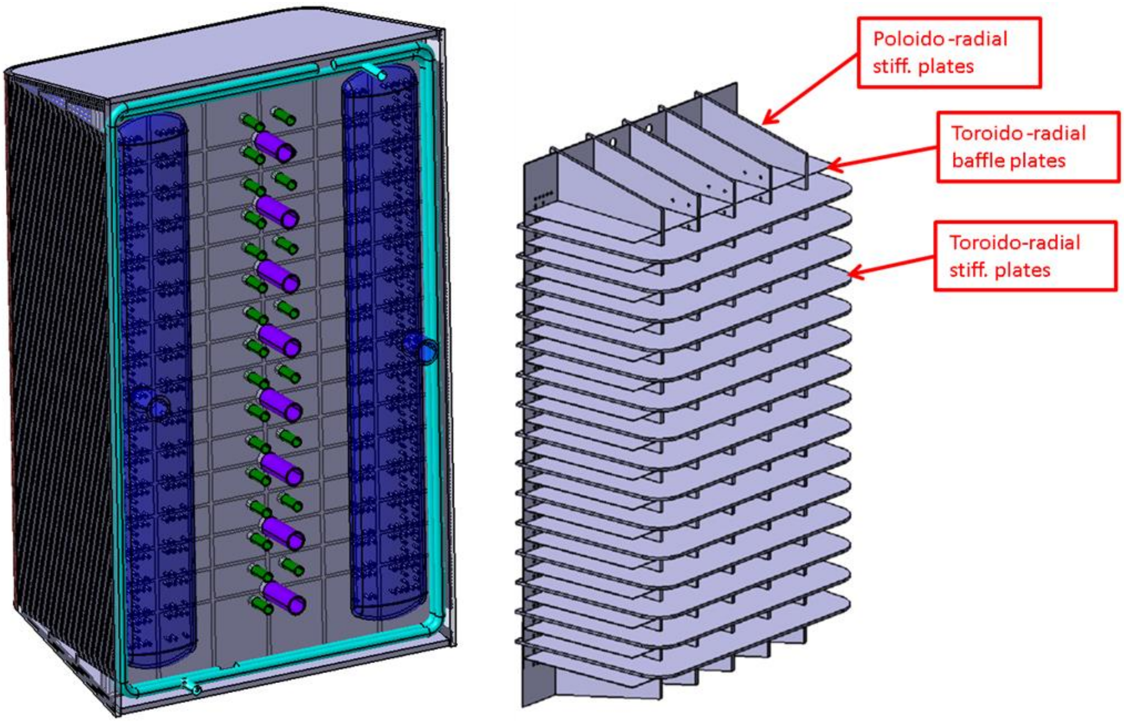

Fig. 3.5 – DEMO WCLL BB 2015 design: equatorial outboard module.

The breeding units are filled with PbLi, which is distributed through a manifold in the toroidal channels [36]. The PbLi enters in the breeding unit from the bottom of the cell, flows in radial direction, from the back to the FW, goes up in poloidal direction and then flows from the FW to the back. A baffle plate of 2 mm thickness, placed at half between two radial-toroidal stiffeners, ensures the PbLi flow path in radial-poloidal direction (see Fig. 3.6). The maximum PbLi velocity at inlet orifices is 5 mm/s, and the average velocity in the BZ is 0.1 mm/s. The modules are cooled by two independent system:

- The First Wall (FW) system, described in detail in § 3.3.1, has the main function of extracting heat due to the heat flux and Neutron Wall Load (NWL);
- The Breeding Zone (BZ), described in detail in § 3.3.2, which have to extract the heating due to nuclear reactions inside the blanket between neutron and PbLi.

The reference thermo-dynamic cycle for BZ and FW systems foresees water entering at 285 °C, and exiting at 325 °C, at 15.5 MPa. The main parameters of WCLL 2016 design are reported in Tab. 3.4.

On the back of the box is the Back Plate (BP), on which attachments to the structure and manifolds to collect the water and the PbLi are fixed (see Sect. 3.3.3).

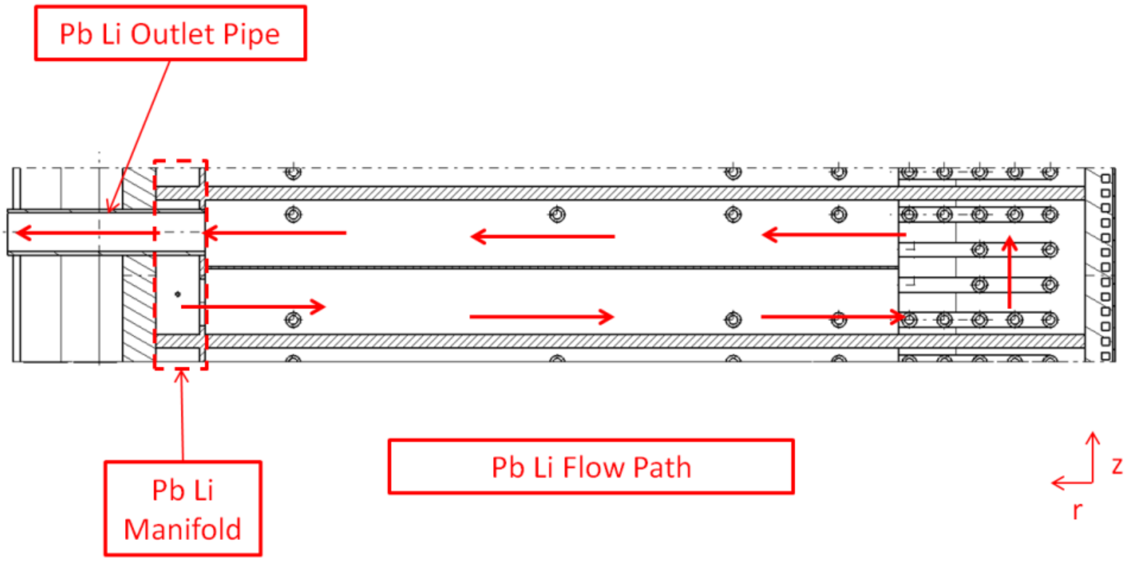

Fig. 3.6 – DEMO WCLL BB 2015 design: PbLi flow path.

A CAD model of the outboard segment was developed, as well as a detailed model of the equatorial outboard module. Moreover, CFD, three-dimensional Finite Element Method (FEM) and neutronics models have been developed to evaluate the design solutions and to provide feedbacks on the performances.

#	Parameter	Unit	Value
1	Fusion Power	***MW***	2037
Pb-17Li-pool/water coolant			
2	Pressure	***MPa***	15.5
3	Inlet temperature	***°C***	285
4	Outlet temperature	***°C***	325
5	Maximum velocity	***m/s***	1.57
FW/water coolant			
6	Pressure	***MPa***	15.5
7	Inlet temperature	***°C***	285
8	Outlet temperature	***°C***	325
9	Maximum velocity	***m/s***	1.24
10	Maximum temperature of the PbLi/steel interface	***°C***	550

Tab. 3.4 – DEMO WCLL 2015 design: main parameters (ENEA) [31].

The layout proposed for WCLL BB design 2015 [35] has showed positive features and the chosen solutions have margins for improvements and optimizations. Nevertheless, drawbacks have been identified on segmentation, being the WCLL BB 2015 based on Multi Module Segment (MMS) approach. The key issues are hereinafter summarized:

- Thermal and thermo-mechanic stress at caps edges
- The segmentation does not allow the complete PbLi drainage of breeding blanket
- The segmentation does not allow the He removal from breeding blanket modules

On the basis of the main outcomes obtained from WCLL 2015 analyses [35], the design was further optimized in 2016 [42]. The main improvement was the development of WCLL blanket design based on the Single Module Segment (SMS) approach (see Fig. 3.7). The conceptual design preserves the same internal structure with a basic elementary cell (i.e. breeding unit) repeated in poloidal direction, and the FW approach, described in detail in Sect. 3.3.1. The BZ coolant system layout is improved to optimize temperature distribution as reported in Sections 3.3.2. The manifold region and BSS have been adapted to the new design, as reported in Sect. 3.3.3.

A new reference thermo-dynamic cycle has been considered in 2016 to improve efficiency of PHTS and BoP, and thus the water, at 15.5 MPa, enters in the BZ and FW systems at 295 °C and exits at 328 °C.

An advanced design has been developed in 2017. The BZ coolant system layout is constituted by a simpler configuration in which the cooling pipes can be assembled in the breeding blanket without crossing the vertical stiffeners (see Fig. 3.8). Moreover, the new design foresees a PbLi flow path fully developed in poloidal direction, with manifolds integrated in the breeding zone.

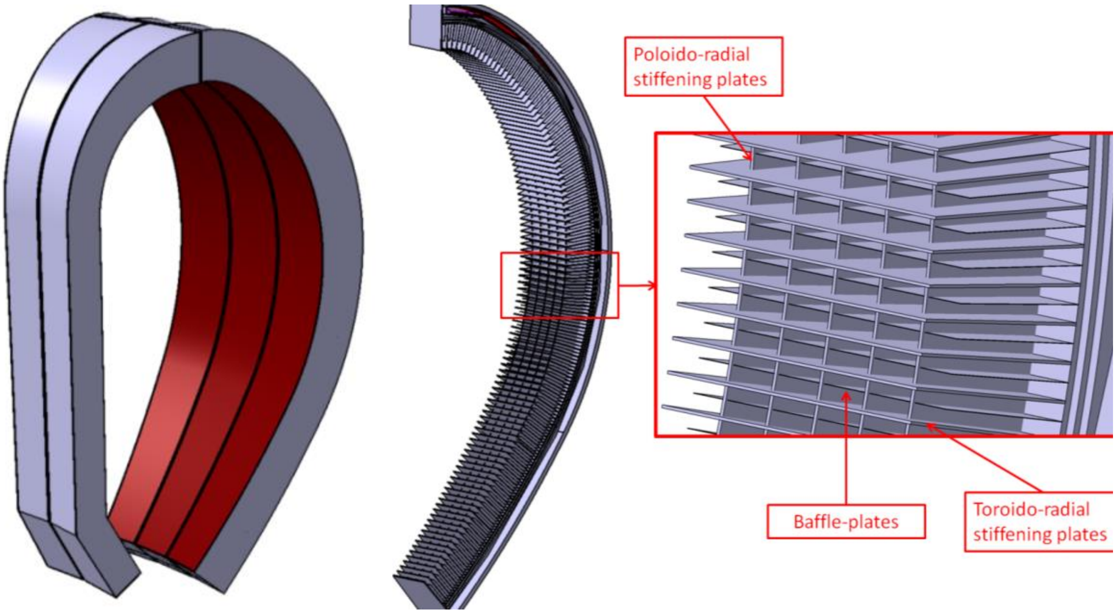

a) WCLL BB sector *b) Outboard segment and internal structures*

Fig. 3.7 – DEMO WCLL BB 2016 design.

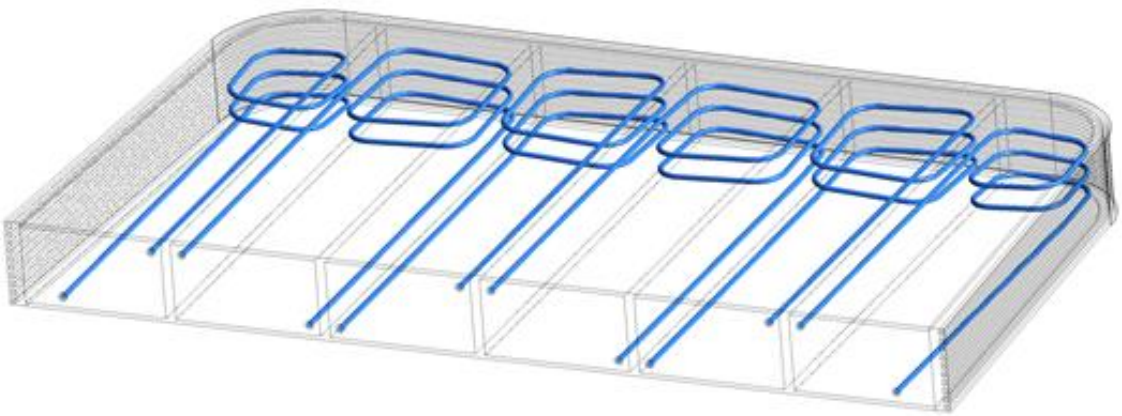

Fig. 3.8 – DEMO WCLL BB 2017 design: detail of the breeding unit.

3.3.1 First Wall

The front part of the box facing to the plasma is the First Wall. It is an integrated part of BB module and it is cooled with an independent water system. The FW cooling geometry is the result of an optimization procedure, accounting for steady state and TM analyses, done with 3D FEM models [33].

The FW is constituted by Eurofer and has a thickness of 25 mm; the plasma facing area is covered by a tungsten layer of 2 mm thickness. The water coolant flows in counter current direction in square channels of 7×7 mm, with a pitch of 13.5 mm, as shown in (Fig. 3.9). The position of FWs channels is symmetrical with respect to the plane of TR and plates, in order to ensure the symmetry of the breeding units. In each breeding unit there are 10 coolant channels. Water enters at 295 °C and exits at 328 °C, at 15.5 MPa.

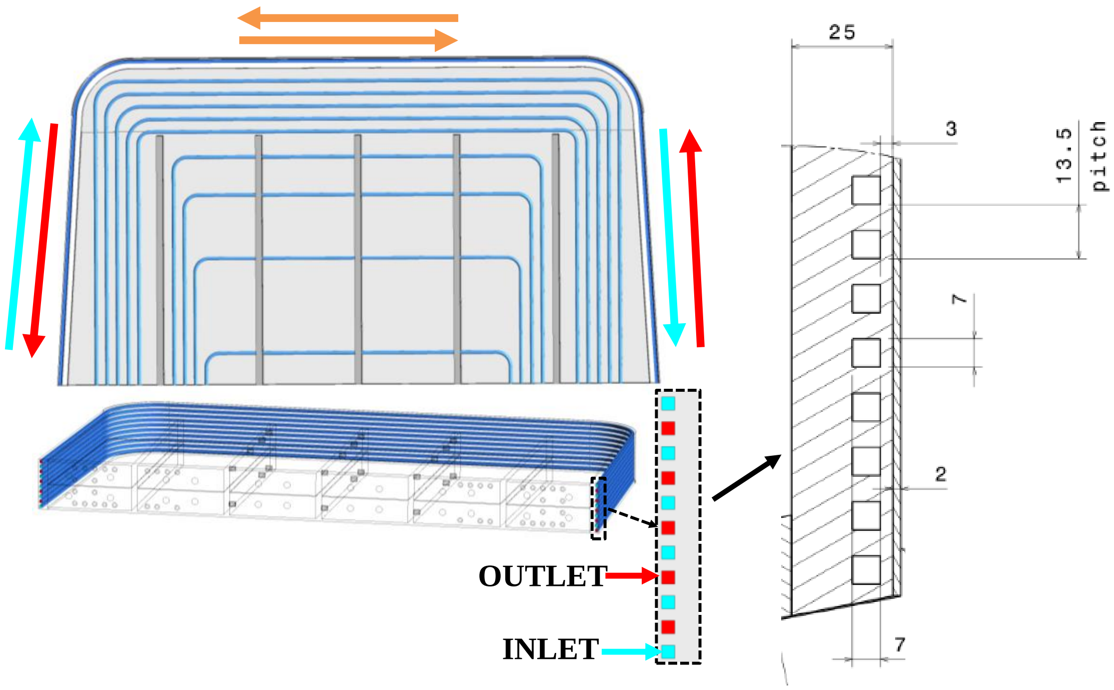

Fig. 3.9 – DEMO WCLL BB 206 design: layout of the FW cooling channels [35][45].

3.3.2 **Breeding Zone**

The Breeding Zone (BZ) is cooled with an independent system. The cooling pipes are radial-toroidal Double-Walled tubes (DWTs) displaced in a horizontal plane. The tube has an external diameter of 13.5 mm, the internal one of 8 mm with a thickness of 1.25 mm. Thus, there is a 0.5 mm space between the two concentric tubes, which is filled with a metal that guarantees the double wall separation ensuring the thermal conduct between the walls. Main relevant pipes dimensions are reported in Fig. 3.10.

The water coolant enters at 295 °C, and exits at 328 °C, at 15.5 MPa (PWR conditions). Considering as reference the breeding unit placed at equatorial plane of the outboard segment, the total number of BZ tubes is 21.

In 2016 an improved coolant system layout was investigated in order to enhance temperature symmetry (Sect. 4.1), this configuration foresees the recirculation of the water in the BZ tubes. In particular, the coolant enters in the first 10 tubes near the FW, flows radial-toroidal direction and it is collected in a manifold, from which the water recirculates in a module and exits in the opposite side, as illustrated in Fig. 3.11.

In 2017 the BZ coolant system layout has been modified to further improve temperature distribution and coolant performances (see Fig. 3.8). It is characterized by a simpler configuration, with a reduced number of pipes and without crossing the vertical stiffeners.

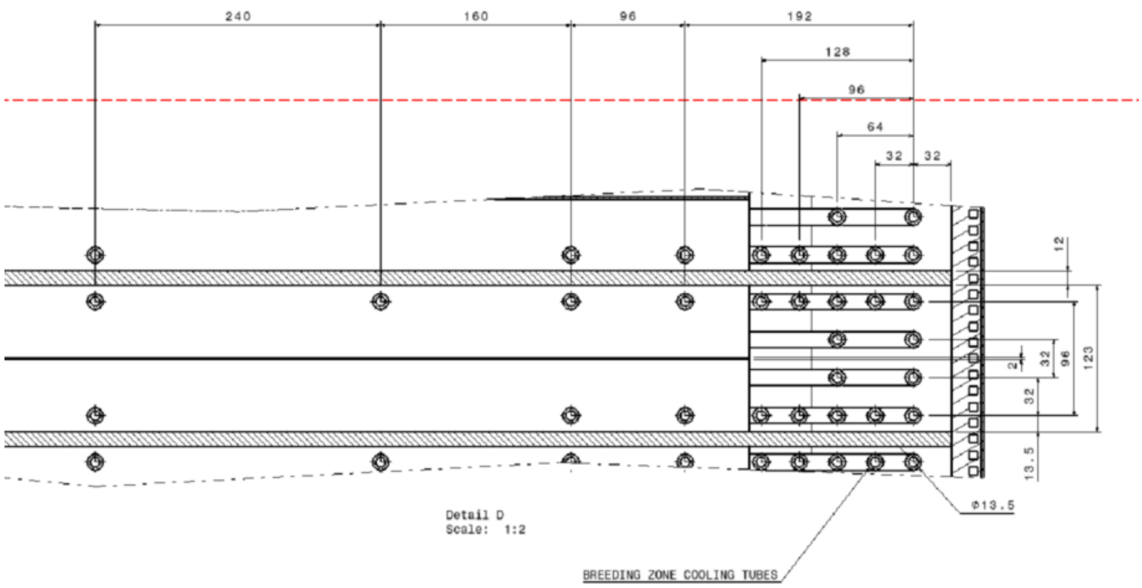

Fig. 3.10 – DEMO WCLL BB 2016 design: Radial-poloidal section of breeding unit with main pipes dimensions [35].

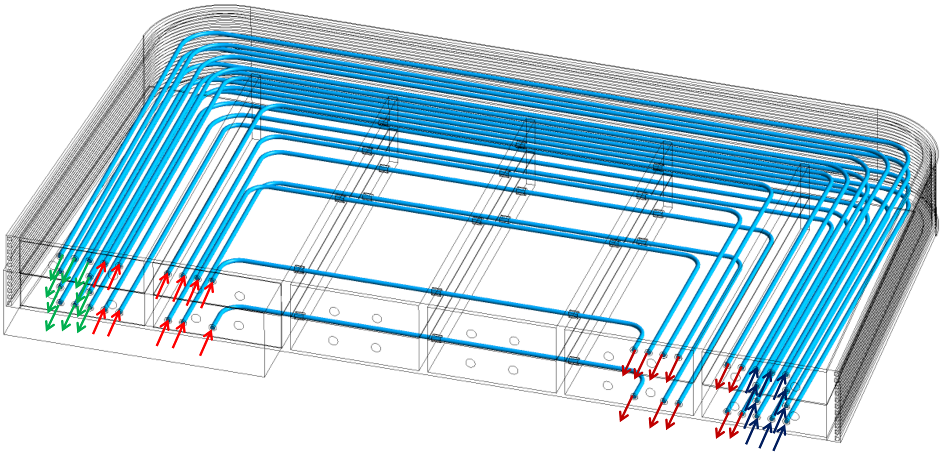

Fig. 3.11 – DEMO WCLL BB 2016 design: BZ coolant system layout [35].

3.3.3 Manifolds and feeding pipes

The WCLL 2015 design was developed on the basis of MMS approach, thus an inlet and outlet manifolds are foreseen for each module and for each system (FW, BZ and PbLi). The BZ water manifolds (inlet and outlet) are place on the back side of the module back plate. The connection with feeding and collecting pipes is at the center of the manifolds. The FW water manifolds are square shaped tubes, placed near the back wall and joined with the FW channels by straight tubes.

The PbLi manifold was formed by the gap between the BP and the BZ (1.48×2.48×0.4), pointed out in Fig. 3.12 a. The stiffening plates divide the manifold in 96 rectangular portions, as depicted in Fig. 3.12 b. The PbLi enters in the gap from eight inlets; each inlet feeds the four central portions of the manifold region, and then the PbLi spreads in toroidal direction though the small orifices realized in the radial-poloidal stiffeners (Fig. 3.12 b). CFD analyses have been performed to evaluate the feasibility of the PbLi manifold [36], as reported in 4.1.

In 2016 design, the manifolds have been adapted to the new configuration based on SMS approach. The BZ and FW water manifolds preserve the same approach of the previous design, but only one manifold (inlet and outlet) is foreseen for the overall segment. The BSS of the segments (inboard and outboard) have a T shape and is joined to the sidewalls and the back walls.

Considering the results of CFD analyses (see Section 4.1), the PbLi manifolds are simplified and are constituted by two gaps of 40 mm placed inside the segment structure and delimited by walls of 30 mm thick. Moreover, CFD thermal analyses of the BSS (see Sect. 4.4) have suggested to integrate the water manifolds in the space between the BP and the BSS to cool the Eurofer structure.

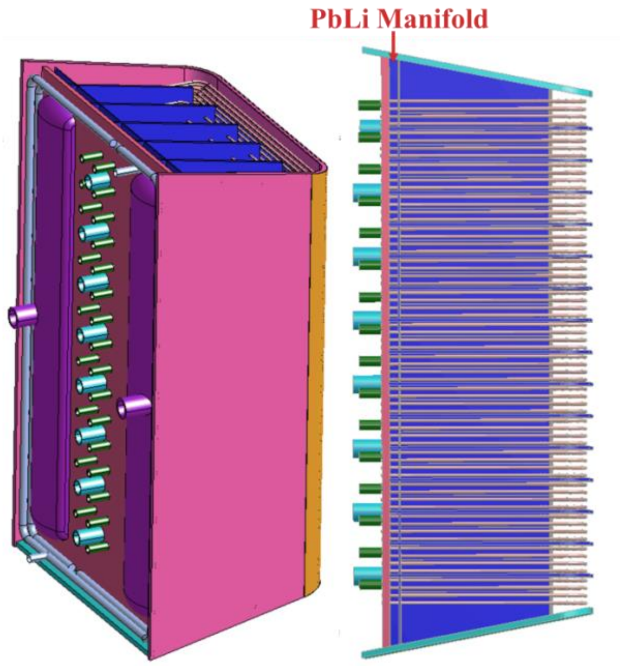

a) Equatorial outboard module

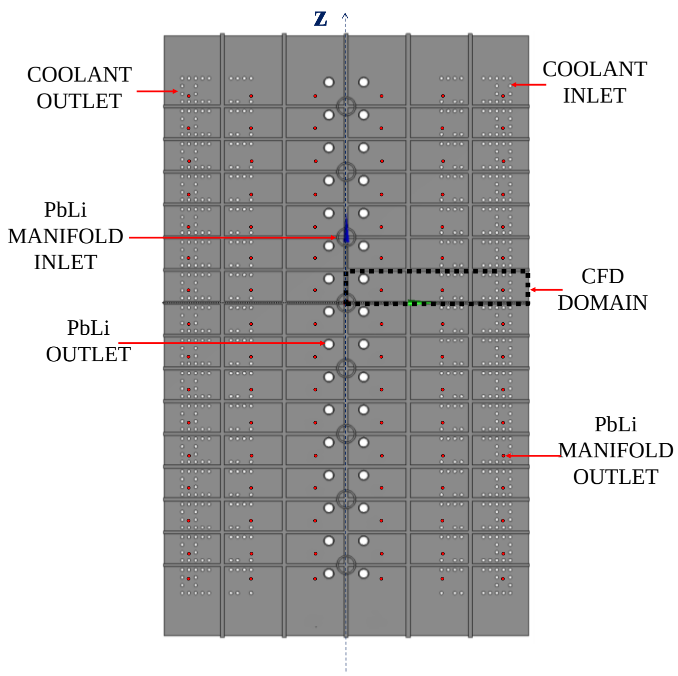

b) *PbLi manifold*

Fig. 3.12 – DEMO WCLL BB 2015 design: PbLi manifold [39].

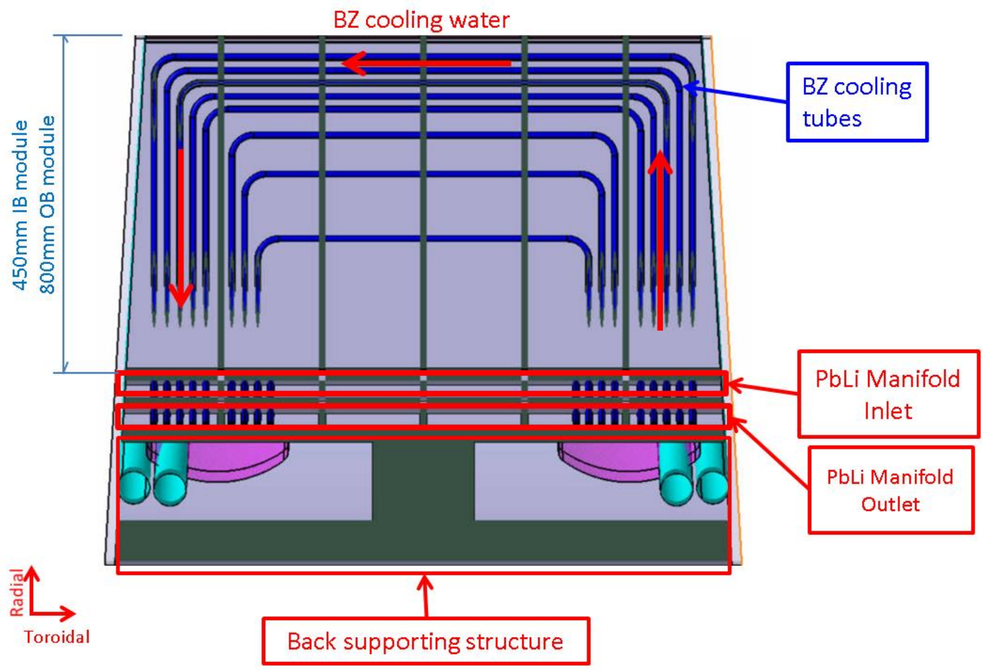

a) Radial-toroidal section of the outboard segment

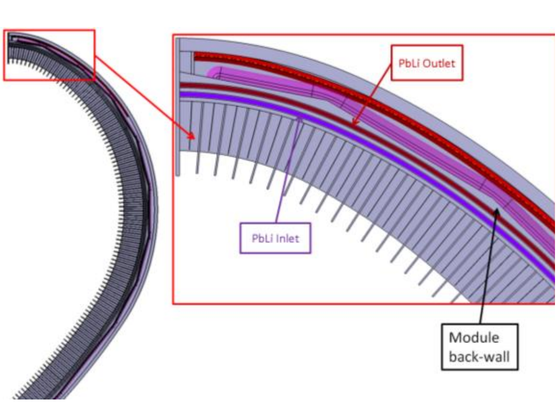

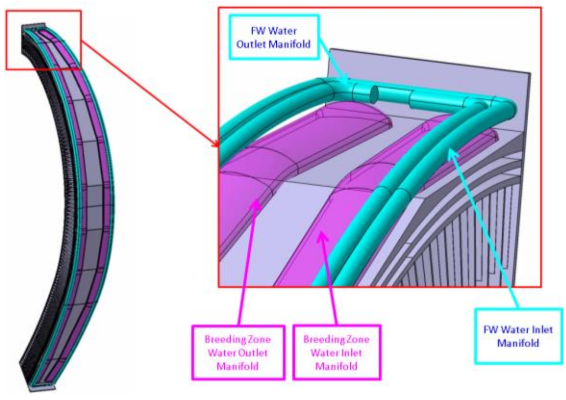

b) Back plate and PbLi manifold region

c) BZ and FW cooling water manifold

Fig. 3.13 – DEMO WCLL BB 2016 design: PbLi and water manifolds.

3.4 Lesson learned and implication on design

The WCLL 2015 design has shown positive features, nevertheless drawbacks and areas for improvements have been identified. As regard the segmentation, the MMS approach does not allow the complete PbLi drainage of breeding blanket, and He removal. Furthermore, due to the discontinuities between modules, caps edges can be affected by thermal and thermo-mechanics stress. Thus, the SMS configuration has been investigated at University of Palermo and compared with the MMS approach to assess thermo-mechanical behavior, mainly in terms of displacements and equivalent stresses.

Taking into account the analyses performed in 2015 on PbLi manifold, and feedbacks from manufacturing, the PbLi manifolds have been simplified in 2016 and adapted to the SMS approach. Nevertheless, considering both water and PbLi, manifolds and feeding/discharging pipes scheme shall be improved and further simplified to enhance the reliability, manufacturability and flexibility of the design.

The BSS has been also adapted to the SMS. Thermal analyses demonstrated that, the proposed design needs active cooling in inboard segment, which is affected by a power deposition about one order of magnitude larger than the outboard. To avoid temperatures exceeding the limits, the manifold region has been integrated in the BSS, thus providing active cooling to the structural material starting from the WCLL BB 2016 design. This approach has been improved in WCLL 2017 design.

As regard the BZ coolant systems, a layout has been proposed in 2016 to enhance the temperature symmetry in toroidal direction [39]. Nevertheless, further improvements are needed to achieve a complete symmetry Moreover, considering the results of the CFD analyses, it was evident that the coolant performances could be enhanced (e.g. reducing tubes number) and the tubes layout could be simplified to satisfy manufacturing requirements (e.g. avoiding pipes crossing vertical stiffeners).

In 2017, CFD analyses on the breeding cell have demonstrated that it is possible to reduce the number of tubes, thus, to enhance cooling, neutronic and thermo-mechanical performances. Moreover, a further step for the realization of WCLL blanket design was the simplification of design (i.e. BZ coolant system and PbLi flow path), to improve manufacturability [44], making the most from the SMS approach.

4 TH ANALYSES OF WCLL BB

4.1 CFD analyses of WCLL 2015 PbLi manifold

CFD analyses have been performed on WCLL BB 2015 design to evaluate the feasibility of PbLi manifold [39]. Considering the design reported in § 3.3.3 a simplified computational domain has been defined. In particular, being the breeding units of the equatorial outboard module equals (with the exception of the top and bottom units), and symmetric with respect the poloidal direction (z-axis in Fig. 3.12 b), the computational domain is reduced at only three portions of the manifold (Fig. 4.1), with dimensions 0.727×0.123×0.04 m. The orifices A, B, C indicated in the figure, are the manifold outlets. The cooling pipes of the BZ, which cross the BP, are neglected in the CFD model.

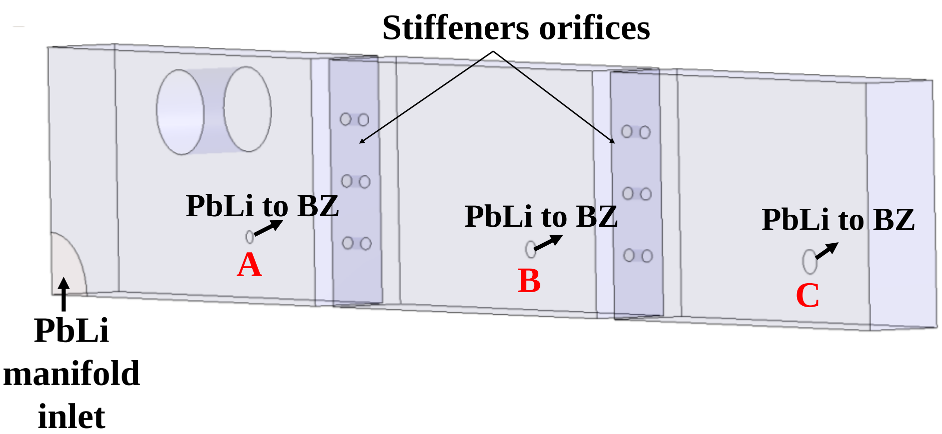

Fig. 4.1 – DEMO WCLL BB 2015 design: CFD model of PbLi manifold.

A preliminary analytical evaluation of the pressure drop in the computational domain is performed to define the diameters of the stiffeners orifices and manifold outlets. The study accounts only the concentrated pressure losses and it is done considering a maximum PbLi velocity of 0.05 m/s in the whole manifold, to limit the MHD issues and to avoid corrosion of Eurofer with PbLi. Furthermore, to ensure the structural integrity of the stiffening plates the number of orifices on stiffening plates is preserved.

The diameter of manifold outlets B and C are defined assuming the diameter of outlet A and stiffening plates orifices, and calculating the pressure drops from inlet and outlet of the manifold. Different values of outlet A and stiffening plate orifice diameters are considered [39].

The analytical analysis demonstrates that, setting the stiffener orifices diameter, the outlet A diameter can assume only values lesser than or equal to the stiffening plate orifices.

The results of the pressure drop at manifold outlets are reported, for different geometries in Tab. 4.1.

#	ΔP_{OA} [Pa]	ΔP_{OB} [Pa]	ΔP_{OC} [Pa]
1	57.77	32.77	26.53
2	88.06	63.06	56.82
3	57.77	44.40	41.07
4	31.17	17.81	14.48
5	57.77	50.02	48.09
6	18.27	10.52	8.59

Tab. 4.1 – Pressure drops at outlet orifices.

The diameters of outlet B and C are calculated starting from the pressure drops, with the reverse equations. Several geometries are selected to be studied with a CFD analysis. The values of diameters are reported in Tab. 4.2, where: ΦSP indicates the diameter of each stiffening plate orifice, ΦA, ΦB, and ΦC are, respectively, the diameter of manifold outlet A, B, C (Fig. 4.1).

#	Φ_{SP} [mm]	Φ_A [mm]	Φ_B [mm]	Φ_C [mm]
1	6.0	6.0	6.9	7.3
2	6.0	5.4	5.9	6.0
3	7.0	6.0	6.4	6.6
4	7.0	7.0	8.1	8.5
5	8.0	6.0	6.2	6.3
6	8.0	8.0	9.2	9.7

Tab. 4.2 – Orifices diameter selected with analytical analysis.

The computational domain considered is fluid. A rough mesh model is used in the calculations. The mesh is formed by tetrahedral elements and is characterized by $2 \cdot 10^6$ nodes and $7 \cdot 10^6$ elements. The selected mesh of the computational domain is used for all the calculations.

The CFD fluid-dynamic simulations are steady state and run in isothermal conditions (energy equation is turned off). The SST (Shear Stress Transport) k-ω turbulence model [45] is completely used in this context. The steady calculations were interrupted when residual RMS errors values were below an acceptable value (i.e. 10^{-4}), and monitor points for selected parameters of interest (i.e. pressure in the domain) reached constant values. The number of iterations needed to achieve steady state conditions was about 200. The material properties of PbLi (see ANNEX A), implemented in CFX, are calculated at constant temperature of 325°C [40]. The PbLi density is 9808.8 kgm^{-3}, and the dynamic viscosity is $1.94 \cdot 10^{-3}$ Pa·s. The total PbLi inlet mass flow rate is 0.0734 kg s^{-1}, the static pressure at the outlet is 0 Pa.

Several simulations are run to investigate the PbLi behavior in the manifold and to optimize the PbLi mass flow rate distribution, maintaining the PbLi velocity below the assumed limit of 0.05 m/s. The CFD analysis confirms the analytical results as shown in Fig. 4.2, where the pressure and velocity fields are reported for Run 5 and Run 6, respectively. In Run 5, the difference of pressure between the manifold and the outlet surfaces A, B, and C, is of the same order of magnitude and equal to 52 Pa. In this case a good mass flow rate distribution is achieved, as the pressure drop between inlet and outlet is greater than the pressure drops at stiffening plate orifices. While, in Run 6, the pressure loss at stiffening plate orifices are not negligible, and bring to have less flow at outlet B and C.

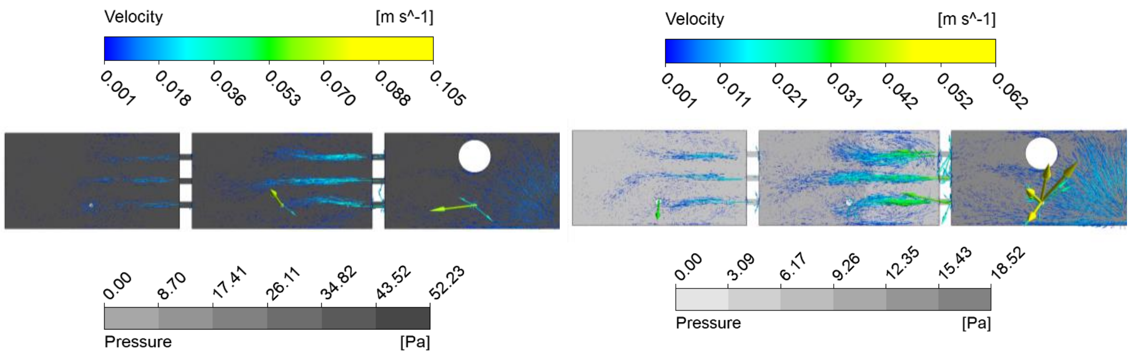

a) *Run 5* *b)* *Run 6*

Fig. 4.2 – CFX results: poloidal-toroidal view of pressure and velocity fields

The PbLi is distributed in all regions, even if stagnant regions are evidenced, in particular near the manifold outlet C. PbLi velocity, represented by the arrows in Fig. 4.2 a) and b), respects the assumed limit in the manifold. The average velocity at manifold outlets is in the range 0.055-0.075 m/s in Run 5, and lower than 0.05 m/s in Run 6. Maximum local values are reached at manifold outlet A. Considering the stiffening plate orifices, the average PbLi velocity is 0.033 m/s in the first set of orifices and 0.017 m/s in the second.

The CFD analysis proves that a homogeneous mass flow rate distribution can be achieved assuming a greater PbLi velocity limit. The evaluation of Eurofer corrosion rate with Sannier equation [41] that PbLi velocity can be increased without deteriorating corrosion effect. The corrosion rate for PbLi at 325 °C, which is the WCLL BB design inlet temperature, is less than 1 µm/yr increasing PbLi velocity up to 0.1 m/s.

Structural analyses are needed to evaluate if the presence of the orifices in the stiffening plates may compromised the structural integrity of the BB box, in normal operation and overpressure conditions. Furthermore, specific MHD analyses are required to evaluate more realistic flow paths in the PbLi manifold and to demonstrate the performances of the selected design.

4.1.1 **Main achievements**

The activity aims at supporting the preliminary design of the PbLi manifold, evaluating the size of the orifices suitable to uniformly distribute the breeder in the BZ. The objective is pursued calculating the pressure drops through the outlet and stiffening plate orifices of the manifold and defining the allowed orifices diameters. Several geometries are selected and investigated through CFD predictive calculations, using ANSYS CFX – 15 code.

The CFD analyses demonstrate that the PbLi distribution in the manifold is feasible increasing the PbLi velocity up to 0.1 m/s, considering Eurofer corrosion issues. Nevertheless, considering the outcomes from analyses and in order to enhance manufacturing and feasibility of the WCLL concept, the PbLi manifold has been modified in 2016 and, further, in 2017 design. MHD analyses are required to evaluate more realistic flow paths in the manifold and to demonstrate the performances of the selected design.

4.2 **CFD analyses of WCLL BB 2016 design**

The preliminary thermo-hydraulic (TH) analyses [39] were carried out to investigate the thermal and fluid-dynamic behavior of WCLL 2016 design, ensuring that the temperature requirement of the structures is met. The analyses focused on the elementary cell of the breeding blanket (i.e. breeding unit), developing a detailed CFD model to obtain a complete temperature distribution both in the fluids domains (i.e. PbLi, water) and solid structures. Several simulations were carried out to evaluate the response of coolant systems under different boundary conditions with the following main objectives:

- To investigate the effect of buoyancy forces in PbLi;
- To investigate the thermal field of PbLi in the Breeding Zone (BZ);
- To study the efficiency of the water coolant system, FW and BZ;
- To quantify the effective extracted power from FW, with respect the deposited power;
- To investigate hot spot, hot regions and issues;
- To optimize the temperature distribution in the water and PbLi systems.

4.2.1 Model and boundary conditions

A three-dimensional finite volume model of the breeding unit of DEMO WCLL blanket was set-up, using ANSYS CFX v15.0 code. The model includes solid domains (i.e. stiffeners, DWTs, FW, and Tungsten layer) and fluid domains (i.e. PbLi and water coolant), schematized in Fig. 4.3 [35][45].

The breeding unit has an average toroidal distance of 1300 mm, the radial dimension is 827 mm and the total height is 135 mm. Half height of radial-toroidal stiffeners is considered in the model, as the periodic condition is applied. The BZ coolant system consists of 21 DWTs with hydraulic diameter of 8 mm and an external diameter of 13.5 mm. The gap of DWT is not modeled. The FW of the breeding unit includes 10 square channels of 7×7 mm.

The physical properties of materials, used in the simulations (i.e. PbLi, water, Eurofer steel and Tungsten) and reported in ANNEX A, have been implemented in CFX code database. The physical properties of solid domains are specified in terms of density, specific heat and thermal conductivity, while fluid domains require also the dynamic viscosity [45].

To simulate the power deposition on WCLL, two thermal loads have been considered for the analysis: the plasma surface heating, due to the charged particles and radiation coming from plasma, and volumetric heat source, due to neutron and photon interaction with materials constituting WCLL. The FW surface is subjected to the power deposition due to particles and radiations arising from plasma. A maximum nominal heat flux of 0.5 MW/m^2 is imposed onto the straight surface of the tungsten, and, concerning the SWs, a cosine-dependent law has been adopted for them [30]. Moreover, a radial distribution of heat power density is applied to the model (i.e. solid structures and PbLi domains) to simulate power deposited by neutrons and photons. As far as a detailed neutronic model was not available for the 2016 WCLL blanket design, the volumetric power density was deduced from neutronic calculations based on the past PPCS-A WCLL blanket design [16]. The past radial distribution profile has been scaled with the 2015 DEMO1 average Neutron Wall Load (NWL) [9] and integrated with the radial model of the WCLL 2015 blanket design [30]. The volumetric generation in the coolant is not considered in the model.

The total power deposited in the breeding unit is 0.346 MW, of which 0.127 MW are deposited in the FW and 0.219 MW in the BZ. Water enters at 285 °C and exits at 325 °C, at 15.5 MPa, the total mass flow rate needed to extract the thermal energy is 1.529 kg/s. The FW and BZ mass flow rate have been evaluated case by case, as indicated in Tab. 4.3.

Concerning the PbLi breeder, buoyancy forces are considered in PbLi domain, thus the heat transfer between fluid domains occurs by means convection and conduction phenomena. The PbLi inlet mass flow rate is 0.146 kg/s., at 325 °C of temperature. A 0 Pa relative pressure is set at outlet surfaces of fluid domains (i.e. FW and BZ coolant, PbLi). The thermal-hydraulic parameters are summarized in Tab. 4.4. The other boundary conditions adopted for all the models are:

- Periodic boundary conditions are imposed on the upper and lower surfaces of radial-toroidal plates, FW and tungsten layer, in poloidal direction, to simulate the presence of the others breeding units;
- Adiabatic condition is applied to SWs, to back walls of PbLi, FW, tungsten and tubes;
- Thermal conduction is enabled in all solid domains, allowing the heat transfer between the solid structures and between solid and fluid domains;
- Inlet mass flow rate and outlet static pressure at flow domain inlet and outlet sections
- No-slip condition at the interface between coolant and the circuit steel walls;
- Reynolds Averaged Navier Stokes (RANS) equations are used in the fluid domains and two-equations k-ω Shear Stress Transport (SST) model is exploited to simulate the turbulence effects.

#	Description	Note
1	FW mflow: 37% of total mflow BZ mflow: 63% of total mflow	Mass flow rate calculated with enthalpy balance
2	FW mflow: 45% of total mflow BZ mflow: 55% of total mflow	Mass flow rate obtained from TM analyses
3	FW mflow: 45% of total mflow BZ mflow: 55% of total mflow	Counter-current flow adopted in BZ system
4	FW mflow: 37% of total mflow BZ mflow: 63% of total mflow	Recirculation adopted in BZ system

Tab. 4.3 – WCLL 2016 CFD analyses.

#	Parameter	Unit	Value
1	FW HF (max)	***MW/m²***	0.5
2	Total power	***MW***	0.346
3	FW power	***MW***	0.127
4	BZ power	***MW***	0.219
5	Coolant (BZ-FW) T_{inlet}	***°C***	285
6	Coolant (BZ-FW) pressure	***MPa***	15.5
7	Total mass flow rate	***kg/s***	1.529
8	PbLi T_{inlet}	***°C***	325
9	PbLi Mass Flow	***kg/s***	0.146

Tab. 4.4 – WCLL 2016 CFD analyses: boundary conditions.

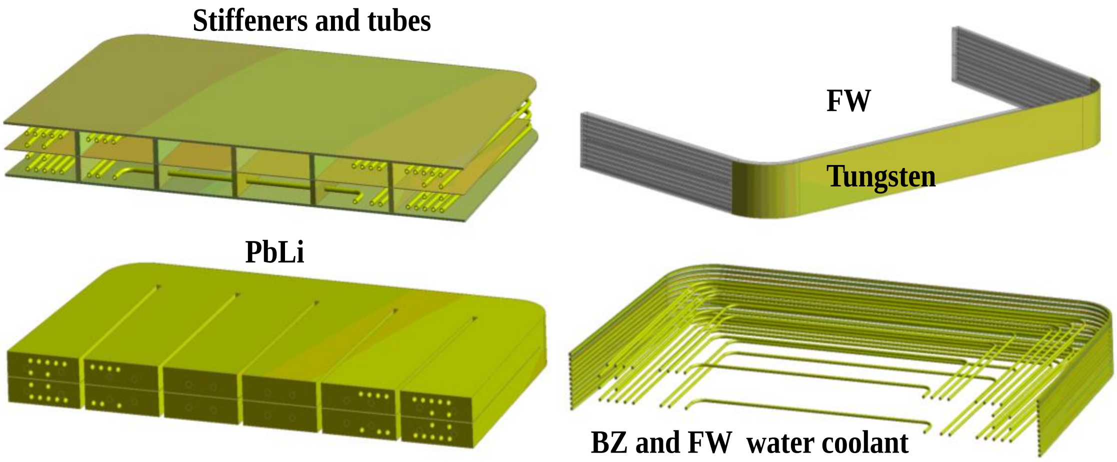

Fig. 4.3 – WCLL 2016 CFD analyses: CFX solid domains (i.e. stiffeners, DWTs, FW and tungsten layer) and fluid domains (i.e. PbLi, FW and BZ coolant).

4.2.2 Mesh features

The models have been meshed using a complex block hexahedral/tetrahedral grid. Sensitivity analyses are pursued to find the best agreement between the geometry discretization precision, mesh quality and the time requested for the calculation.

Many local controls have been inserted to define properly the geometry. For this purpose, different code tools have been exploited, such as the sizing control, the sweep method, and the inflation control near the solid walls. Despite the complexity of the domains, satisfactory results in terms of quality of the mesh have been achieved. The number of nodes, elements and the average values skewness and orthogonal quality of the selected mesh are reported in Tab. 4.5. A mesh detail of the selected mesh can be appreciated in Fig. 4.4. The major features of the mesh can be summarized as follows:

- Structured hexahedral mesh in the BZ coolant and FW coolant domain using the inflation layers technique at the coolant/solid interface;
- Structured hexahedral mesh in solid structure;
- Tetrahedral elements in PbLi domain with inflation layers at the PbLi/solid interface to allow a better description of the velocity gradients in those regions.

Parameter	**Value**
Nodes	14×10^6
Elements	28×10^6
Average Skewness	0.2938
Average Orth. Quality	0.831

Tab. 4.5 – WCLL 2016 CFD analyses: mesh statistics.

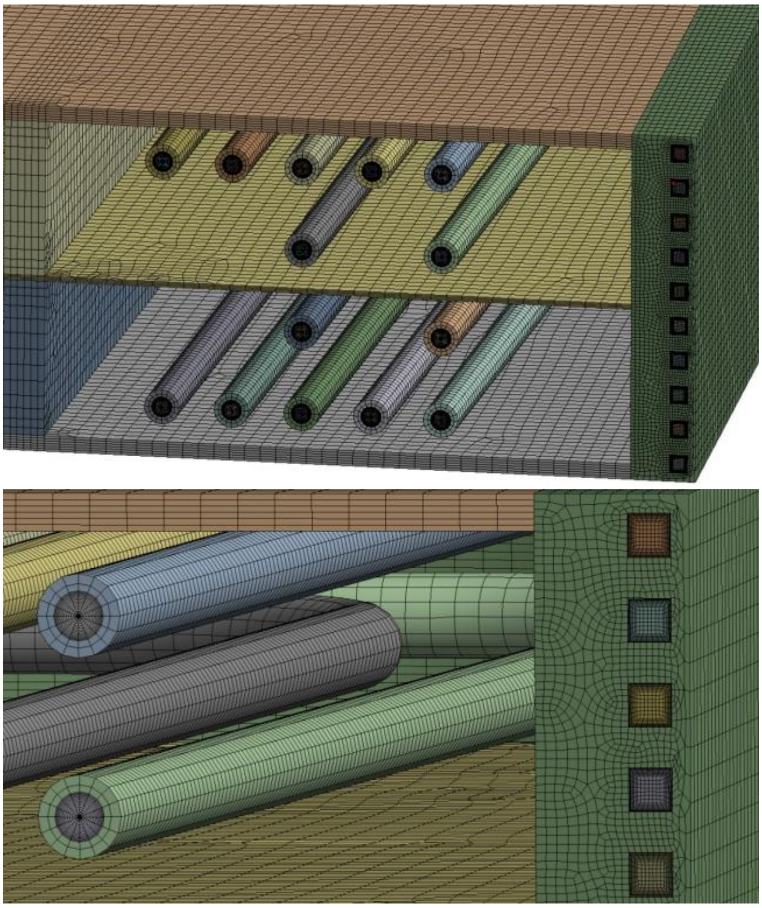

Fig. 4.4 – WCLL 2016 CFD analyses: detail of mesh model in solid and fluid domains.

4.2.3 **Results**

The water coolant of BZ system of Case 1 and 2 enters in the right side of the breeding unit and exits from the left side, flowing in radial-toroidal direction, as indicated in Fig. 4.5. Assuming the same total mass flow rate (1.529 kg/s.), the two simulations differ for the mass flow rate distribution between FW and BZ coolant systems. In Case 1 the FW mass flow rate is 37% of total mass flow rate, and the BZ mass flow rate is 63%. The mass flow rate of each system is calculated with the enthalpy balance, considering the power deposited in the system and water thermo-dynamic cycle (285-325 °C). Equal inlet mass flow is assumed in FW channels, instead BZ mass flow is distributed in the tubes depending upon tube length and the nuclear heating deposited near the tube.

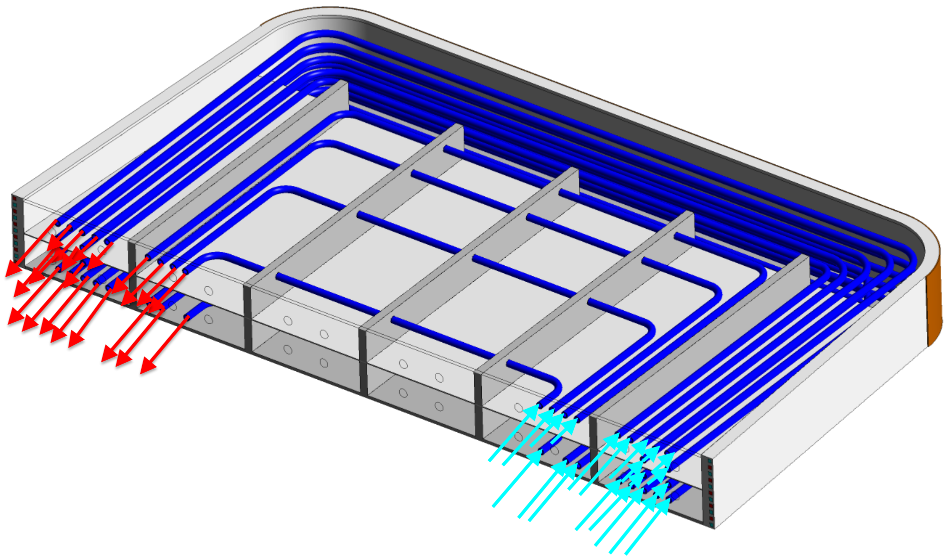

Fig. 4.5 – WCLL 2016 CFD analyses, Case 1 and Case 2 BZ coolant system layout. Blue rows indicate water inlet; red rows indicate water outlet.

A detailed analysis of the results is performed, to evaluate the efficiency of FW and BZ systems. The average outlet temperature of FW and BZ coolant of 329.1 °C and 322.2 °C, respectively (see Tab. 4.8). The results demonstrate that, being the FW outlet temperature greater than theoretic value (325 °C), and the BZ outlet temperature lower, the FW coolant system extracts part of the power of the BZ system. The comparison between the power deposited and the power extracted by FW and BZ systems confirms this result. The difference between the power deposited and the power extracted in the FW and BZ systems, which is equal to 12.72% and -7.86%, respectively (see Tab. 4.5).

The analysis demonstrates that the calculation of mass flow distribution between the two systems cannot be based only on the enthalpy balance, due to the radial and toroidal volumetric power density distribution. Thus, a sensitivity analysis is performed to improve coolant systems efficiency.

	Power deposited [MW]	Extracted Power [MW]	Error [%]
FW	0.127	0.1433	***12.72***
BZ	0.219	0.2016	***-7.86***
Total	0.346	0.3449	***-0.29***

Tab. 4.6 – WCLL 2016 CFD analyses, Case 1, comparison between power deposited and power extracted un FW and BZ systems.

In Case 2, a mass flow rate distribution based on thermo-mechanical (TM) results [33] has been considered in the CFD model. The FW and BZ mass flow rates are, respectively, 45% and 55% of total mass flow. In Tab. 4.7 the mass flow rates of each BZ tube are reported: the tubes are labeled from 1 to 9 in toroidal direction, starting from the first line near the right Side Wall (SW) and from 1 to 4 in poloidal direction (i.e. 1_1).

#	BZ tubes	Mass flow rate [kg/s]
1	1_1; 1_2; 1_3; 1_4	0.0736
2	2_1; 2_4	0.0502
3	3_1; 3_2; 3_3, 3_4	0.0441
4	4_1; 4_4	0.0336
5	5_1; 5_4	0.0419
6	6_1; 6_4	0.0383
7	7_1; 7_4	0.0264
8	8_1	0.0199
9	9_1; 9_4	0.0046

Tab. 4.7 – WCLL 2016 CFD analyses, Case 2 BZ mass flow rate.

The results of the simulation show a better distribution of outlet temperature in the two coolant systems: the average coolant outlet temperature is 323.5 °C in the FW and 324.7 °C in BZ coolant system. Moreover, a reduction of maximum temperature is noted in the FW coolant system and Eurofer structure. Fig. 4.6 and Fig. 4.7 show the FW coolant bulk temperature in the two simulations; it is noted that the maximum temperature in Case 1 is about 337 °C, and in Case 2 is reduced to 330 °C. The counter-current flow of FW water coolant ensures the temperature symmetry in toroidal direction, as also demonstrated by temperature distribution in FW Eurofer. Fig. 4.10 presents the thermal field of FW Eurofer in Case 2.

As regard the BZ system, the bulk temperature is investigated grouping the tubes, according to temperature distribution, and calculating the average temperature at different sections (see Fig. 4.8 and Fig. 4.9). The trend of the average BZ coolant temperature as function of position in the tubes presents a maximum average temperature of about 330 °C in Case 1 and 327 °C in Case 2.

Considering that the average coolant velocity is 1.3 m/s in the BZ system and 2.0 m/s in FW system, which is well below the assumed limit (7 m/s), there is margin to further improve cooling performances.

As regard the breeding region, Case 1 and Case 2 present a similar thermal field in PbLi and stiffeners domains; the ΔT between maximum temperatures is about 1 °C (see Tab. 4.8). The temperature in solid structures remain well below the Eurofer maximum allowable value (550 °C) in both simulations. Nevertheless, it was noted an asymmetric temperature distribution in toroidal direction, as shown in Fig. 4.11 and Fig. 4.12, where PbLi and solid structures temperature map obtained in Case 1 is reported, respectively. This asymmetry is mainly due to the BZ coolant system layout, as cold water enters in the right side of the breeding unit and hot water exits from left side. The toroidal asymmetry is an issue, as it is source of thermal stress for the Eurofer structures. Moreover, the toroidal asymmetry determines the presence of two regions with different PbLi density and, due to the buoyancy forces, there is a PbLi net flow in toroidal direction in addition to the dominant radial-poloidal flow.

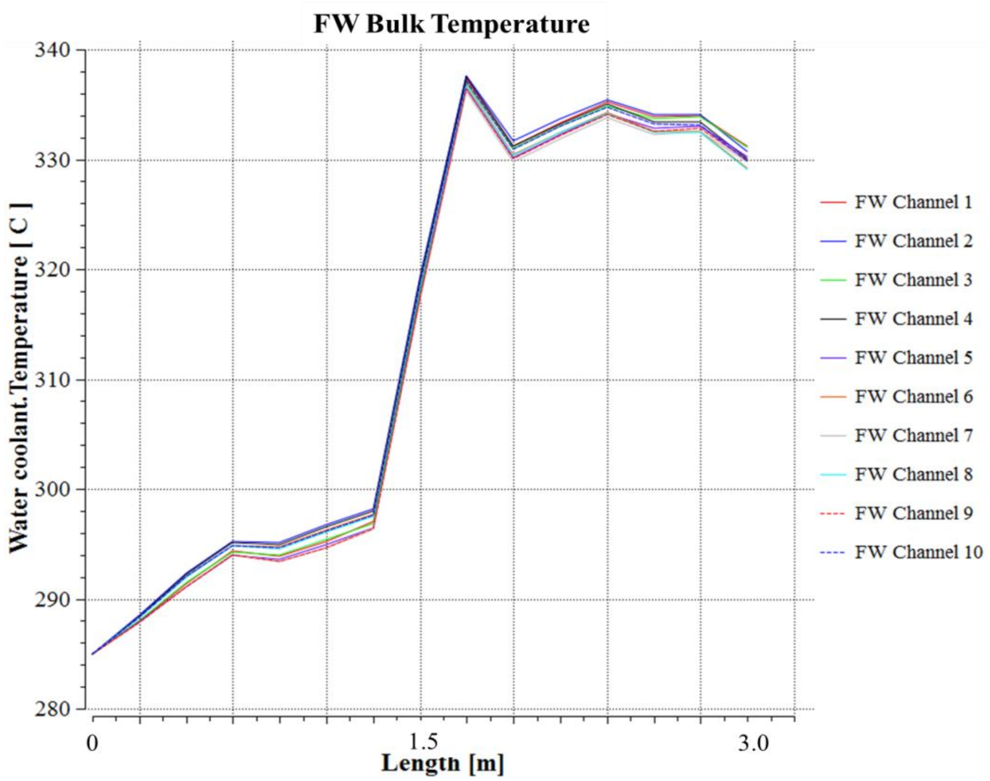

Fig. 4.6 – WCLL 2016 CFD analyses Case 1, FW coolant bulk temperature.

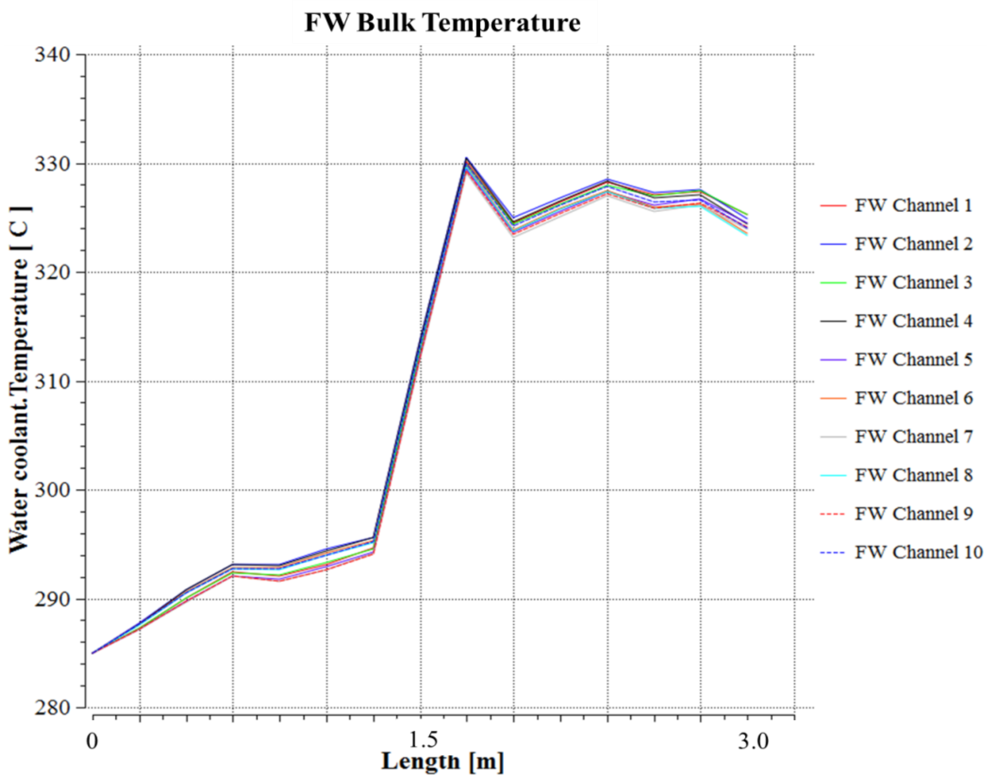

Fig. 4.7 – WCLL 2016 CFD analyses, Case 2, FW coolant bulk temperature.

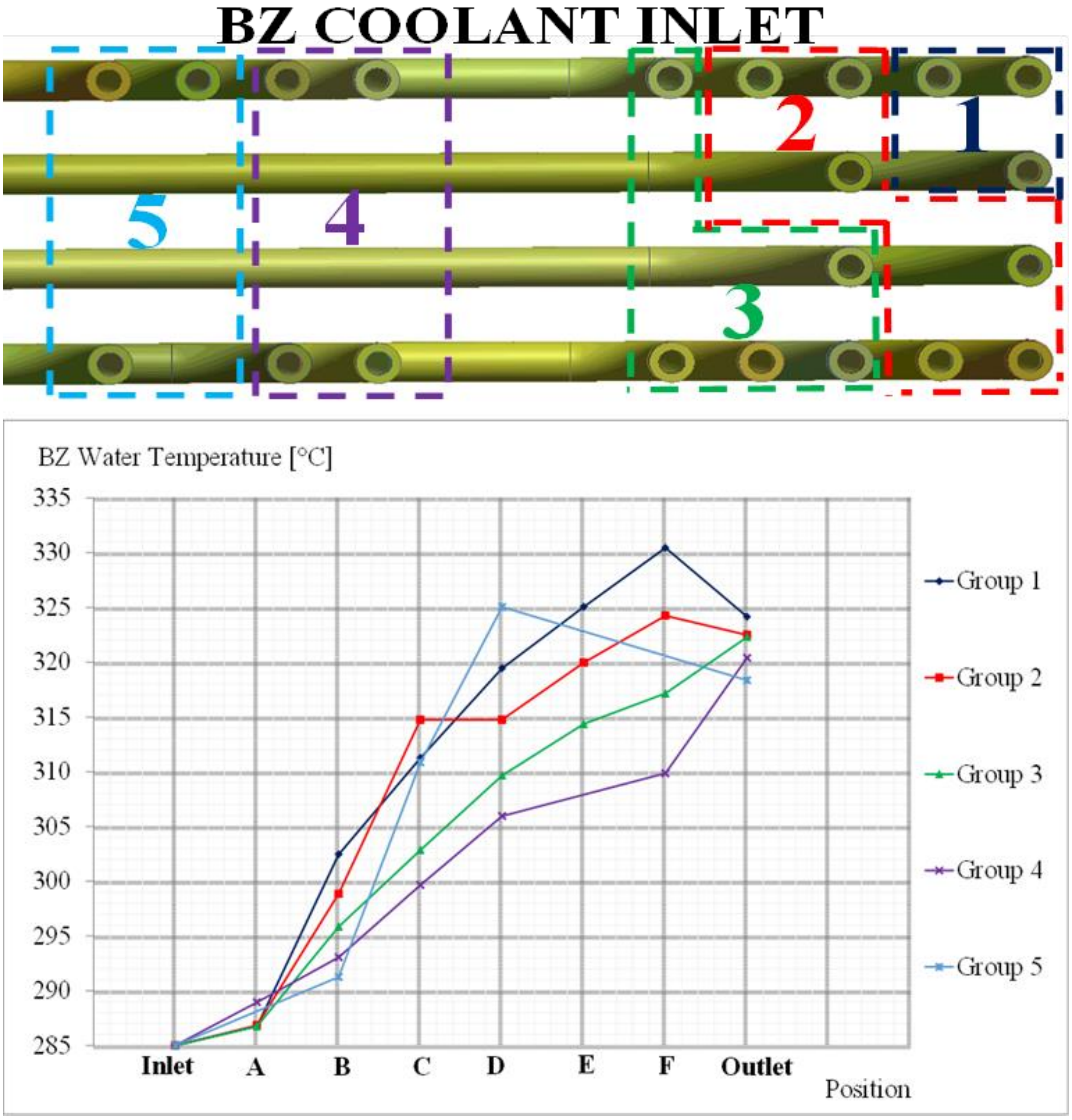

Fig. 4.8 – WCLL 2016 CFD analyses, Case 1, BZ water temperature VS position.

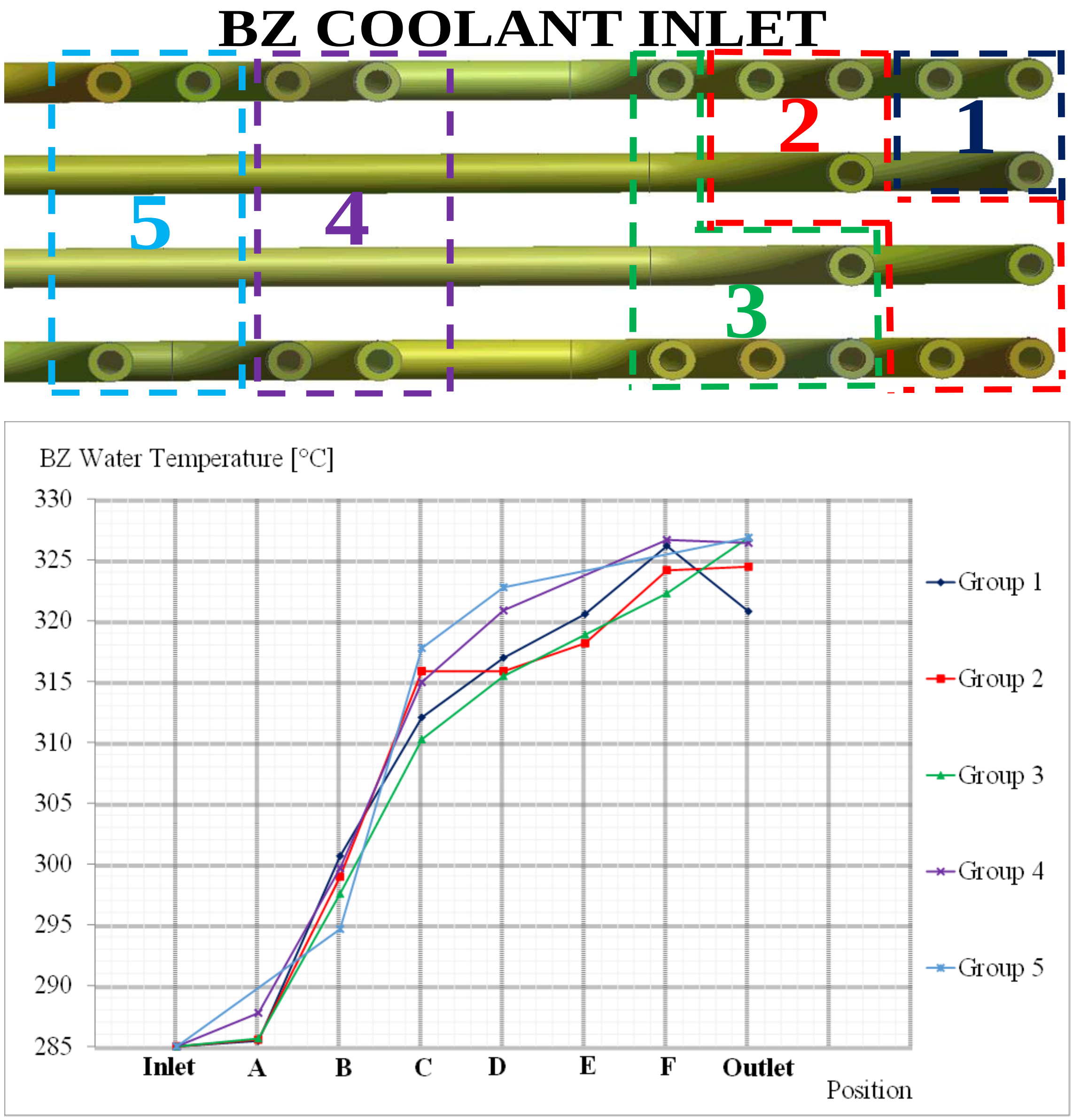

Fig. 4.9 – WCLL 2016 CFD analyses, Case 2, BZ coolant temperature VS position.

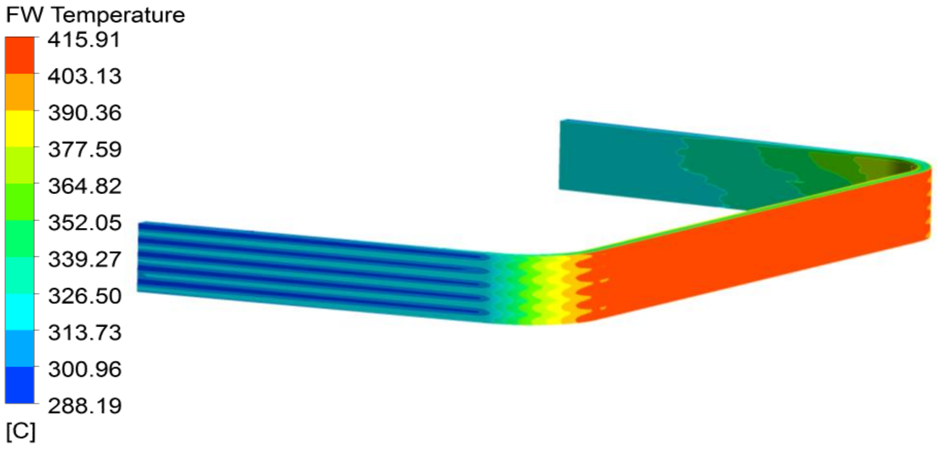

Fig. 4.10 – WCLL 2016 CFD analyses, Case 2, FW Eurofer temperature.

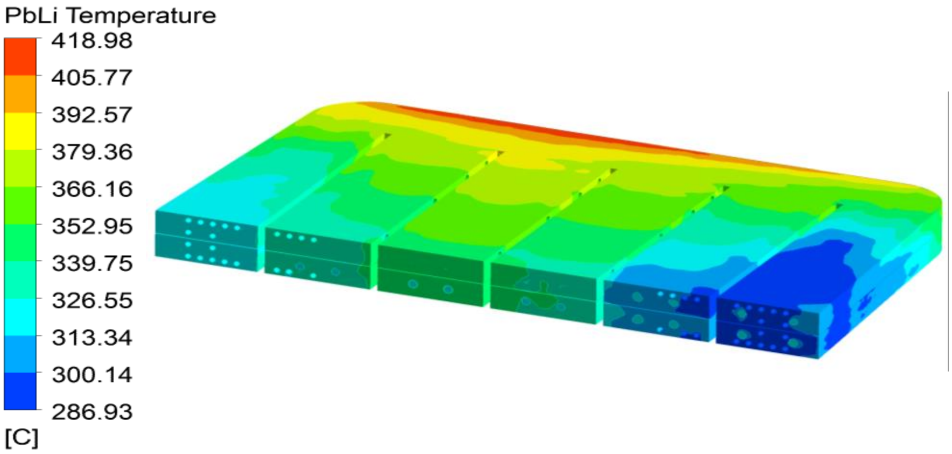

Fig. 4.11 – WCLL 2016 CFD analyses, Case 1, PbLi temperature.

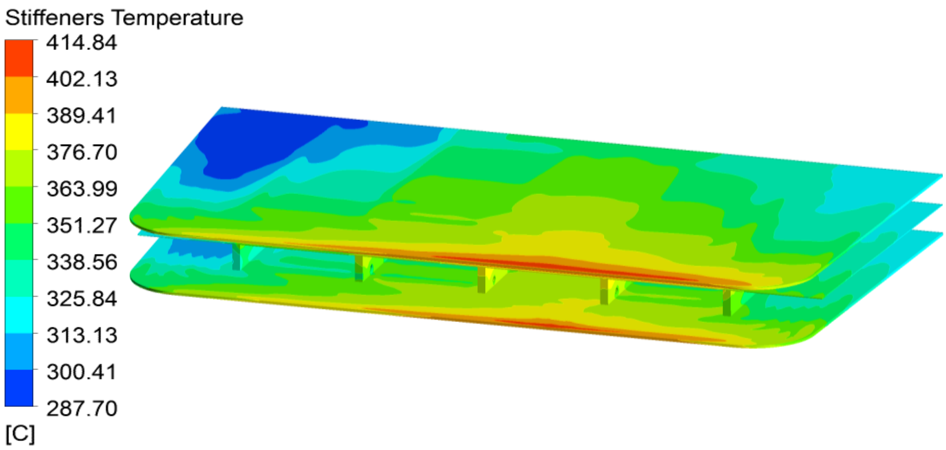

Fig. 4.12 – WCLL 2016 CFD analyses, Case 1, stiffeners temperature.

In order to achieve a temperature symmetry in toroidal direction two alternative BZ coolant system layouts have been investigated. In Case 3, a counter-current flow path was simulated, as schematized in Fig. 4.13, assuming the same mass flow rate distribution of Case 2.

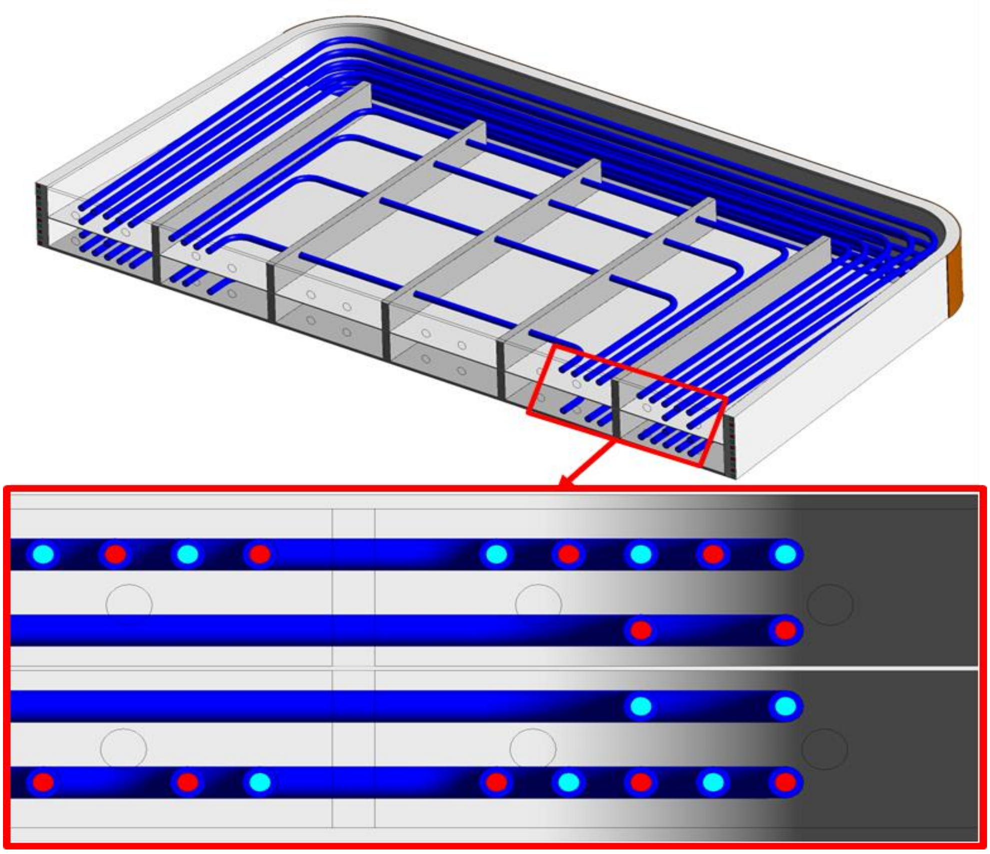

Fig. 4.13 – WCLL 2016 CFD analyses, Case 3, BZ coolant system layout: inlet (blue) and outlet (red) orifices.

The results of CFD simulation show that this configuration ensures temperature symmetry in toroidal direction, as shown in Fig. 4.14, where a radial-toroidal view of PbLi is reported, respectively. and in Fig. 4.15 illustrates the radial-toroidal temperature of Eurofer structures, showing that the maximum temperature is still below 500 °C. Moreover, a good outlet temperature distribution is achieved in BZ coolant system with an average outlet temperature of 325.8 °C, as reported in Tab. 4.8. Nevertheless, the counter-current flow in BZ system requires water (inlet and outlet) manifolds that are difficult to be integrated with current design, considering the available space between the back plate and the BSS and constraints of DEMO 2015 specifications.

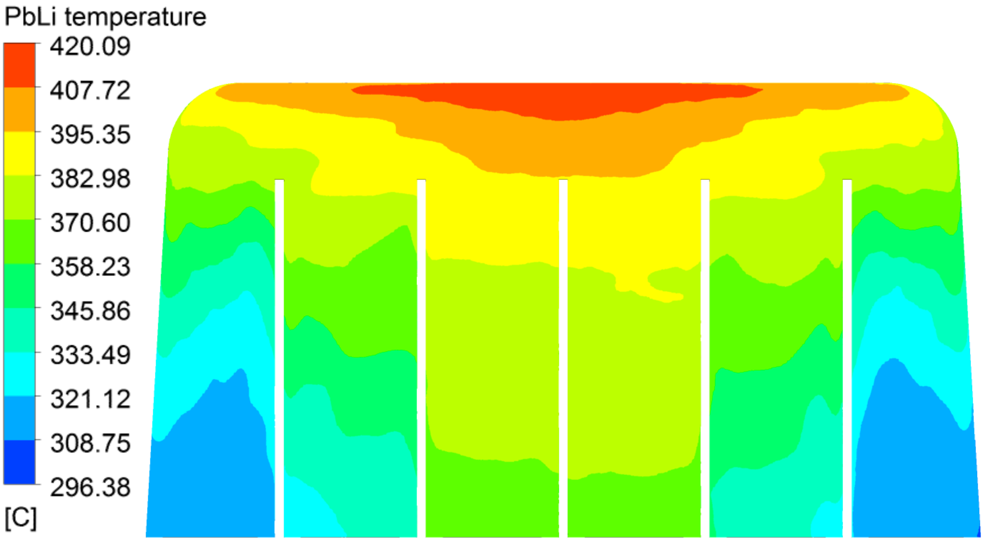

Fig. 4.14 – WCLL 2016 CFD analyses, Case 3, radial-toroidal view of PbLi temperature distribution.

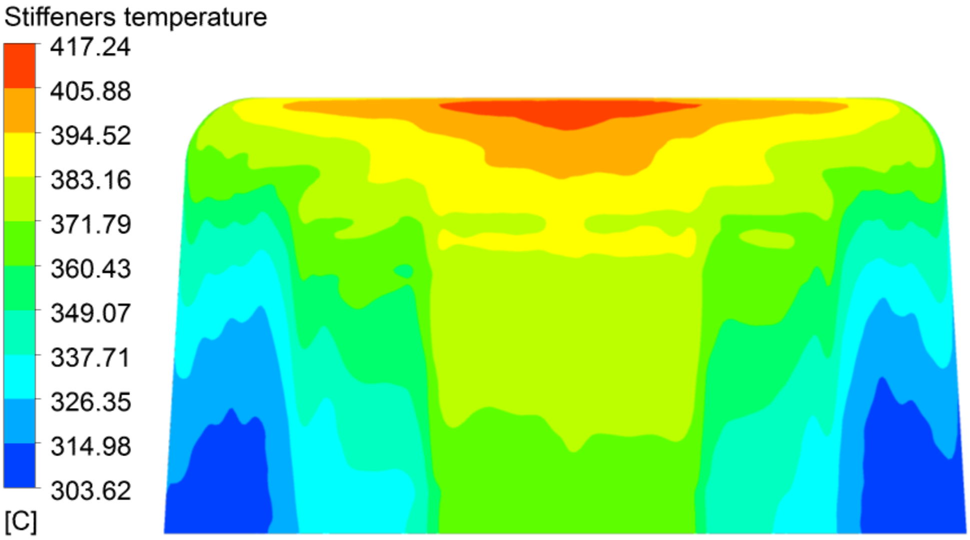

Fig. 4.15 – WCLL 2016 CFD analyses, Case 3, radial-toroidal view of stiffeners temperature.

In Case 4 BZ water enters in the 10 tubes near the FW, flows in radial-toroidal direction, it is collected in a manifold and then recirculates into the other 11 tubes in the opposite direction, as represented in Fig. 4.16. The same mass flow rate distribution of Case 1 is assumed for BZ and FW systems, and equal flow is assumed at BZ tubes inlet.

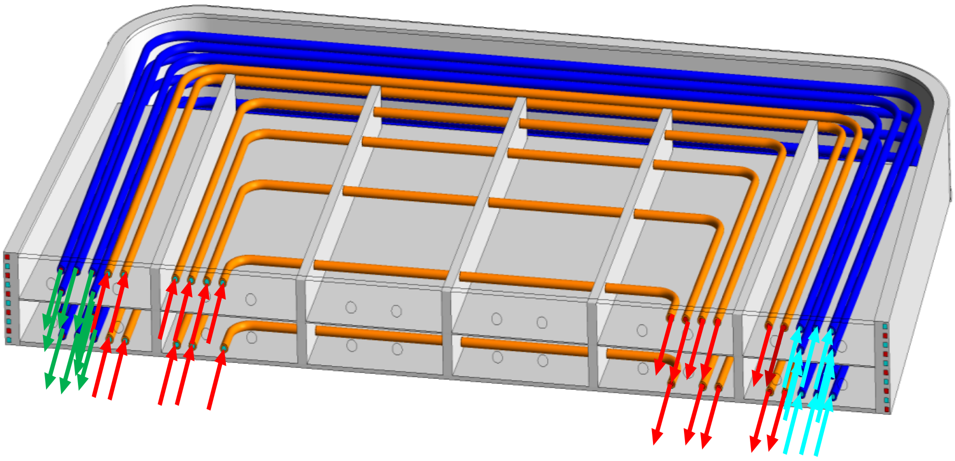

Fig. 4.16 – WCLL 2016 CFD analyses, Case 4, BZ coolant system layout.

The results of the analyses show that the symmetry of thermal field in toroidal direction is improved with respect Case 1 and Case 2 (see Fig. 4.20), and BZ coolant efficiency is enhanced, as water velocity is increased up to 2.67 m/s. Moreover, the maximum temperature of Eurofer stiffeners (408 °C) is decreased with respect previous cases, as illustrated in Fig. 4.21. Nevertheless, the temperature symmetry and coolant efficiency can be further improved.

As regard BZ coolant system, outlet temperature is more homogenous and maximum temperature is reduced, as demonstrated in Tab. 4.8 and Fig. 4.17, where the surface temperature of BZ coolant can be appreciated. The maximum value indicated in Fig. 4.17 is greater than the value in Tab. 4.8 as the table reports bulk temperatures, instead the figure shows the surface temperature.

The BZ coolant system layout, presented in Case 4, is the only configuration that can be integrated successfully with current WCLL design. The CFD analyses carried out demonstrate that there is margin to enhance cooling performances, as the average coolant velocity is below the assumed limit (7 m/s) and the maximum temperature is always lower than 500 °C. Cooling performances can be maximized, for example, reducing the number of tubes. Further studies are needed, and alternative configurations should be investigated, to improve temperature symmetry in toroidal direction, and to simplify the design (i.e. avoiding pipes crossing vertical stiffeners).

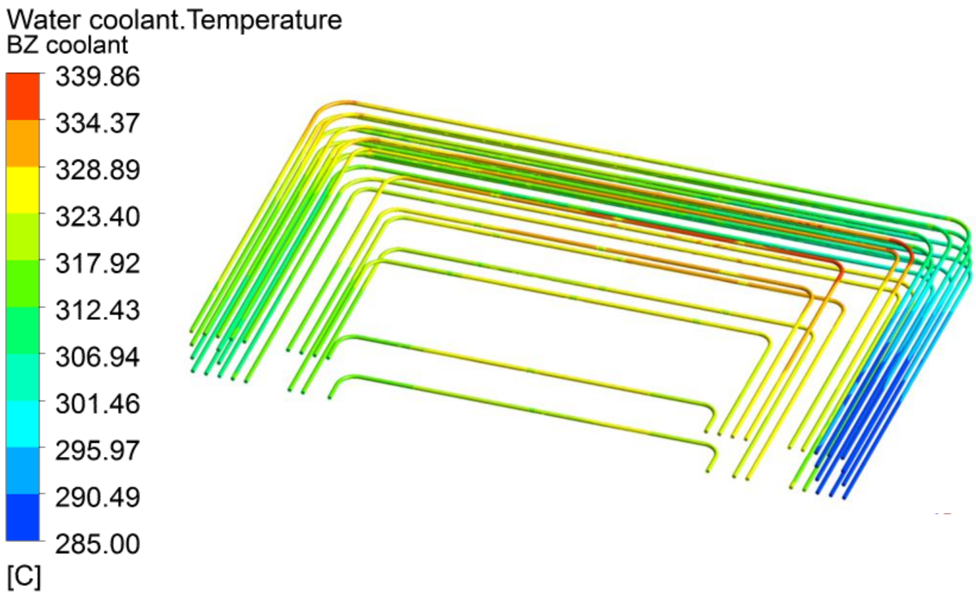

Fig. 4.17 – WCLL 2016 CFD analyses, Case 4, BZ coolant-tube interface temperature.

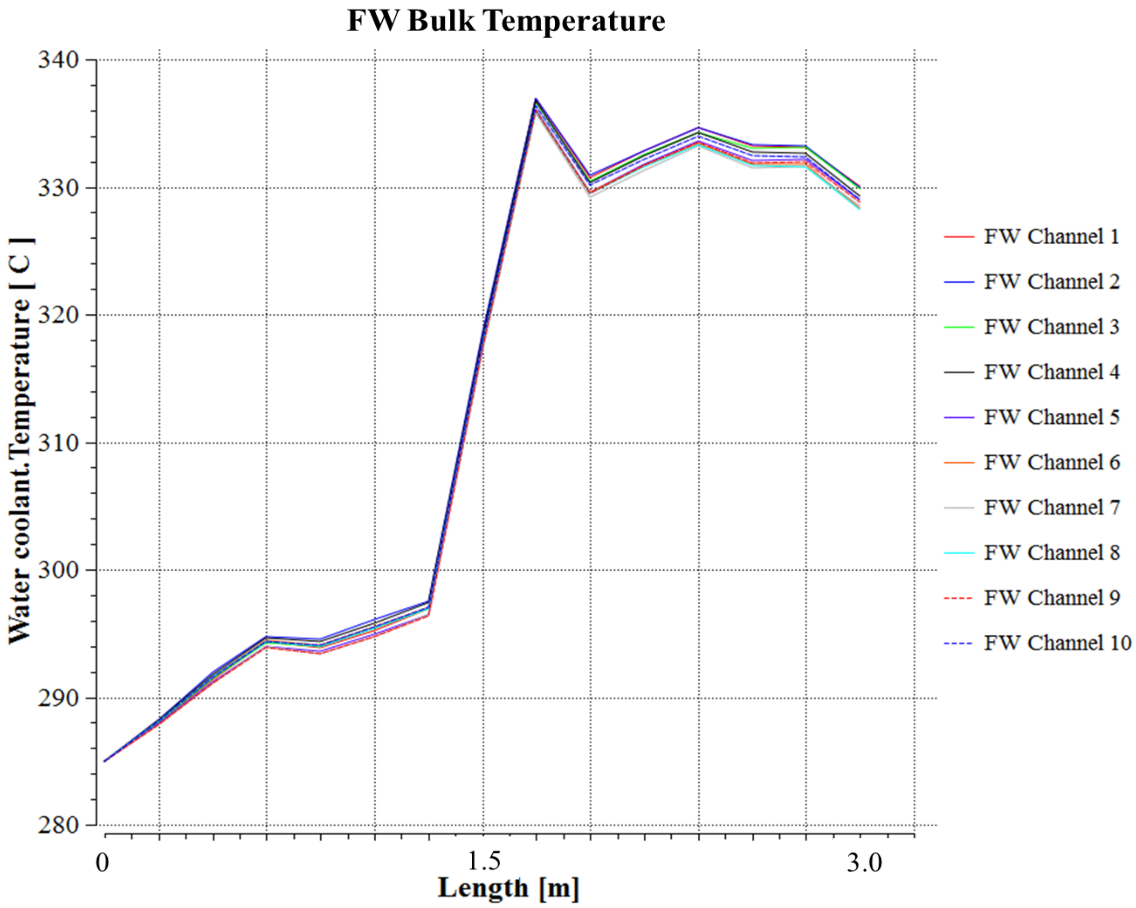

Fig. 4.18 – WCLL 2016 CFD analyses, Case 4, CFX FW coolant bulk temperature.

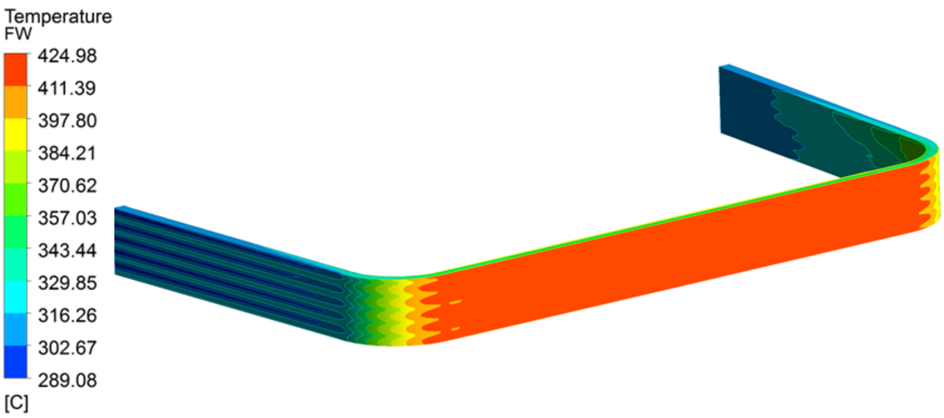

Fig. 4.19 – WCLL 2016 CFD analyses, Case 4, FW Eurofer temperature.

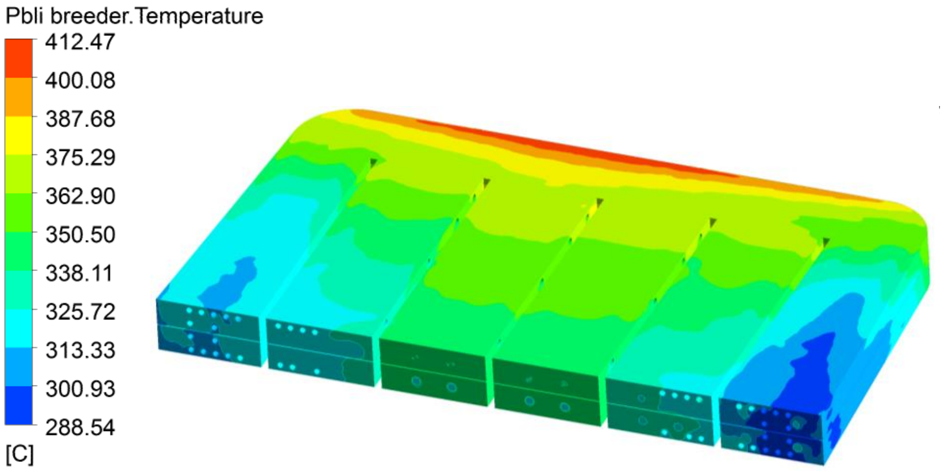

Fig. 4.20 – WCLL 2016 CFD analyses, Case 4, PbLi temperature.

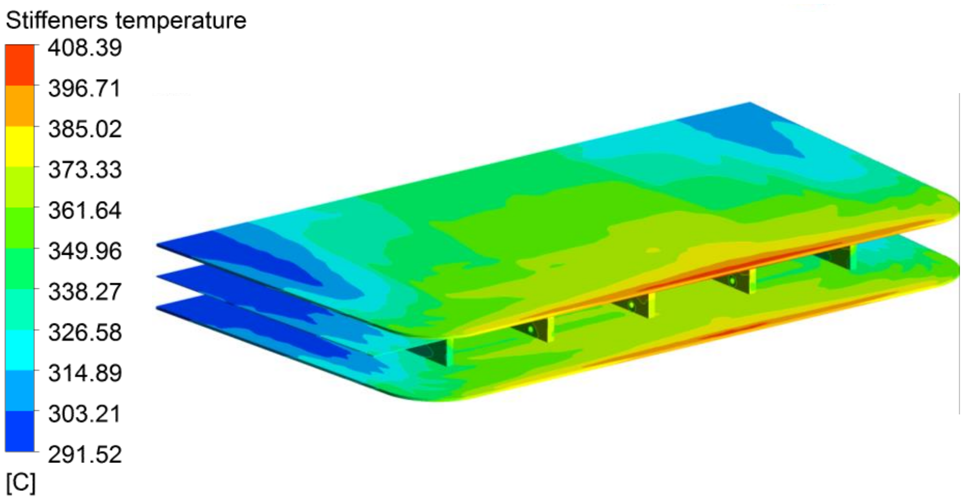

Fig. 4.21 – WCLL 2016 CFD analyses, Case 4, stiffeners temperature.

#	Description	Case 1	Case 2	Case 3	Case 4
1	PbLi T_{min} [°C] T_{max}[°C]	 286.9 418.9	 286.8 417.3	 296.85 420.05	 288.7 412.4
2	Eurofer structures T_{min} [°C] T_{max}[°C]	 287.6 414.8	 287.6 413.1	 304.35 417.25	 291.5 408.3
3	FW Eurofer T_{min} [°C] T_{max} [°C]	 289.4 425.4	 288.3 415.8	 286.05 422.25	 289.25 424.9
4	Tungsten T_{min} [°C] T_{max} [°C]	 312.7 433.2	 308.6 423.6	 304.85 434.15	 312.5 432.8
5	BZ coolant T_{min} [°C] T_{max} [°C]	 284.9 332.7	 284.9 339.5	 284.95 343.45	 284.9 330.4
6	FW coolant T_{min} [°C] T_{max} [°C]	 284.9 350.0	 284.9 342.0	 284.95 344.75	 284.9 349.6
7	BZ coolant avg T_{out} [°C]	322.2	324.7	325.8	322.4
8	FW coolant avg T_{out} [°C]	329.1	323.5	323.4	328.1
Minimum and maximum temperature are bulk values					

Tab. 4.8 – WCLL 2016 CFD analyses, temperature in solid and fluid domains.

4.2.4 Main achievements

The CFD analyses performed in 2016 demonstrate that the BZ and FW coolant systems of WCLL breeding blanket present excellent coolant performances, maintaining the maximum temperature in PbLi and solid domains well below the limit (550 °C).

The preliminary analysis (Case 1) highlights that the FW systems extracts part of the power deposited in the BZ, demonstrating the limit of the analytical evaluation of the mass flow rates based only on the enthalpy balance. Moreover, the mass flow rate in BZ tubes should be defined taking into account the effective radial and toroidal profile of volumetric power in the BZ. These results are confirmed by the analysis carried out considering the mass flow rate distribution obtained with thermo-mechanical analyses.

The domains of BZ are characterized by an asymmetry in toroidal direction of thermal field, this is due to the BZ coolant system layout. To improve the temperature symmetry two alternative configurations were investigated. The first foresees a counter-current flow path of water in the BZ coolant system. This configuration is an ideal solution which ensures an excellent temperature symmetry in toroidal direction, nevertheless it is difficult to be manufactured because the available space in the manifolds region. The second coolant scheme is based on the recirculation of water in the BZ tubes. This configuration is promising, as the coolant performances are enhanced, and it is the only solution that can be integrated in the manifolds region, even if further improvements on temperature distribution are needed.

Moreover, being water velocity in FW and BZ systems well below the assumed limit (7 m/s), there are margins to reduce the number of cooling tubes and thus to improve cooling performances.

4.3 CFD analyses of WCLL BB 2017 design

The main objective of the analyses performed in 2017 is to enhance thermal-hydraulic performances, improving the design on the basis of main outcomes from the studies carried out in 2016. In particular, the new configuration should satisfy the following main characteristics:

- Temperature symmetry in toroidal direction;
- Maximized cooling performances;
- Reduced number of tubes;
- Simplified coolant system layout, enhancing manufacturability (i.e. avoiding pipes crossing vertical stiffeners) and flexibility.

4.3.1 Model and boundary conditions

Several BZ coolant system layouts have been investigated, considering different pipes geometries (i.e. U-shaped tubes, helical tubes, wavy tubes), that are illustrated in Fig. 4.22. The configurations present a simple layout, as they can be easily assembled in the breeding zone, without crossing vertical stiffeners. This configuration of the breeding unit presents the following modifications with respect the WCLL 2016 design. The radial-poloidal stiffening plates have been extended until the FW and the baffle plate has been removed, changing the PbLi flow path from the radial-poloidal direction to a poloidal flow through the holes made in the radial-toroidal stiffening plates. The FW coolant layout is maintained, with coolant flowing in counter-current direction in 10 channels.

In the preliminary CFD analyses, the PbLi is isolated. This assumption is conservative from the temperature distribution point of view, as the temperature profile into the BZ is driven only by buoyancies effects. Further analyses will be carried out, once the reference configuration will be selected, to optimize the holes dimensions and distribution in the stiffening plates.

For each configuration thermal-hydraulic steady state analyses have been performed in order to assess the coolant systems efficiency in removing the deposited power, as well as sensitivity analyses to evaluate the response of the systems under different boundary conditions (i.e. changing number of pipes in each toroidal channel, mass flow rates). The complete list of the simulations is reported in Tab. 4.10, and the relevant results are discussed in Sect. 4.3.3.

For each configuration, a 3D finite volume model has been set-up to realistically reproduce the geometric and flow features of WCLL breeding unit, and to obtain a complete and detailed temperature distribution both in fluid and solid domains.
The same thermal loads and boundary conditions of WCLL 2016 CFD analyses have been considered in the simulations (see Sect. 4.2.1).

A new thermo-dynamic cycle is assumed as reference for WCLL BB 2017 design, in order to improve efficiency of PHTS and BoP. The thermo-dynamic cycle, still based on PWR conditions, foresees water coolant entering at 295 °C and exiting at 328 °C, at 15.5 MPa. The total mass flow rate, calculated using RELAP5/Mod3.3 properties [45], is 1.787 kg/s. The mass flow rate of BZ and FW systems is and 1.011 kg/s and 0.776 kg/s, respectively and it is calculated on the base of thermo-mechanical analyses. As regard the PbLi, static condition is assumed with an initial temperature of 325 °C. The complete set of thermo-dynamic parameters is reported in Tab. 4.9.

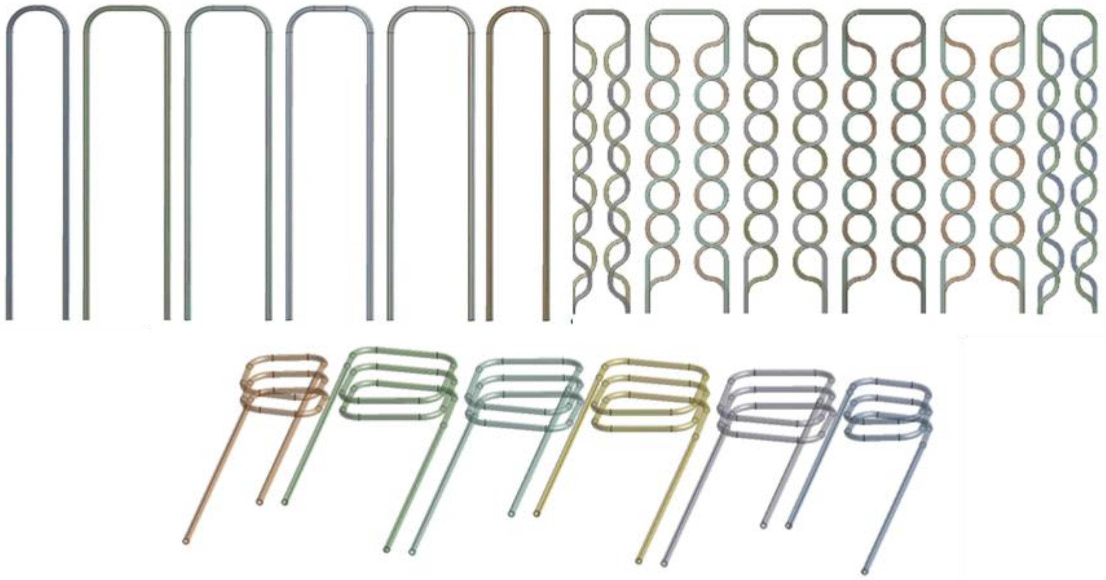

Fig. 4.22 – WCLL BB 2017 CFD analyses: BZ coolant geometries to be investigated.

#	Parameter	Unit	Value
1	FW HF (max)	$MW\ m^{-2}$	0.5
2	Coolant (BZ-FW) T_{inlet}	***°C***	295
3	Coolant (BZ-FW) Pressure	***MPa***	15.5
4	FW Power	***MW***	0.127
5	BZ Power	***MW***	0.219
6	FW Mflow	***kg/s***	0.776
7	BZ Mflow	***kg/s***	1.011
8	Total Mflow	***kg/s***	1.786
9	PbLi T_{inlet}	***°C***	325

Tab. 4.9 – WCLL BB 2017 CFD analyses: boundary conditions.

#	ID	DESCRIPTION	NOTE
1	2017_breeder_unit	• 24 tubes • Constant mflow rate in BZ system	Collectors are not optimized
2	20170623_breeder_unit_2tubes	• 12 tubes • Constant mflow rate in BZ system	
3	20170628_breeder_unit_1tube	• 6 tubes • BZ mflow central channels: 0.773 kg/s • BZ mflow side channels: 0.238 kg/s	
4	2017_03_20_breeder_unit_spring01	• 12 HC tubes • Constant mflow rate	
5	2017_03_20_breeder_unit_spring02	• 12 HC tubes • BZ mflow central channels: 0.773 kg/s • BZ mflow side channels: 0.238 kg/s	
6	2017_03_20_breeder_unit_1spring_02	• 6 HC tubes • Constant mflow	BZ inlet at top
7	2017_03_20_breeder_unit_1spring_04	• 6 HC tubes • BZ mflow central channels: 0.773 kg/s • BZ mflow side channels: 0.238 kg/s	
8	2017_03_20_breeder_unit_1spring_05	• 6 HC tubes • BZ mflow central channels: 0.773 kg/s • BZ mflow side channels: 0.238 kg/s • Buoyancies forces disactived	
9	2017_breeder_unit_4tubes_03	• 24 curved tubes • Constant mflow rate in BZ system	
10	2017_breeder_unit_2Ctubes_05	• 12 curved tubes • BZ mflow evaluated on the basis of effective power deposited in each toroidal cell	
*HC: HELICAL			

Tab. 4.10 – WCLL 2017 design: CFD simulations.

4.3.2 **Mesh features**

The 3D finite volume models have been meshed using the same approach of WCLL 2016 model (see Sect. 4.2.2). Nevertheless, the mesh model of PbLi domain has been better defined to find the best geometry discretization precision, considering the time requested for calculations. The main parameters that characterized the mesh are reported in Tab. 4.11. A mesh detail can be appreciated in Fig. 4.23.

Parameter	**Value**
Nodes	15×10^6
Elements	52×10^6
Average Skewness	0.24
Average Orth. Quality	0.86

Tab. 4.11 – WCLL BB 2017 design: mesh statistics.

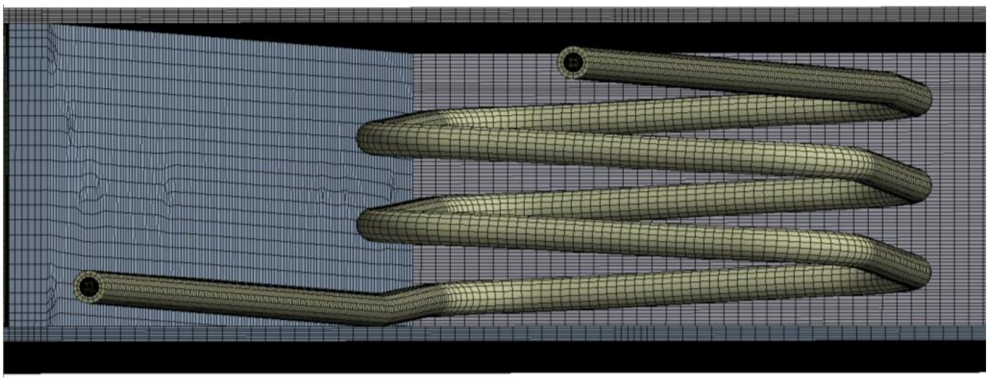

a) Detail of BZ HC tube mesh

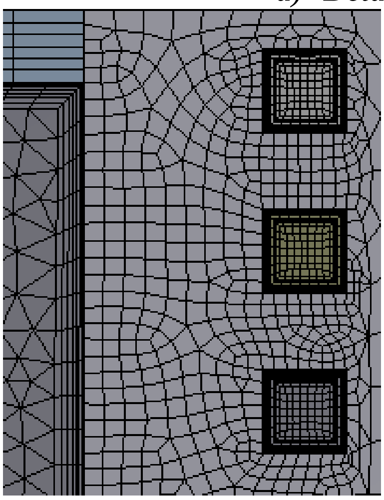

b) Detail of FW Eurofer and coolant mesh

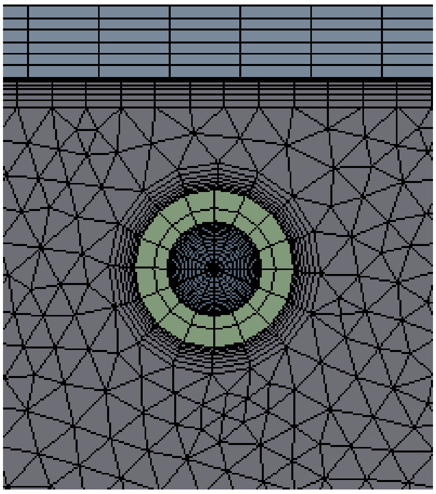

c) Detail of PbLi and BZ tube mesh

Fig. 4.23 – WCLL BB 2017 analyses, mesh of Case 7: detail of fluid and solid domains.

4.3.3 **Results**

In Case 1 the BZ coolant system is characterized by 24 U-shaped tubes, as shown in Fig. 4.24. The analysis is carried out considering constant and equal mass flow rate in each BZ tube. The water is distributed in the pipes symmetrically with respect the poloidal-toroidal plane.

The CFD analyses demonstrates that this configuration ensures the temperature symmetry in toroidal direction, as shown in the PbLi and Eurofer domains. Fig. 4.25 presents an isometric view of PbLi thermal field (Fig. 4.25 a) and the temperature distribution in poloidal-toroidal direction, at plane A. It is noted that the buoyancies forces drive the PbLi flow path, as there is a stratification in poloidal direction. The temperature distribution obtained in Eurofer structures is reported in Fig. 4.26, presenting a maximum value of 409 °C, which is well below the limit (550 °C). The maximum and minimum temperature of all domains are summarized in Tab. 4.13.

As regard the BZ and FW coolant systems, the average outlet temperature is 328 °C and 327 °C, respectively, as reported in Tab. 4.14. Due to the temperature distribution in PbLi domain, the BZ coolant system presents a maximum temperature in the tubes at the top of the breeding unit, as shown in Fig. 4.27, where the temperature at coolant-tube interface is reported. It is noted that the outlet temperature is not uniform, thus, the mass flow rate distribution in the BZ tubes should take into account the different power density in the toroidal channels and the influence of the FW system. Tab. 4.14 summarized the main parameters (i.e. maximum and minimum temperature) of BZ and FW coolant systems.

The average outlet velocity of water in BZ and FW systems is 1.32 m/s and 2.41 m/s, respectively, thus, there is margin to improve cooling efficiency.

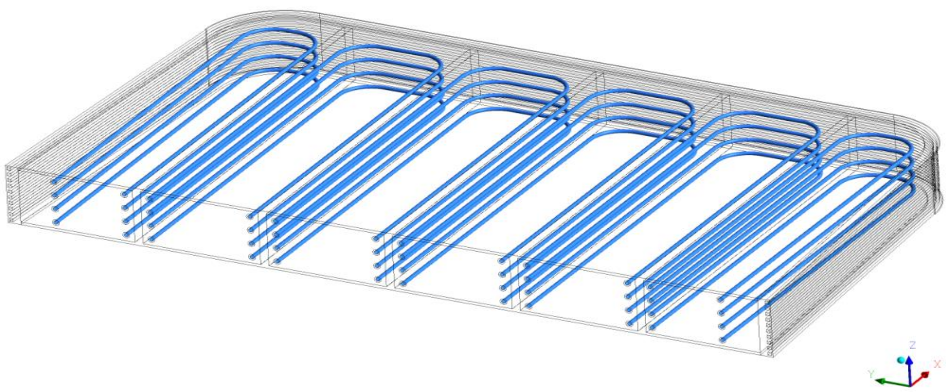

Fig. 4.24 – WCLL 2017 analyses: breeding unit with 24 U-shaped tubes

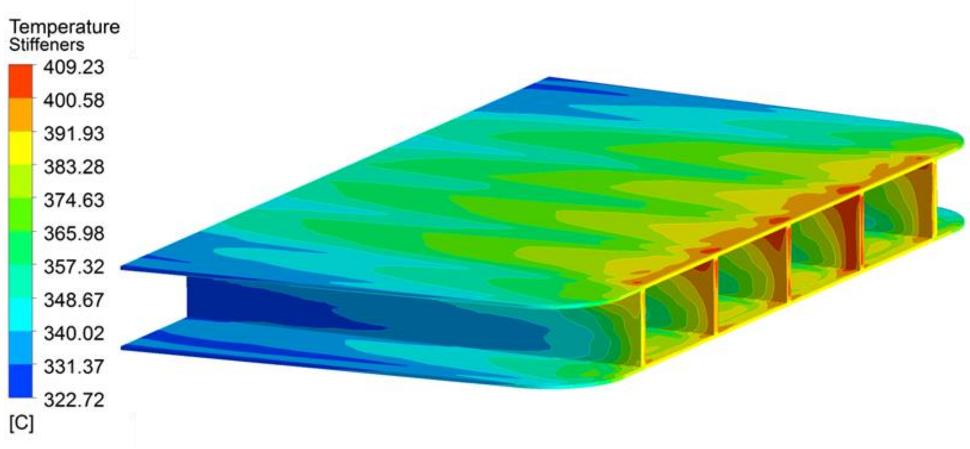

Fig. 4.25 – WCLL 2017 analyses, 24 U-shaped tubes: CFD stiffeners temperature.

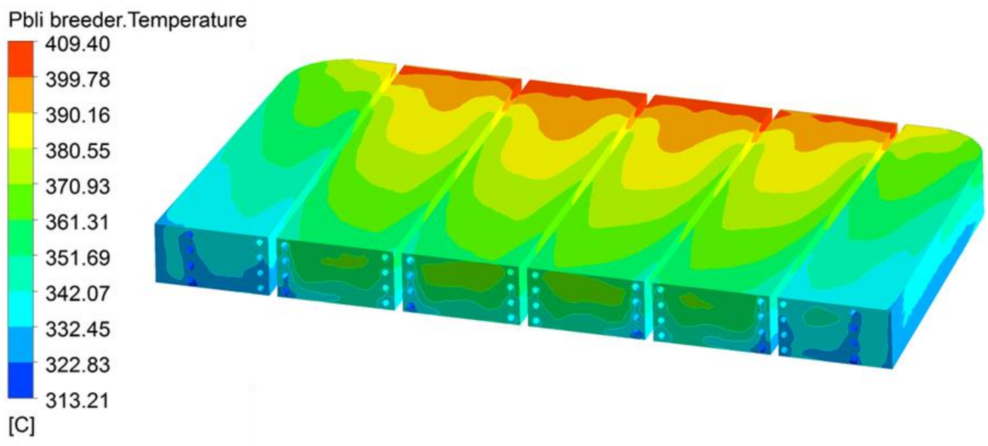

a) Isometric view of PbLi domain

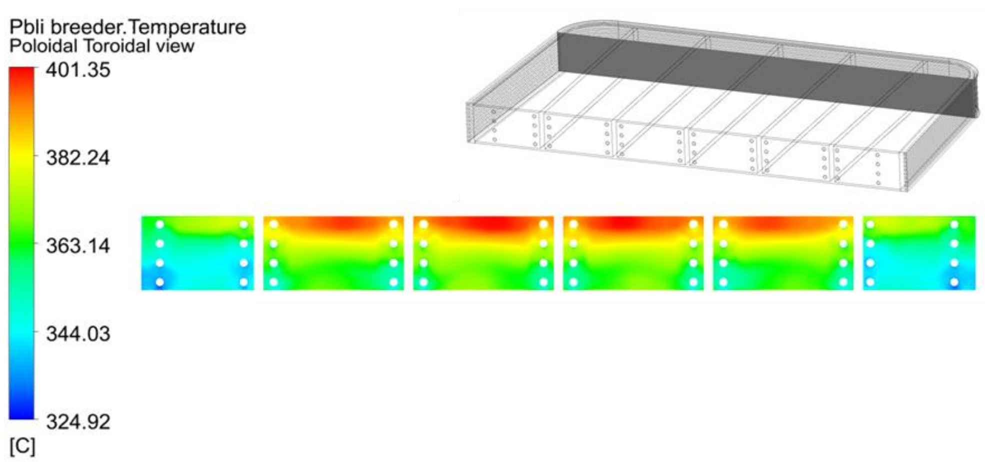

b) Poloidal-toroidal view of PbLi domain

Fig. 4.26 – WCLL 2017 analyses, 24 U-shaped tubes: CFD PbLi temperature.

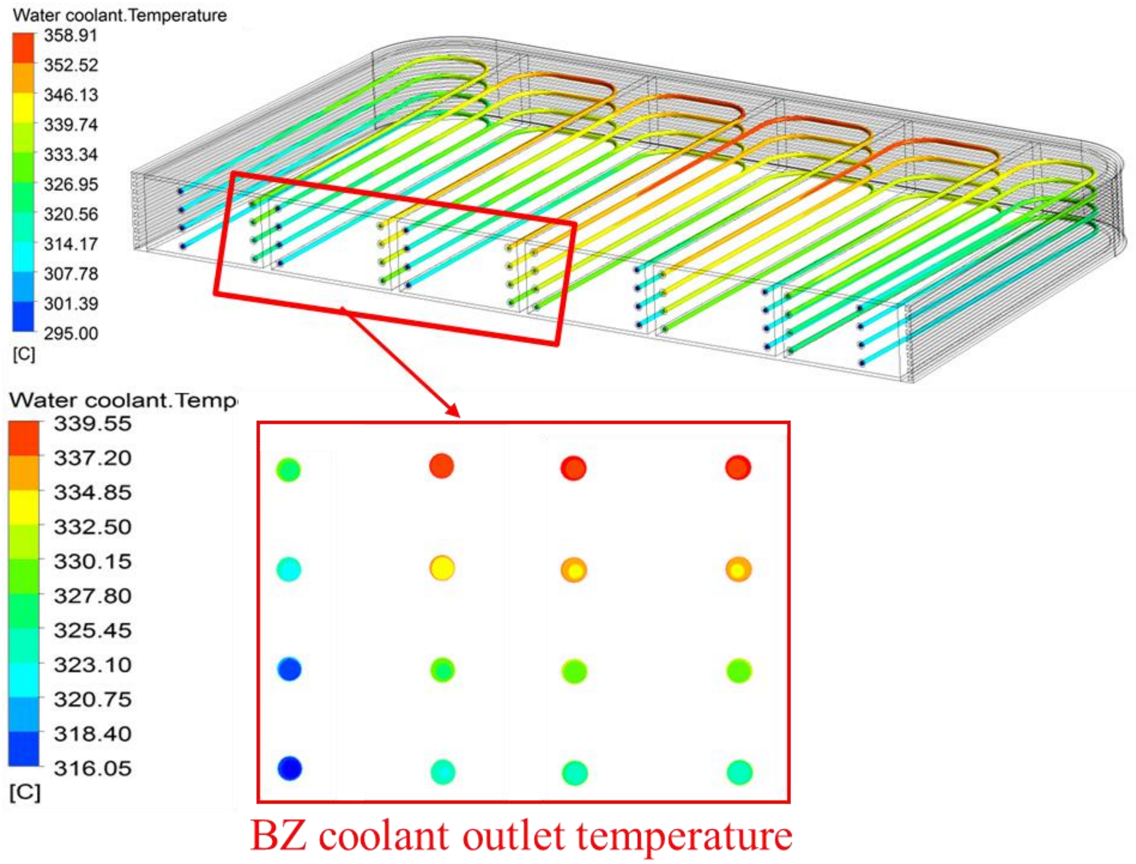

Fig. 4.27 – WCLL 2017 analyses, 24 U-shaped tubes: BZ tube-coolant interface temperature.

The BZ coolant system of Case 2 is characterized by 12 U-shaped tubes. A scheme of WCLL breeding unit is reported in Fig. 4.28. The analysis is carried out considering constant and equal mass flow rate in each BZ tube. Maintaining the symmetry with respect the poloidal-toroidal plane, the water is distributed and collected reducing the number of manifolds.

The CFD analyses demonstrates that toroidal symmetry is maintained, and the maximum temperature in PbLi and stiffeners is still below the limit. In particular, as shown in Fig. 4.29 and in Fig. 4.30, which present the thermal field of PbLi and stiffeners respectively, the maximum temperature is about 435 °C. The maximum and minimum temperatures of the other domains (fluid and solid) are summarized in Tab. 4.15.

Tab. 4.15 presents the main parameters of BZ and FW coolant systems. The average coolant outlet temperature is 327.6 °C in the FW and 328.9 °C in the BZ. The temperature distribution at BZ outlet presents, as in the previous case, a higher temperature in pipes at top, due to the constant mass flow rate.

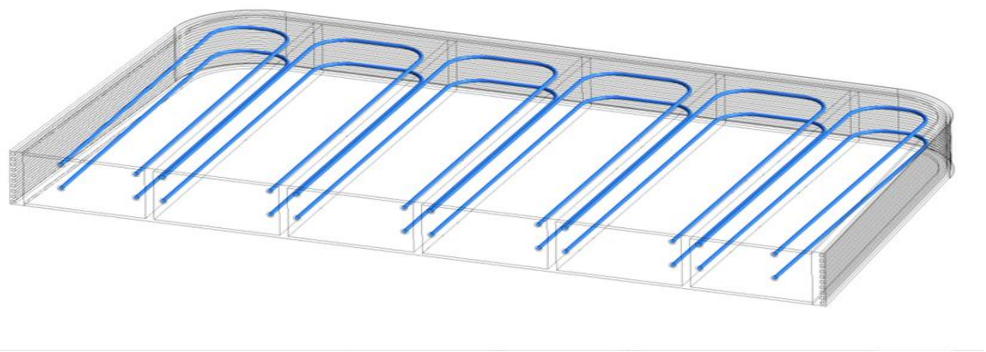

Fig. 4.28 – WCLL 2017 analyses: breeding unit with 12 U-shaped tubes.

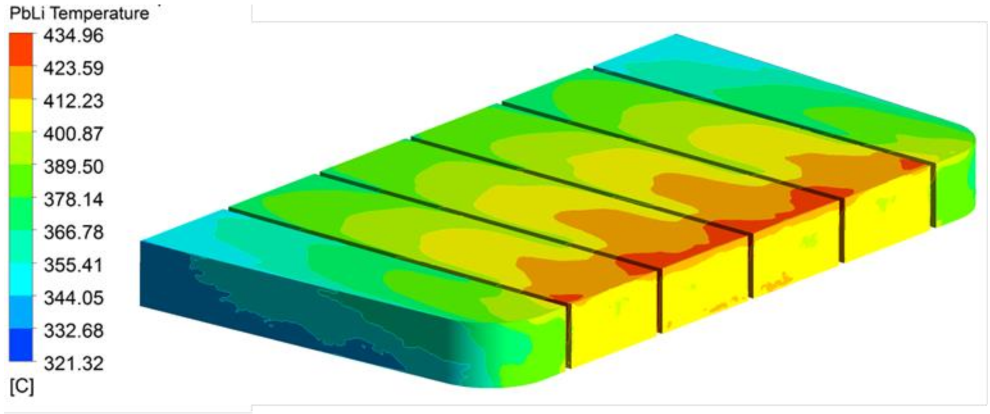

Fig. 4.29 – WCLL 2017 analyses, 12 U-shaped tubes: PbLi temperature.

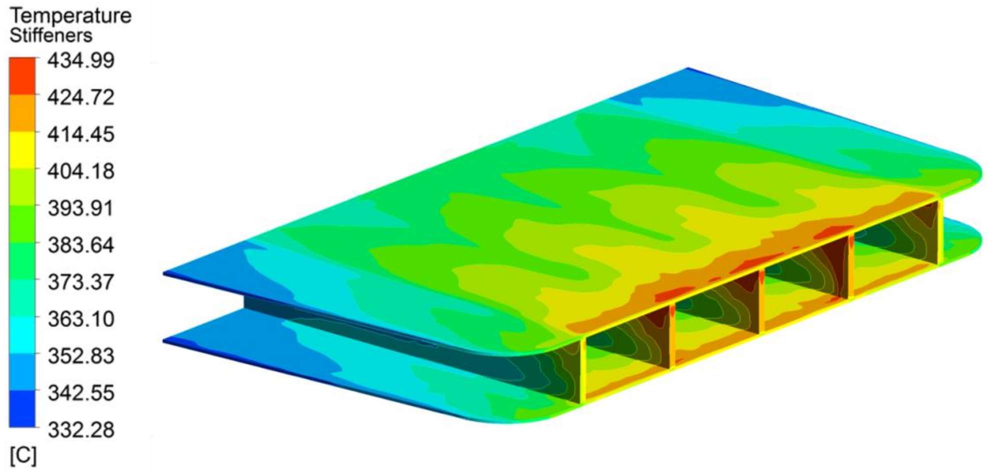

Fig. 4.30 – WCLL 2017 analyses, 12 U-shaped tubes: stiffeners temperature.

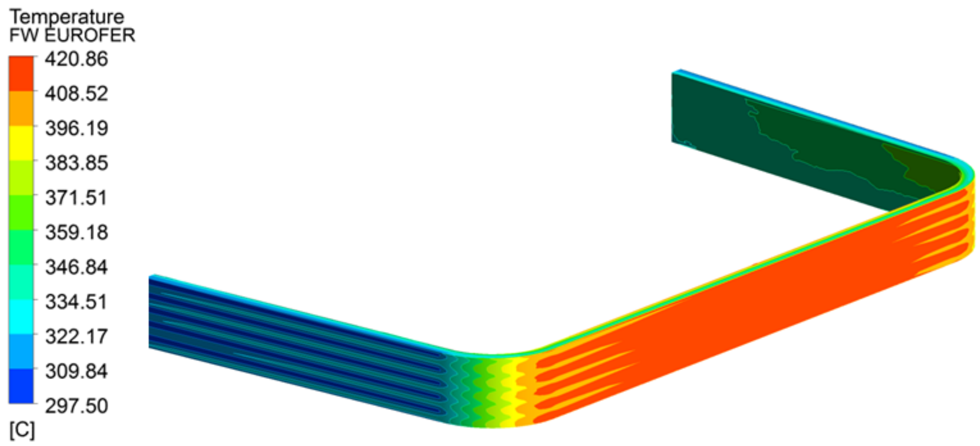

Fig. 4.31 – WCLL 2017 analyses, 12 U-shaped tubes: FW Eurofer temperature.

In Case 3, the BZ coolant system is characterized by 6 U-shaped tubes, as shown in Fig. 4.32. Considering the outcomes from previous analyses, the mass flow rate is calculated considering the effective power extracted by pipes in different toroidal channels. It is assumed in the side channels a mass flow rate equal to 0.238 kg/s and in the central channels of 0.773 kg/s. The BZ water is distributed assuming the same approach of Case 2. The main advantage of this configuration is the reduction of pipes in the breeding blanket, and thus of Eurofer.

The BZ outlet temperature has been homogenized, due to the balanced mass flow rate distribution, with an average value of 325.7 °C, and the difference between the maximum and minimum temperature of 1°C, as shown in Fig. 4.33, where the BZ thermal field, with a detail of outlet temperature is reported. Nevertheless, the BZ outlet temperature in this case is lower than the FW outlet temperature (332 °C), this is due to an increase of the power extracted by the FW systems. New iterations are needed to optimize mass flow rate between coolant systems. Tab. 4.17 summarizes the main coolant parameters of FW and BZ systems. It is noted that coolant performances are enhanced, being the BZ coolant velocity increased up to 5 m/s.

Th CFD analyses demonstrate that the coolant efficiency is ensured also with this configuration, as the stiffeners and PbLi temperature is well below the limit. In particular, as shown in Fig. 4.34 and Fig. 4.35, the maximum temperature is about 483 °C in PbLi and stiffeners domains, respectively. It is noted that the maximum temperature of FW Eurofer is increased up to 459 °C, and it is higher than the maximum temperature of Tungsten layer (427 °C), this is mainly due to the reduction of coolant in the BZ and to the PbLi thermal field, with local hot spot at the top pf breeding unit. This result is also confirmed by the temperature distribution of FW Eurofer domain in Fig. 4.36, which shows that the maximum temperature is reached in the inner side of the FW. The maximum and minimum temperature of all domains are summarized in Tab. 4.18.

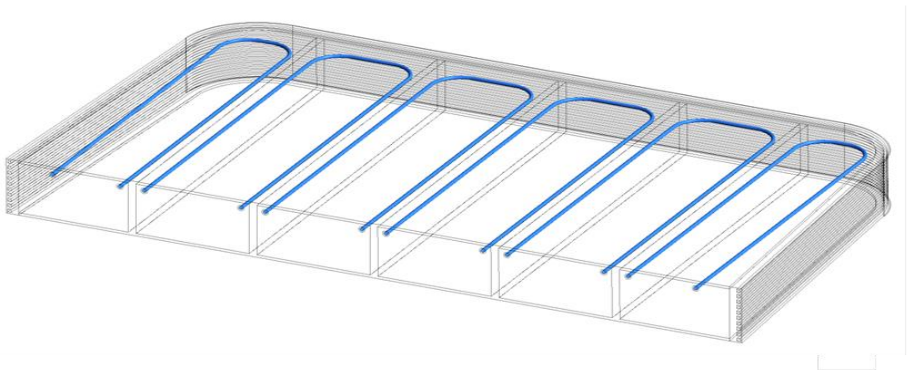

Fig. 4.32 – WCLL 2017 analyses: breeding unit with 6 U-shaped tubes.

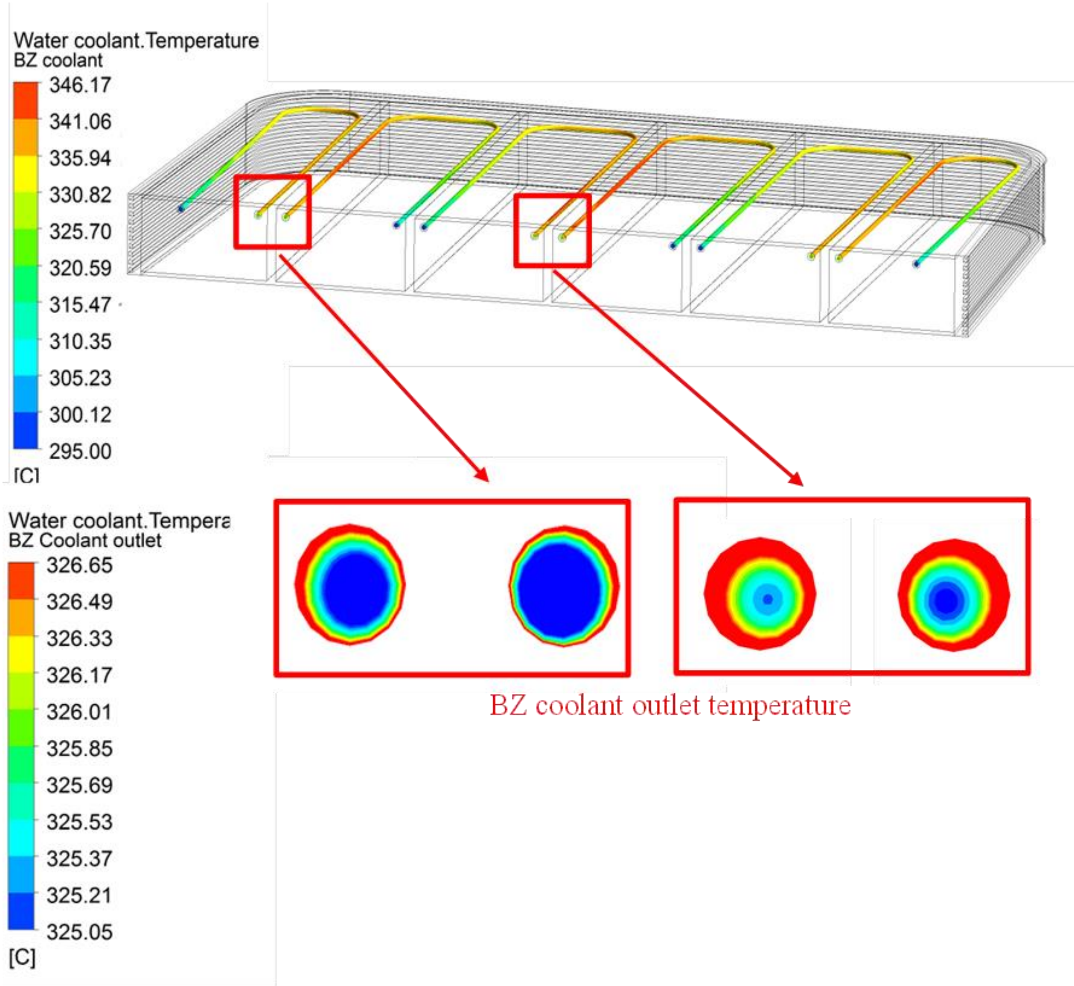

Fig. 4.33 – WCLL 2017 analyses, 6 U-shaped tubes: BZ coolant/tubes interface and coolant outlet temperature.

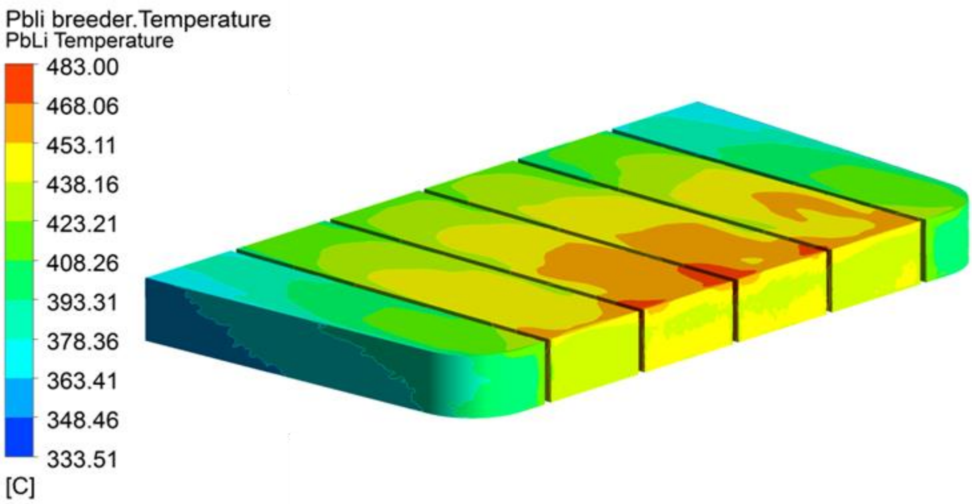

Fig. 4.34 – WCLL 2017 analyses 6 U-shaped tubes: PbLi temperature.

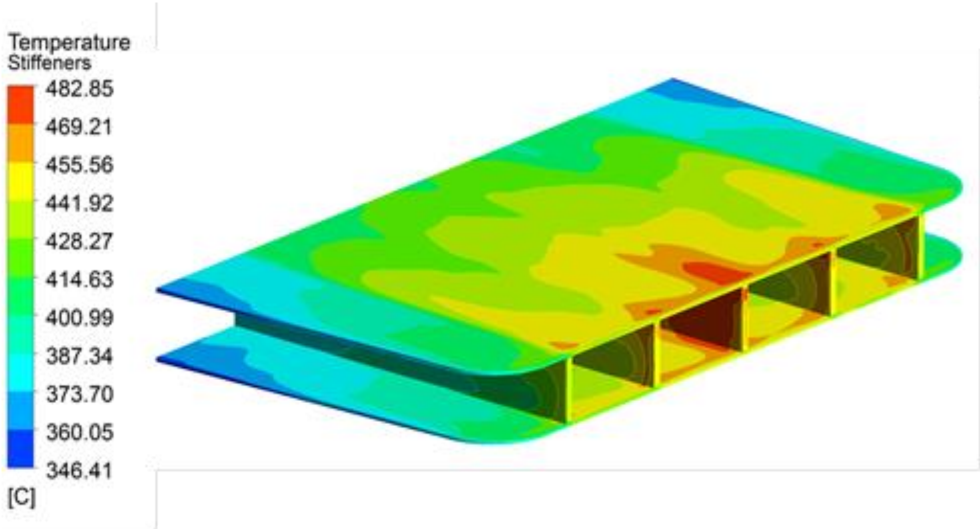

Fig. 4.35 – WCLL 2017 analyses, 6 U-shaped tubes: stiffeners temperature.

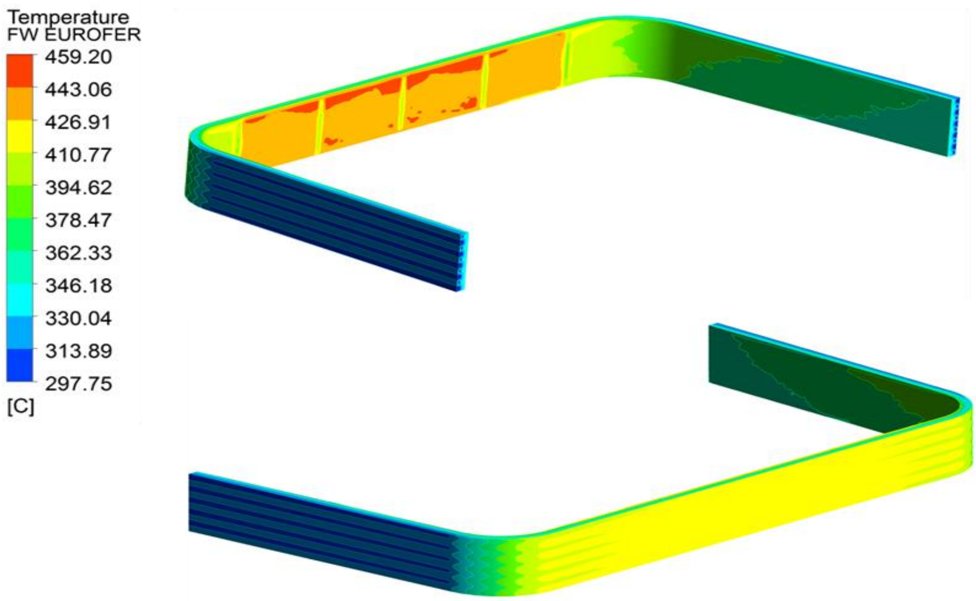

Fig. 4.36 – WCLL 2017 analyses, 6 U-shaped tubes: FW Eurofer temperature.

Taking into account the main outcomes from previous analyses, an advanced layout has been investigated, which foresees helical (HC) tubes. This configuration has the main advantage of reducing the overall number of pipes, ensuring the cooling in the first 15 cm near the FW, where there is the higher volumetric power density.

Sensitivity analyses have been performed, in particular two configurations have been investigated in detail, the first one foresees 12 HC tubes in the breeding unit, and the second 6 HC tubes, as illustrated in Fig. 4.37 and Fig. 4.38.

In the both cases the BZ mass flow rate is evaluated considering the toroidal distribution of power heating, and thus in the side channels the mass flow rate is 0.238 kg/s, and in the central channels is 0.773 kg/s. The water distributed maintaining symmetry with respect the poloidal-toroidal plane and minimizing the number of manifolds. In particular, there are three outlet manifolds and two inlet manifolds, which are integrated in the available space between the BP and the BSS.

The preliminary analyses demonstrate that temperature symmetry is ensured, nevertheless the outlet temperature is not homogenized. Fig. 4.39 shows the BZ coolant temperature at coolant/tubes interface and in detail the outlet temperature. It is noted that there is a difference of 5 °C between the top and the bottom outlets, this is due to two main reasons. The first is linked to the HC tubes position, as the top outlet corresponds to the HC tubes nearest the FW, which are affected by a higher power density. Thus, the evaluation of mass flow rate in BZ coolant tubes should consider the radial power density. The second cause is the PbLi thermal field: being PbLi isolated, it is driven only by buoyancies forces and thus hot regions are located at the top of the breeding unit. In Case 7, the BZ outlet temperature presents a more uniform distribution, with a difference of 1.5 °C between the maximum and the minimum value. It can be appreciated in Fig. 4.42, where the BZ coolant-tube interface temperature and a detail of the outlet temperature is reported.

Case 5 presents excellent cooling performances, with maximum temperature in PbLi domain of 401 °C, as shown in Fig. 4.40, and in stiffeners of 398.6 °C, as illustrated in Fig. 4.41. These results demonstrate that there is margin to further reduced the number of tubes. Indeed, considering Case 8, it is noted that maximum temperatures are well below the limit, and in particular in PbLi and stiffeners domains are 434.9 °C and 432.7 °C, respectively. The thermal field of PbLi and stiffens domains can be appreciated in Fig. 4.43 and in Fig. 4.44. The minimum and maximum temperatures of the overall domains are reported in Tab. 4.20 and in Tab. 4.21.

The FW outlet bulk temperature is 327.1°C for the Case 5 while in Case 8 is 328.8°C. The reduced number of tubes in Case 8, determines an increase of FW outlet temperature. As regard the BZ outlet bulk temperature, in Case 5 is 328.1 °C and in Case 8 is equal to

327.8 °C. It is noted (see Tab. 4.19 and Tab. 4.22) that BZ cooling performances are enhanced, being the water velocity increased from 2.6 m/s (Case 5) up to 5 m/s.

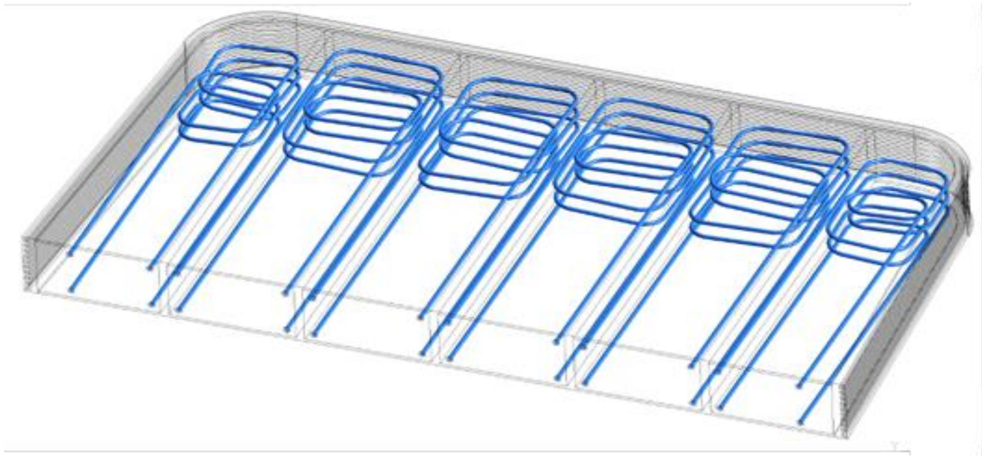

Fig. 4.37 – WCLL 2017 analyses: breeding unit with 12 HC tubes.

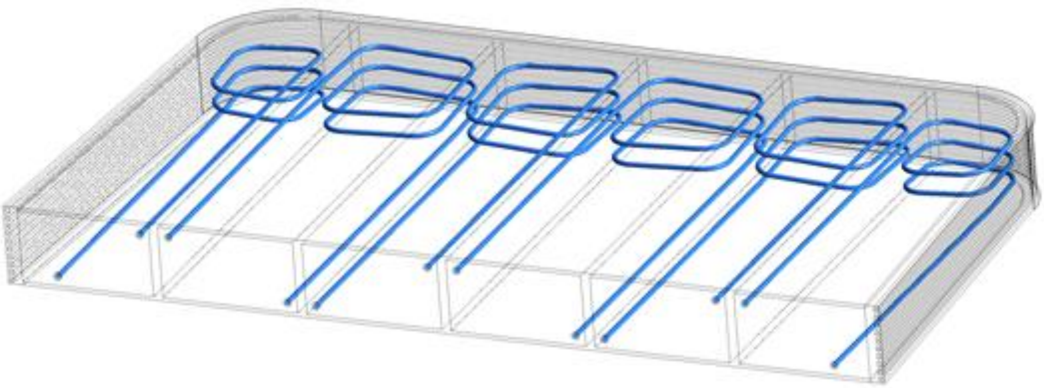

Fig. 4.38 – WCLL 2017 analyses: breeding unit with 6 HC tubes

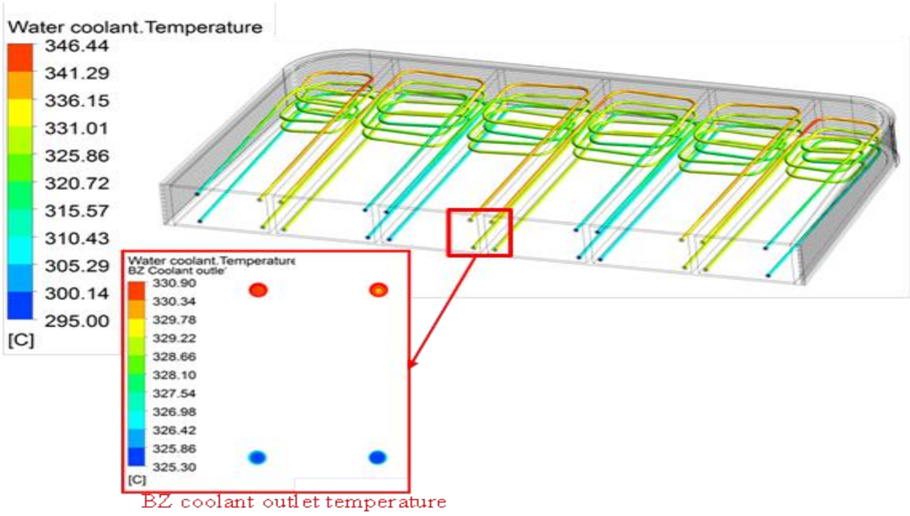

Fig. 4.39 – WCLL 2017 analyses, 12 HC tubes: BZ coolant/tubes temperature and in detail coolant temperature.

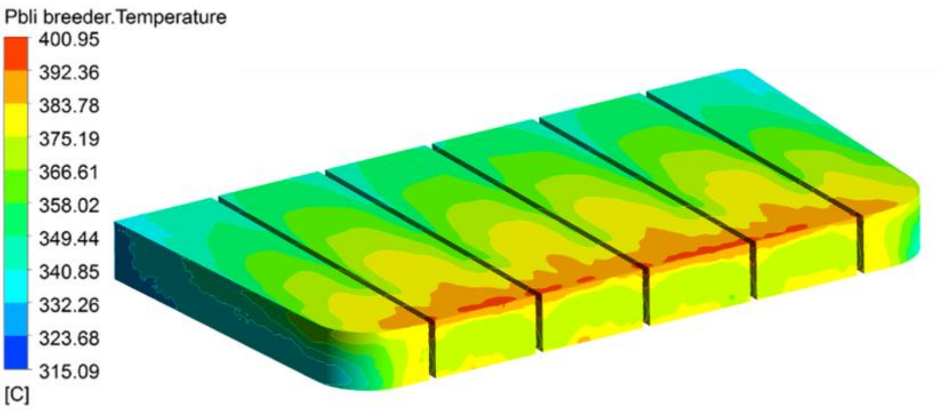

Fig. 4.40 – WCLL 2017 analyses, 12 HC tubes: PbLi temperature.

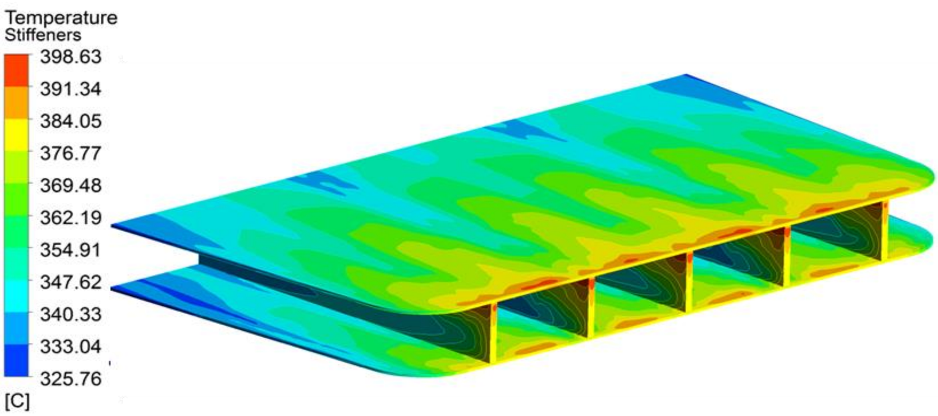

Fig. 4.41 – WCLL 2017 analyses, 12 HC tubes: stiffeners temperature.

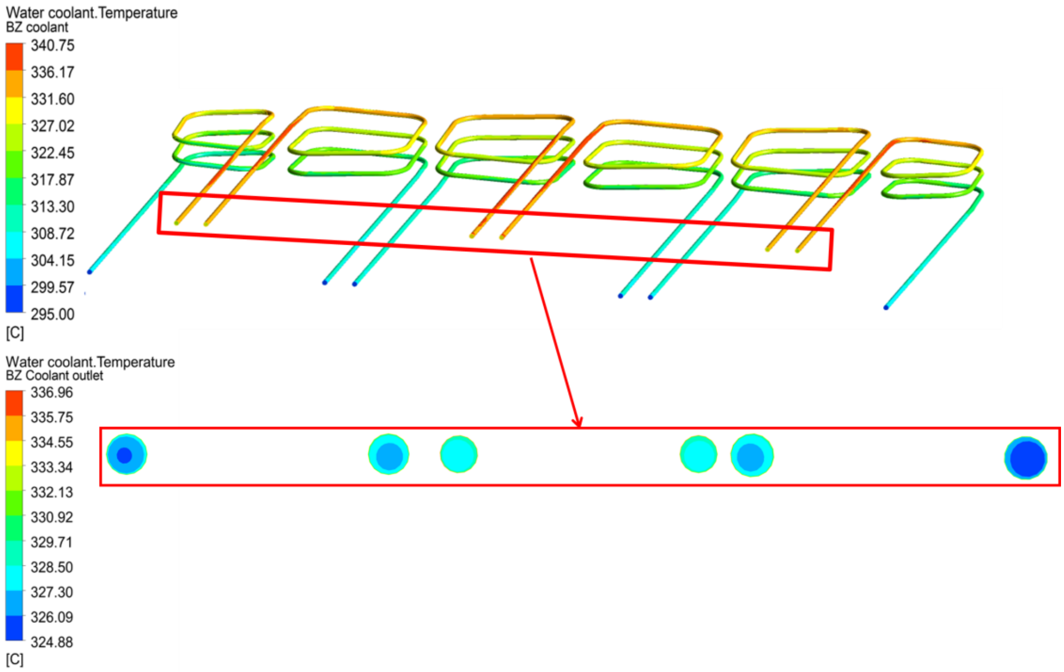

Fig. 4.42 – WCLL 2017 analyses, 6 HC tubes: BZ coolant/tubes temperature and in detail coolant temperature.

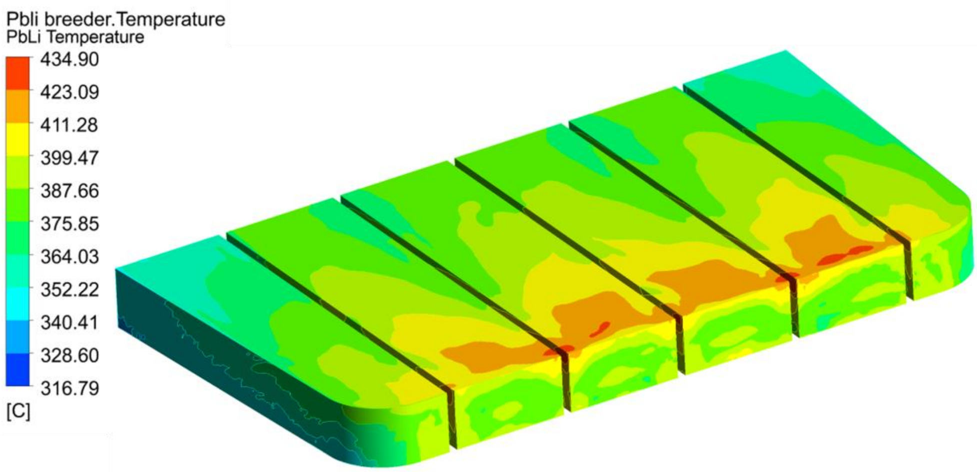

Fig. 4.43 – WCLL 2017 analyses, 6 HC tubes: PbLi temperature.

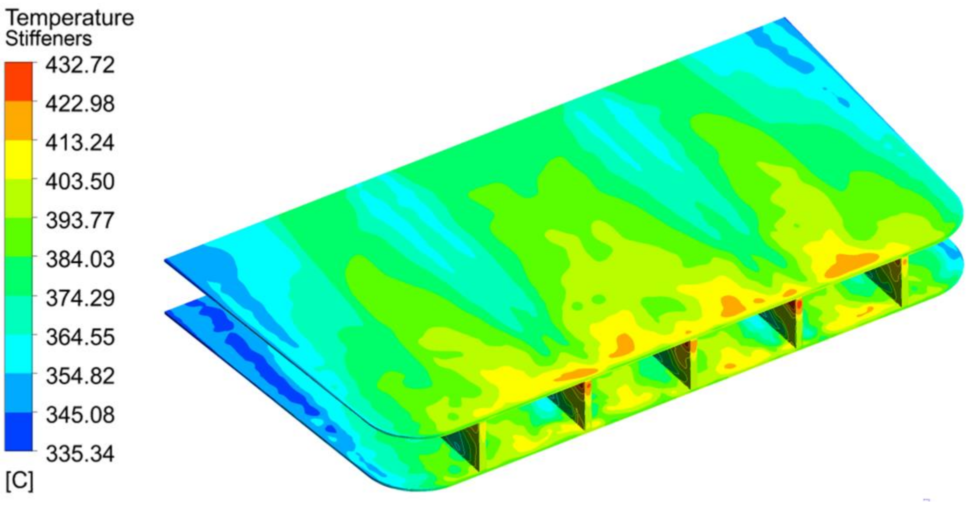

Fig. 4.44 – WCLL 2017 analyses, 6 HC tubes: stiffeners temperature.

The last configuration is characterized by wavy tubes. In the first simulation 24 tubes have been considered (Fig. 4.45), with constant mass flow rate in BZ and FW coolant systems. In the second case the number of tubes is reduced to 12 [47].

In Case 10, the BZ mass flow rate is evaluated on the basis of the effective power extracted by each tube, assuming a symmetric distribution in toroidal direction. The mass flow rates for each pipe of BZ systems are reported in Tab. 4.12.

#	**Mflow rate [kg/s]**	**T out [°C]**
1	0.0736	327.35
2	0.0548	324.75
3	0.1043	329.75
4	0.0817	327.55
5	0.1071	329.85
6	0.0840	327.75
7	0.1071	329.85
8	0.0840	327.75
9	0.1043	329.85
10	0.0817	327.65
11	0.0736	327.45
12	0.0548	324.85

Tab. 4.12 – WCLL 2017 analyses, 12 wavy tubes: BZ mass flow rates.

The results show that, thanks to the new BZ water coolant path, the thermal field is symmetric (Fig. 4.47 and Fig. 4.48) in both cases (Case 9 and Case 10). In particular, due to the mass flow rate optimization performed in Case 10, the temperature field in this configuration is more uniform than Case 9.

The maximum temperature reached in the PbLi is 403.5°C and 414.2°C for Case 9 and Case 10 respectively (Fig. 4.47 and Fig. 4.50). The same behavior can be appreciated in the stiffeners with a maximum temperature of 402.9°C and 415.1°C for the above cited cases (Fig. 4.48 and Fig. 4.51). The absolute maximum temperature achieved is in the FW where the heat flux of 0.5 MW/m^2. In both cases investigated, the maximum temperature limit (550°C) is respected. The maximum and minimum temperatures of the all domains, for Case 9 and Case 10, are reported in Tab. 4.23 and Tab. 4.24, respectively.

The FW outlet bulk temperature is 326.75°C for the Case 9 while in the optimized Case 10 is 328.15°C. Considering that the mass flow rate in the FW channel is the same in Case 9 and 10, the bulk outlet difference is due to a more efficient distribution of the power extraction between the FW and the BZ in the Case 10 that allows an outlet temperature equal to the desired one (328°C).

It is important to note also that, although the BZ outlet temperature is practically the same for the Case 9 and 10 (327.9°C), the difference between the minimum and maximum temperatures at the BZ channel outlet is greater in the Case 9 (16.62°C) than in the Case 10 (10.38°C). This means that, in the BZ, the temperature distribution between the channels is more uniform. Moreover, due to the smaller number of tubes in the BZ for the Case 10, the pressure drop is about for times the one of the Case 9 (0.0214 MPa and 0.0054 MPa, respectively).

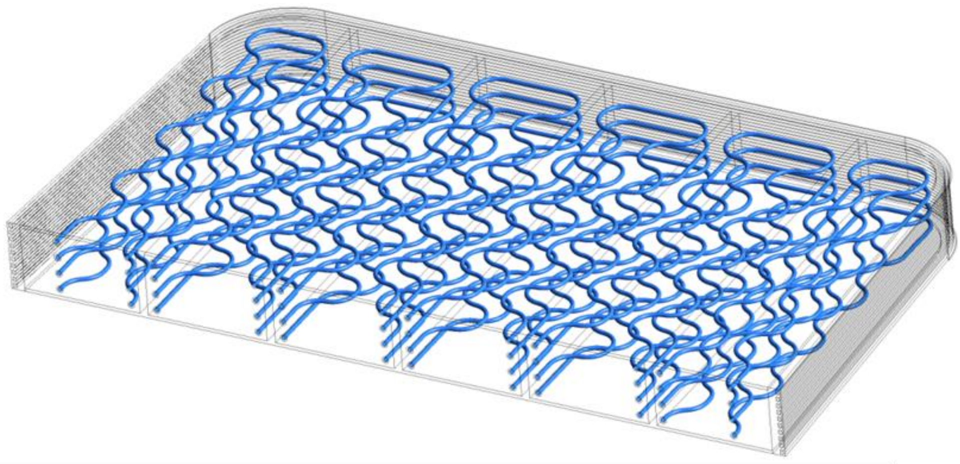

Fig. 4.45 – WCCL 2017 CFD analyses: breeding unit with 24 wavy tubes.

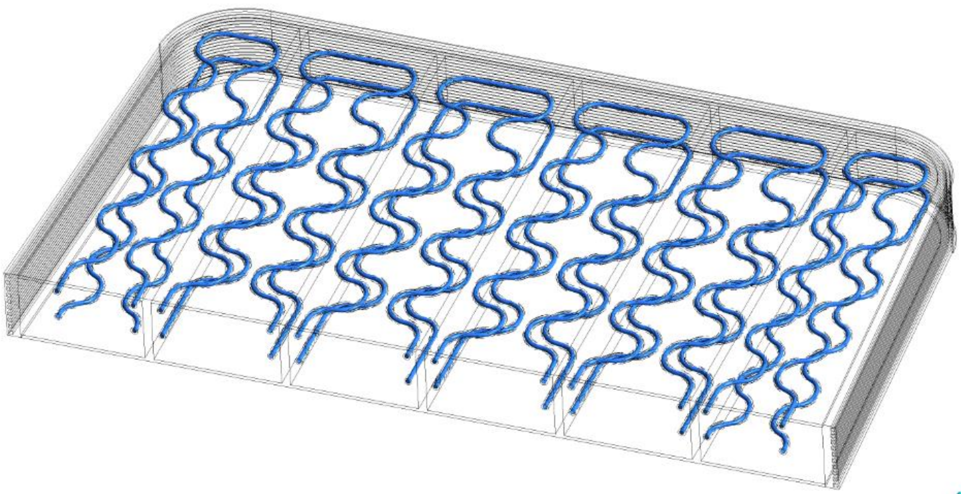

Fig. 4.46 – WCCL 2017 design 12 wavy tubes

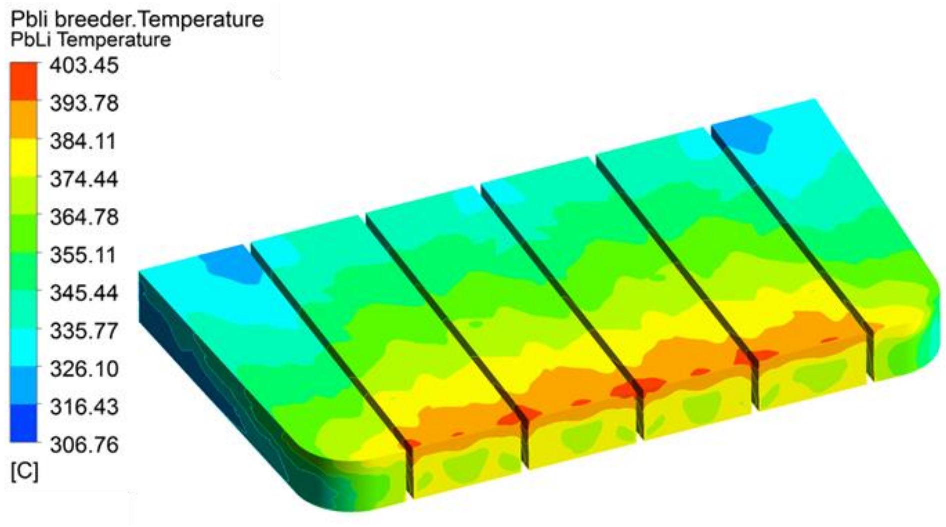

Fig. 4.47 – WCCL 2017 CFD analyses, 24 wavy tubes, PbLi temperature.

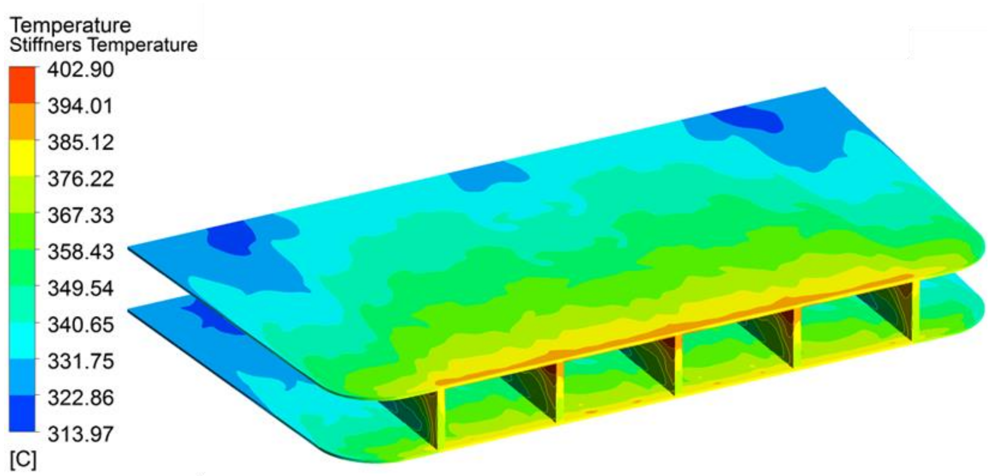

Fig. 4.48 – WCCL 2017 CFD analyses, 24 wavy tubes, stiffeners temperature.

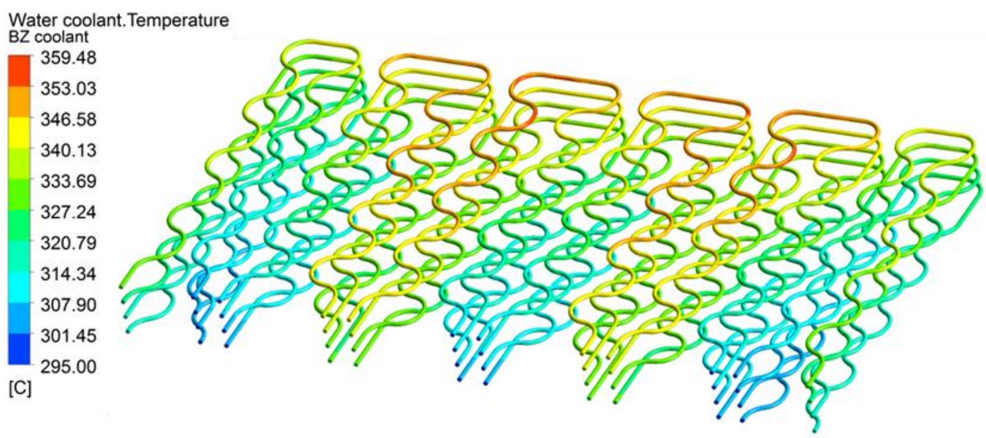

Fig. 4.49 – WCCL 2017 CFD analyses, 24 wavy tubes, BZ coolant temperature.

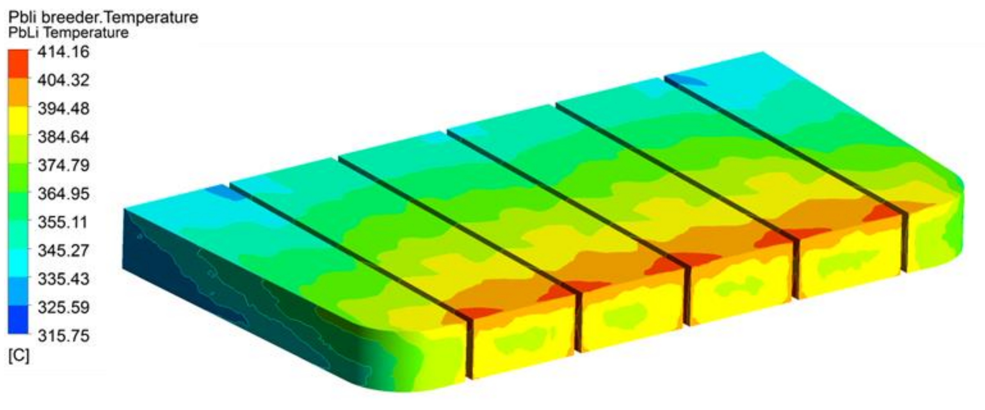

Fig. 4.50 – WCCL 2017 CFD analyses, 12 wavy tubes, PbLi temperature.

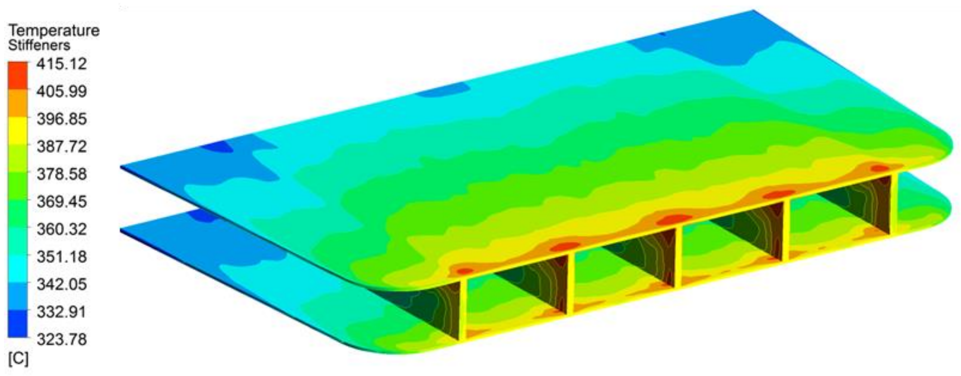

Fig. 4.51 – WCCL 2017 CFD analyses, 12 wavy tubes, stiffeners temperature.

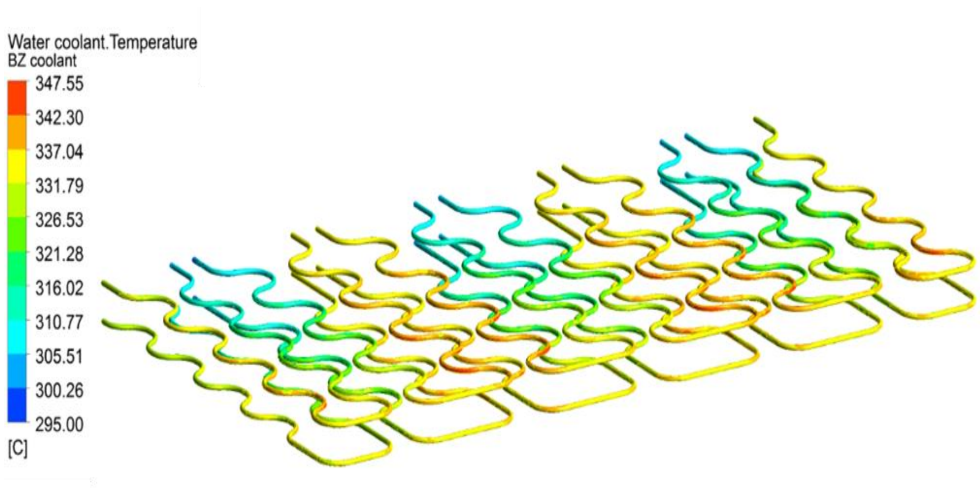

Fig. 4.52 – WCCL 2017 CFD analyses, 12 wavy tubes, BZ coolant temperature.

#	Description	Unit	BZ	FW
1	T in	*°C*	295.0	295.0
2	T out (avg)	*°C*	328.2	327.2
3	T out min	*°C*	316.1	327.8
4	T out max	*°C*	339.6	326.6
5	V (avg)	*m/s*	1.32	2.41

Tab. 4.13 – WCLL 2017 analyses, 24 U-shaped tubes: BZ and FW coolant temperature.

#	Description	T min [°C]	T max [°C]
1	PbLi	313.85	409.45
2	Eurofer structures	322.75	409.25
3	FW Eurofer	297.45	417.39
4	Tungsten	315.85	424.95
5	BZ coolant	294.95	341.85
6	FW coolant	294.95	342.95

Tab. 4.14 – WCLL 2017 analyses, 24 U-shaped tubes: maximum and minimum temperature in solid and fluid domains.

#	Description	Unit	BZ	FW
1	T in	*°C*	295.0	295.0
2	T out (avg)	*°C*	327.6	328.9
3	T out min	*°C*	316.9	328.5
4	T out max	*°C*	334.8	329.1
5	V (avg)	*m/s*	2.62	2.43

Tab. 4.15 –WCLL 2017 analyses, 12 U-shaped tubes: Temperature in BZ and FW systems in Case 2.

#	Description	T min [°C]	T max [°C]
1	PbLi	322.65	434.95
2	Eurofer structures	334.65	434.99
3	FW Eurofer	297.50	420.86
4	Tungsten	316.35	423.95
5	BZ coolant	294.95	338.15
6	FW coolant	294.95	344.05

Tab. 4.16 – WCLL 2017 analyses, 12 U-shaped tubes: temperature in solid and fluid domains.

#	Description	Unit	BZ	FW
1	T in	*°C*	295.0	295.0
2	T out (avg)	*°C*	325.7	331.7
3	T out min	*°C*	325.0	331.5
4	T out max	*°C*	326.6	332.0
5	V (avg)	*m/s*	5.19	2.46

Tab. 4.17 – WCLL 2017 analyses, 6 U-shaped tubes: BZ and FW coolant temperature.

#	Description	T min [°C]	T max [°C]
1	PbLi	335.55	483.05
2	Eurofer structures	350.15	482.85
3	FW Eurofer	297.75	459.20
4	Tungsten	317.85	426.85
5	BZ coolant	294.95	330.35
6	FW coolant	294.95	345.95

Tab. 4.18 – WCLL 2017 analyses, 6 U-shaped tubes: temperature in solid and fluid domains.

#	Description	Unit	BZ	FW
1	T in	*°C*	295.0	295.0
2	T out (avg)	*°C*	328.1	327.1
3	T out min	*°C*	325.3	326.6
4	T out max	*°C*	330.9	327.7
5	V (avg)	*m/s*	2.63	2.41

Tab. 4.19 – WCLL 2017 analyses, 12 HC tubes: temperature in BZ and FW systems.

#	Description	T min [°C]	T max [°C]
1	PbLi	316.05	400.95
2	Eurofer structures	327.45	398.65
3	FW Eurofer	297.05	415.65
4	Tungsten	314.85	424.85
5	BZ coolant	294.95	332.55
6	FW coolant	294.95	343.35

Tab. 4.20 – WCLL 2017 analyses, 12 HC tubes: temperature in solid and fluid domains.

#	Description	Unit	BZ	FW
1	T in	*°C*	295.0	295.0
2	T out (avg)	*°C*	327.8	328.8
3	T out min	*°C*	325.5	328.2
4	T out max	*°C*	330.8	329.5
5	V (avg)	*m/s*	5.24	2.43

Tab. 4.21 – WCLL 2017 analyses, 6 HC tubes: temperature in BZ and FW systems.

#	Description	T min [°C]	T max [°C]
1	PbLi	317.65	434.95
2	Eurofer structures	335.45	432.65
3	FW Eurofer	413.55	416.75
4	Tungsten	315.65	425.95
5	BZ coolant	294.95	330.25
6	FW coolant	294.95	344.35

Tab. 4.22 – WCLL 2017 analyses, 6 HC tubes: temperature solid and fluid domains.

#	Description	T min [°C]	T max [°C]
1	PbLi	309.95	402.05
2	Eurofer structures	314.05	402.95
3	FW Eurofer	297.45	413.95
4	Tungsten	316.75	423.95
5	BZ coolant	294.95	342.45
6	FW coolant	294.95	344.15

Tab. 4.23 – WCLL 2017 analyses, 24 wavy tubes: temperature of solid and fluid domains.

#	Description	T min [°C]	T max [°C]
1	PbLi	315.75	414.16
2	Eurofer structures	323.95	415.15
3	FW Eurofer	297.55	414.45
4	Tungsten	317.45	424.55
5	BZ coolant	294.95	331.45
6	FW coolant	294.95	344.75

Tab. 4.24 – WCLL 2017 analyses, 12 wavy tubes: temperature of solid and fluid domains.

4.3.4 **Main achievements**

The CFD analyses performed in 2017 have the main objectives of enhancing cooling performances, simplifying the design and reducing the overall length of tubes. Several BZ coolant systems layout have been investigated.

The main outcomes from the analyses are:

- The configuration with twelve U shaped tubes is the simplest solution, with reduced overall tube lengths and cooling performances improved. Further analyses are needed to optimize mass flow rate distribution between FW and BZ systems
- The configuration with six HC tubes is the most promising solution. The main advantage of this configuration is that the overall length of pipes is reduced with respect previous design preserving the cooling of BZ region near the FW where the volumetric power density is higher. The BZ coolant velocity is increased up to 5 m/s, and thus the HTC maximized, minimizing tube surface.
- The analyses have been performed with conservative assumptions, as the PbLi is assumed isolated and static. Indeed, the hot spots visible at the edges between the horizontal and vertical stiffening plates are due to the missing representation of the holes in the CFD model. The design of the opening dimension is currently under investigation and this feature will be considered in the next analyses.
- Two design solutions are under development which are based on the outcomes from CFD analyses. In particular, the first solution preserves the internal structures of WCLL 2016 design and considers the HC tubes for the BZ coolant systems. Analyses are ongoing to evaluate the holes dimensions in radial-toroidal stiffening plates. In particular, CFD analyses should verify Pbli flow path in the breeding unit. An alternative solution, foresees the PbLi flowing in polidal direction in channels made by radial-poloidal and poloidal–toroidal stiffeners. In this case, U-shaped tubes will be considered.
- Design choices should be confirmed by MHD analyses. In particular, feedbacks are needed to evaluate which is the influence of MHD issues and thus which is the effective thermal field in the BZ.

4.4 Thermal analyses of Back Supporting Structure

A preliminary thermal analysis of the outboard and inboard segment Back Supporting Structure (BSS) is carried out to investigate thermal behavior of BSS without cooling. Considering the outboard segment, sensitivity analyses were performed to investigate thermal field when applied different boundary conditions. As regard the inboard segment, sensitivity analyses are carried out to identify a cooling system capable of maintaining the temperature below the limit (550 °C).

The following assumptions are considered:

- Opaque body: the phenomenon affects only the surface and not the volume
- Gray surface: the spectral absorptivity and the emissivity are independent of wavelength
- Diffuse surface: intensity independent from direction
- Convective heat transfer neglected

All simulations are performed adopting as boundary conditions the heat exchange in a blackbody cavity, with back temperature, front Vacuum Vessel (VV), of 200 °C, and front temperature, front BB of 300 °C. The emissivity is assumed equal to 0.4. A radial-poloidal volumetric power density is applied to inboard and outboard segments. The poloidal volumetric power density is obtained scaling the radial volumetric power density obtained by neutronics analyses with neutron wall loads [30].

Several CFD calculations are performed to investigate the thermal behavior under different boundary conditions. The list of calculations is summarized in Tab. 4.25 and Tab. 4.26, for outboard and inboard segment, respectively.

#	ID	DESCRIPTION
1	2016_11_16_outboard_r01	Geom. Outboard BSS BP radiation heat transfer at T = 300 °C VV radiation heat transfer at T = 200 °C Radial and poloidal volumetric heat power density
2	2016_11_16_outboard_r02	Geom. Outboard BSS BP radiation heat transfer at T = 300 °C VV radiation heat transfer at T = 200 °C +100% of volumetric heat power density
3	2016_11_16_outboard_r03	Geom. Outboard BSS BP radiation heat transfer at T = 300 °C VV radiation heat transfer at T = 200 °C Constant maximum volume power density (24452 W/m3)

Tab. 4.25 – CFD sensitivity analyses of outboard segment BSS.

#	ID	DESCRIPTION
1	2016_11_16_inboard_r0	Geom. BSS Inboard BP radiation heat transfer at T = 300 °C VV radiation heat transfer at T = 200 °C Radial and poloidal volumetric heat power density
2	2016_11_16_inboard_r01	Geom. BSS Inboard BP radiation heat transfer at T = 300 °C VV radiation heat transfer at T = 200 °C Radial and poloidal volumetric heat power density 1 cooling channel on BSS
3	2016_11_16_inboard_r02	Geom. BSS Inboard BP radiation heat transfer at T = 300 °C VV radiation heat transfer at T = 200 °C Radial and poloidal volumetric heat power density 7 cooling channels on BSS
4	2016_11_16_inboard_r03	Geom. BSS Inboard BP radiation heat transfer at T = 300 °C VV radiation heat transfer at T = 200 °C Radial and poloidal volumetric heat power density 9 cooling channels on BSS
5	2016_11_16_inboard_r04	Geom. BSS Inboard BP radiation heat transfer at T = 300 °C VV radiation heat transfer at T = 200 °C Radial and poloidal volumetric heat power density Constant temperature on front surface (T=300 °C)
6	2016_11_16_inboard_r05	Geom. BSS Inboard BP radiation heat transfer at T = 300 °C VV radiation heat transfer at T = 200 °C Radial and poloidal volumetric heat power density Constant temperature on front surface (T=330 °C)

Tab. 4.26 – CFD sensitivity analyses of inboard segment BSS.

A preliminary thermal analysis of outboard segment BSS is performed to evaluate the thermal field under normal operation. The geometry model of outboard BSS is shown in Fig. 4.53. The BSS is divided in 7 sections in poloidal direction and in 4 sections in radial direction (indicated with letter from A to D), to assign a radial-poloidal distribution of the volumetric power density (see Tab. 4.27).

The results of the reference case (Case 0), demonstrate that, in normal operation, the outboard segment presents a good thermal distribution without cooling, as the maximum temperature is 305.92 °C, reached in the internal volume, where the thickness is greater (Fig. 4.54). The back surface (VV direction) maintains the temperature well below 300 °C.

Two sensitivity analyses were performed, to evaluate the thermal behavior of the BSS when applied a greater volumetric power density. In Case 1 the volumetric power density is incremented of 100 %. The maximum temperature reached in this case is 320.78 °C, as shown in Fig. 4.55. In Case 2 a constant volumetric power density, equal to the maximum valued (24452 MW/m3) is applied to all sectors. The results demonstrate that there is an increase of BSS temperature, but the maximum value is 334.40 °C and it is still below the limit (550 °C). The main difference with respect the previous cases is that the hot regions have moved close the back surface, as shown in Fig. 4.56.

	NWL [MW/m^2]	A [W/m^3]	B [W/ m^3]	C [W/ m^3]	D [W/ m^3]
OB1	0.8	14598	5104	2171	1152
OB2	1.17	21350	7464	3176	1686
OB3	1.34	24452	8549	3637	1930
OB4	1.33	24270	8485	3610	1916
OB5	1.24	22628	7911	3366	1786
OB6	1.12	20438	7145	3040	1613
OB7	1.01	18431	6443	2741	1455

Tab. 4.27 – Outboard segment BSS volumetric power density.

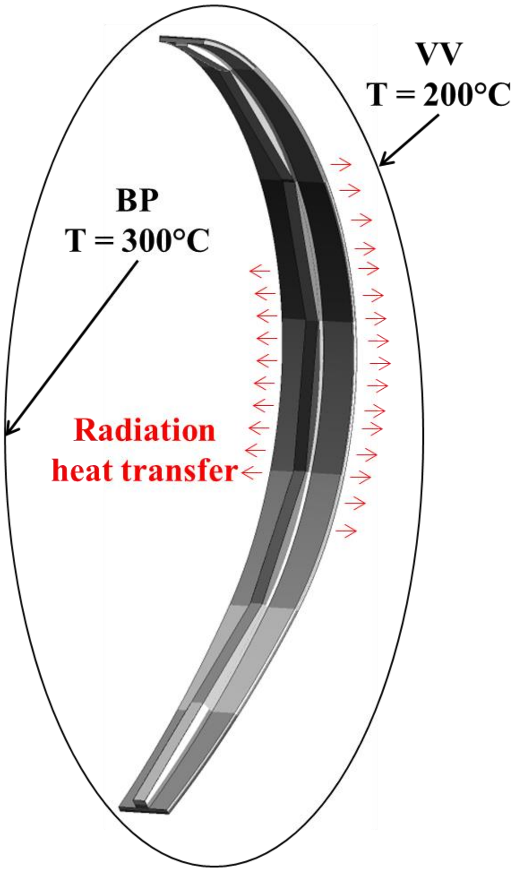

a) Outboard segment

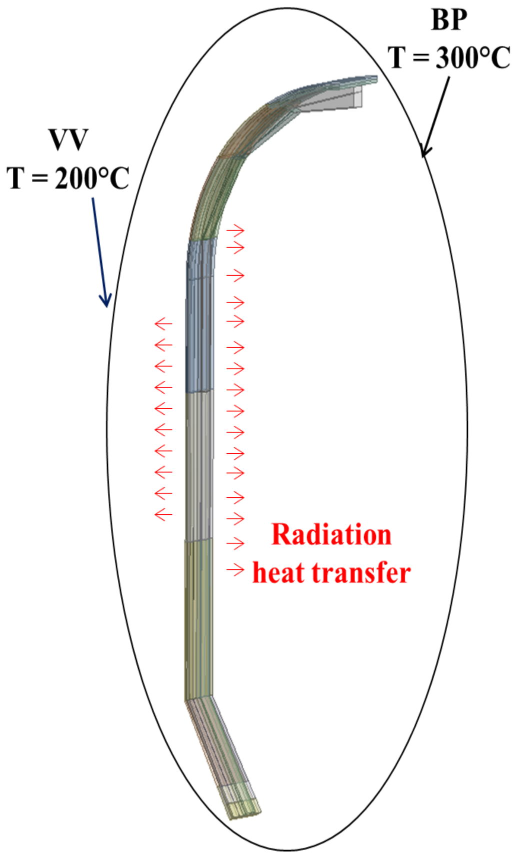

b) Inboard segment

Fig. 4.53 –WCLL BB, BSS geometry model.

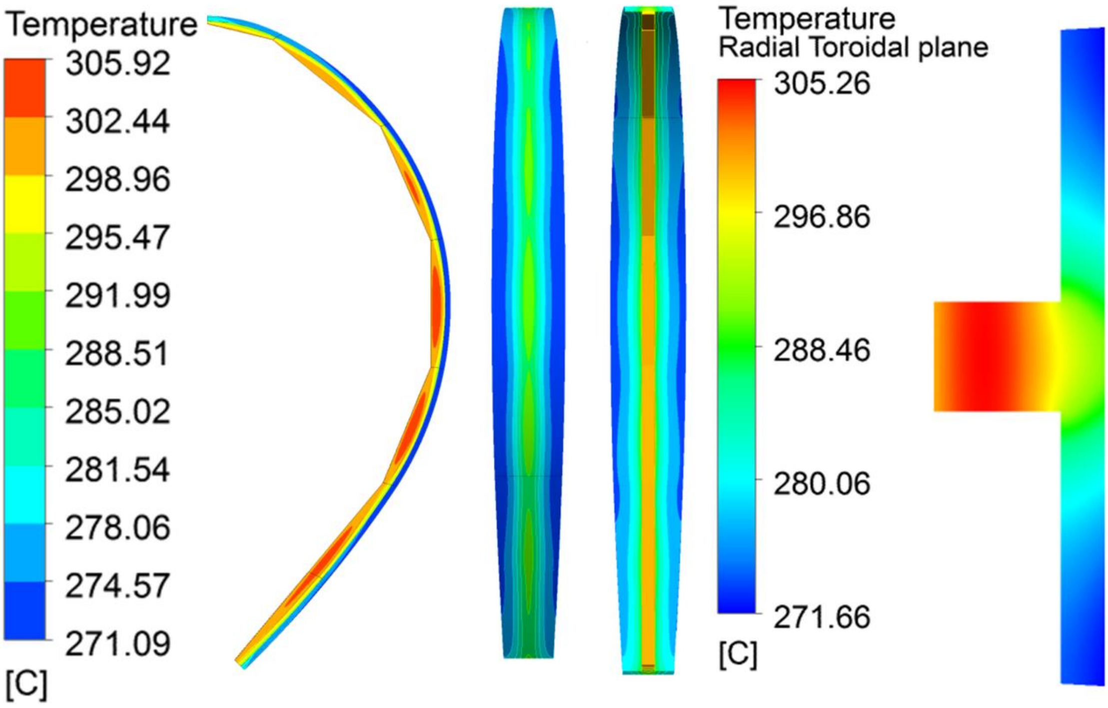

a) Side, back and front view *b) RT view at mid plane*

Fig. 4.54 – CFX temperature of outboard BSS: Case 0.

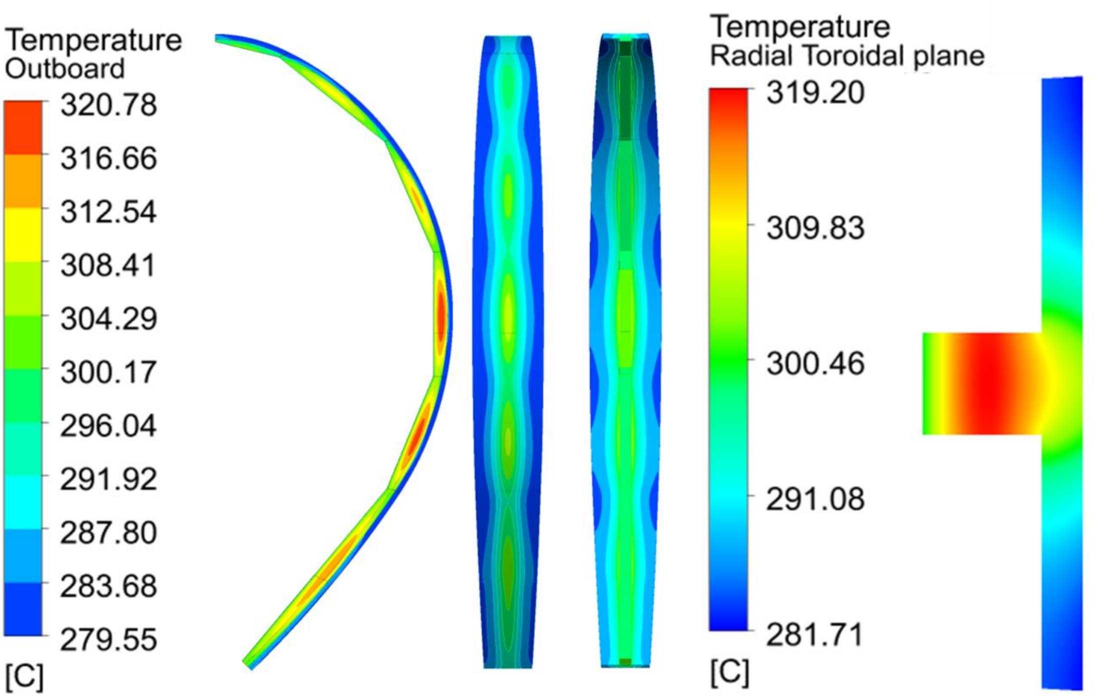

a) Side, back and front view *b) RT view at mid plane*

Fig. 4.55 – CFX temperature of outboard BSS: Case 1.

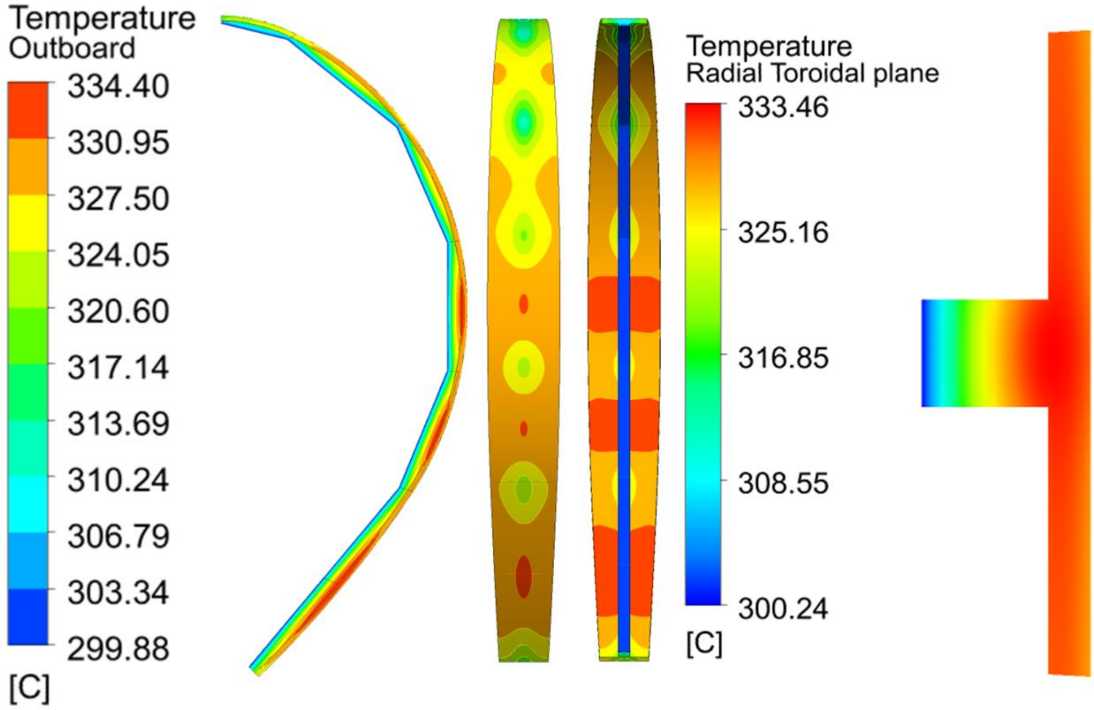

a) Side, back and front view *b) RT view at top plane*

Fig. 4.56 – CFX temperature of outboard BSS: Case 2.

The inboard segment BSS is divided in 7 sections in poloidal direction and in 3 sections in radial direction (indicated with letter from A to D), to assign the radial-poloidal volumetric power density reported in Tab. 4.28.

	NWL [MW/m^2]	A [W/m^3]	B [W/m^3]	C [W/m^3]
IB1	0.64	137833	103040	74589
IB2	0.75	161523	120750	87409
IB3	1.1	236900	177100	128200
IB4	1.07	230439	172270	124704
IB5	0.8	172291	128800	93236
IB6	0.82	176598	132020	95567
IB7	0.9	193827	144900	104891

Tab. 4.28 – Inboard segment BSS volumetric power density.

The first preliminary analysis is performed to evaluate the thermal field of the BSS. The results show that the inboard BSS temperature is higher than outboard segment, due to the greater volumetric power density. The maximum temperature is 512.20 °C (see Fig. 4.57), which is slightly lower than the limit value (550 °C), thus the BSS has to be cooled.

Starting from the results of the results of the preliminary analysis, a set of sensitivity analysis is performed to investigate cooling solutions. First, the geometry is modified making one slots on BSS back wall where an Heat Transfer Coefficient (HTC) of 25000 W/m^{2}K is applied to simulate the heat exchange with water at 285 °C and 15.5 MPa. The HTC used is an approximate but conservative value. The objective of the analysis is to evaluate the area of influence of the cooling channel. The results demonstrate that the influence of one channel is limited, as shown in Fig. 4.58.

In Case 2, 5 channels on the back and 2 on the front face of the BSS are made, whit the same boundary conditions of previous case. In this simulation the maximum temperature is reduced to 473 °C, as the influence of HTC is reduced in the central thickness.
Finally, in Case 3, 9 channels are made, two of them on the lateral surface of the central thickness. The temperature results of the calculation are shown in Fig. 4.60. The maximum temperature is 424.97 °C: the coolant channels do not affect the central thickness.

In Case 4 and Case 5 a different cooling solution is investigated: it is assumed that whole front surface is cooled with water, maintaining the temperature at 300 °C and 330 °C, respectively. The results of simulations are reported in Fig. 4.61. The maximum temperature reached in Case 4 is 368 °C, which is well below the limit (550 °C).

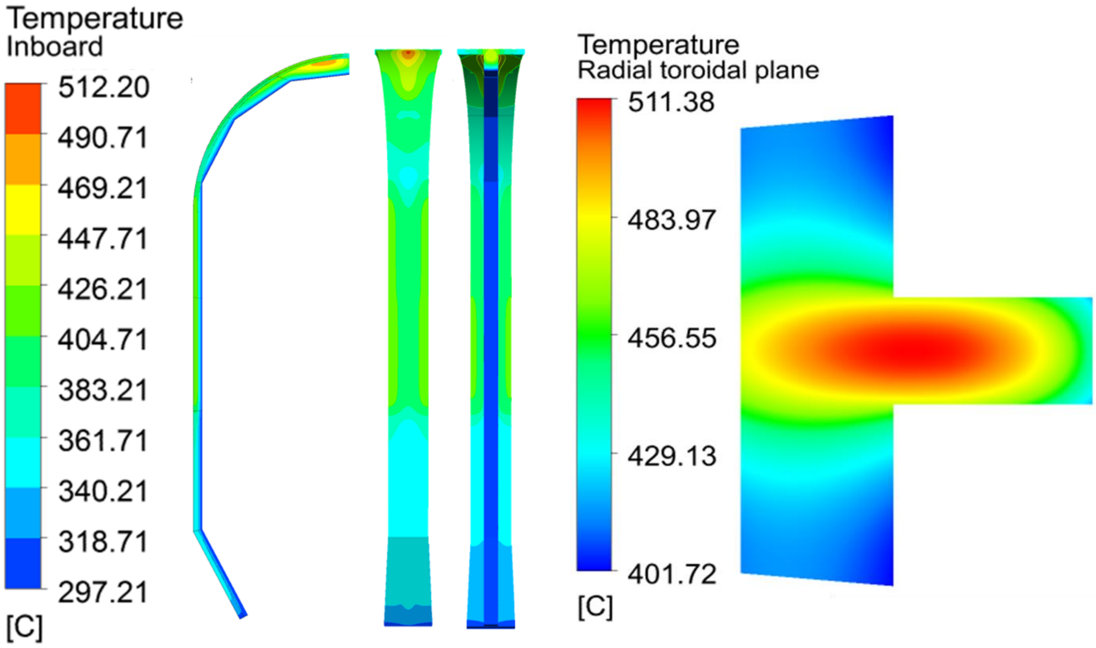

a) Side, back and front view *b) RT view at top plane*

Fig. 4.57 – CFX temperature of inboard BSS: Case 0.

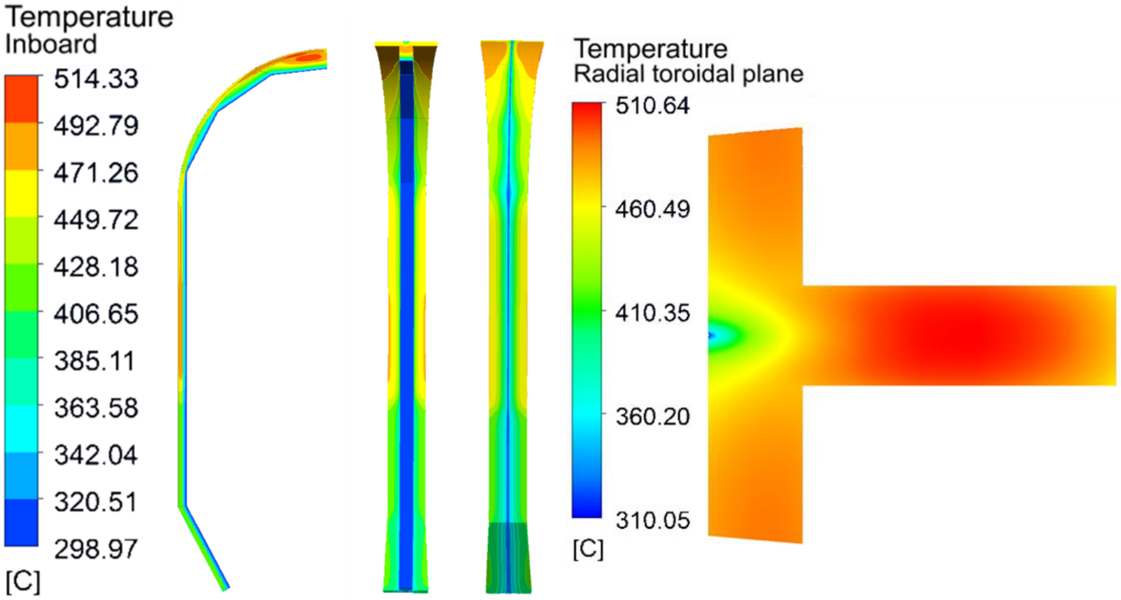

a) Side, back and front view *b) RT view at top plane*

Fig. 4.58 – CFX temperature of inboard BSS: Case 1.

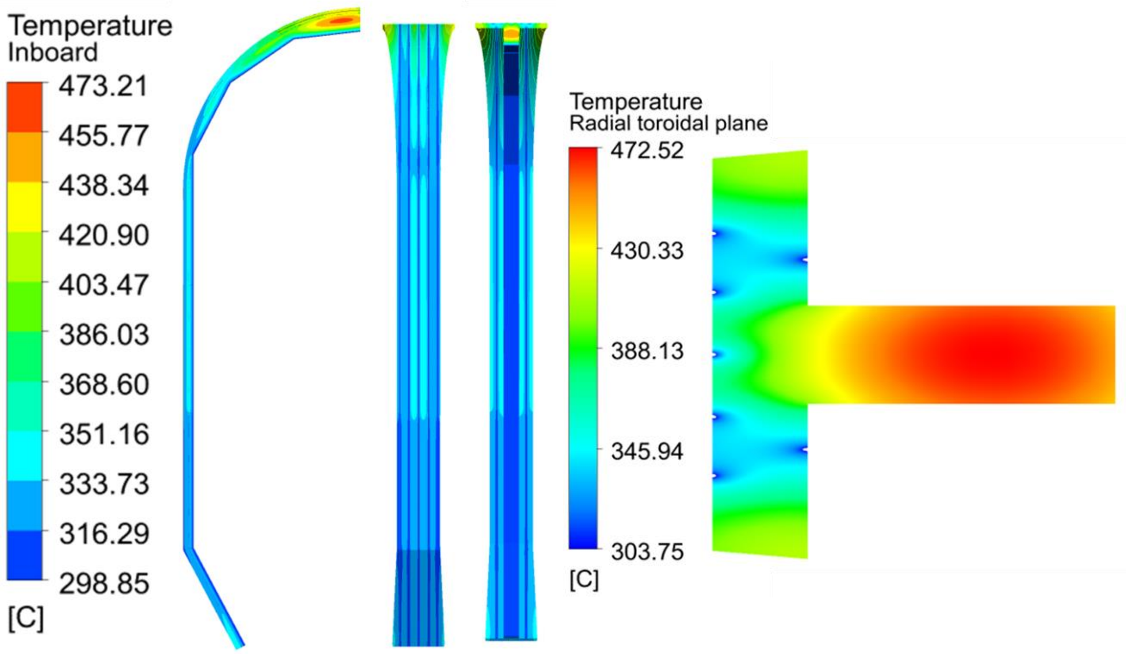

a) Side, back and front view *b) RT view at top plane*

Fig. 4.59 – CFX temperature of inboard BSS: Case 2.

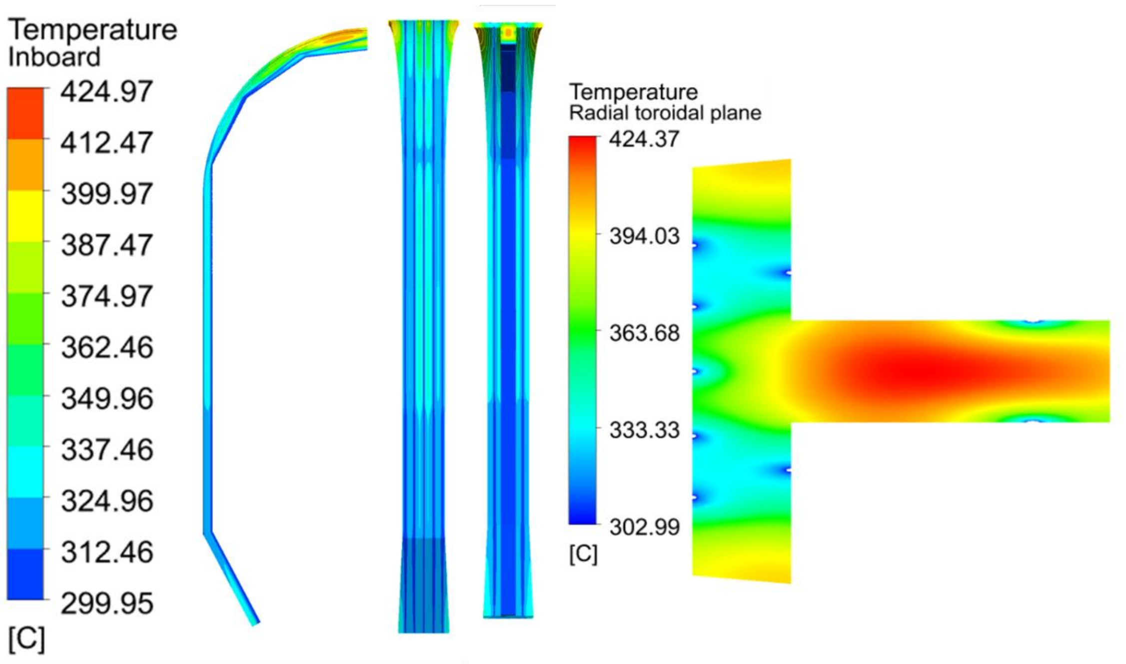

a) Side, back and front view *b) RT view at top plane*

Fig. 4.60 – CFX temperature of inboard BSS: Case 3.

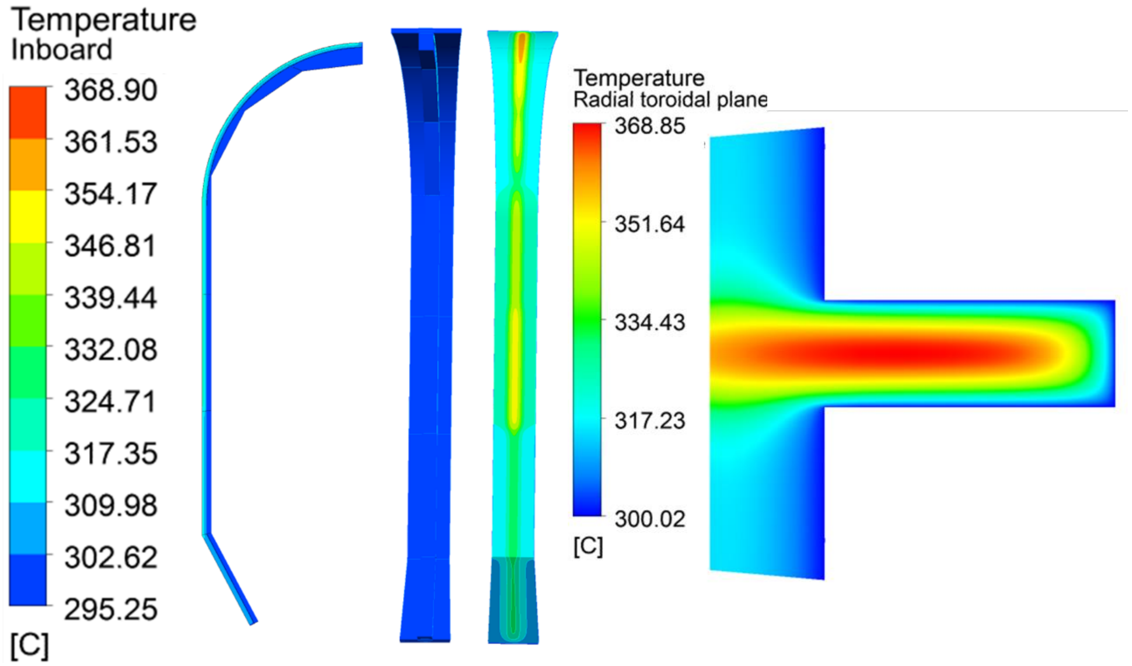

a) Side, back and front view *b) RT view at top plane*

Fig. 4.61 – CFX temperature of inboard BSS: Case 4.

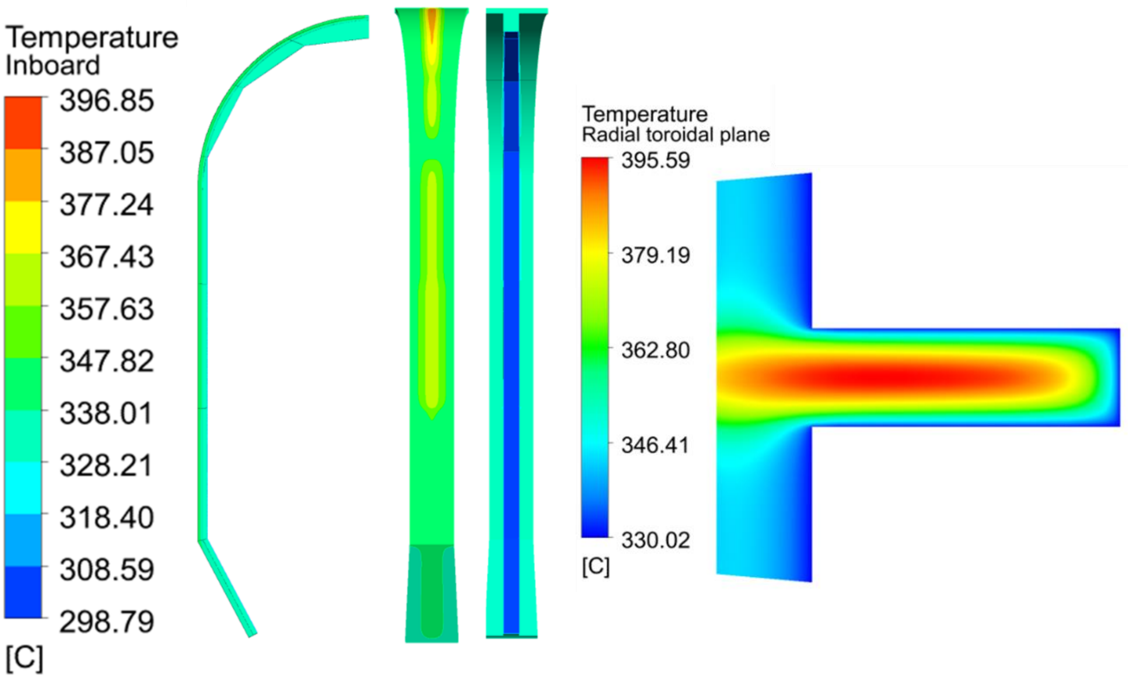

a) Side, back and front view *b) RT view at top plane*

Fig. 4.62 – CFD analyses of Inboard BSS Case 5.

4.5 Main achievements

The thermal analyses performed on outboard and inboard segment BSS demonstrate that the outboard BSS temperature is well the limit (550 °C), even increasing the volumetric power density up to 100%. Thus, refrigeration of outboard segment is not needed.

Contrary, the inboard segment BSS is affected by a power density which is one order of magnitude greater than the power density of outboard segment. The preliminary thermal analyses show that the inboard BSS temperature is over the limit, thus cooling is needed. Several analyses have been performed to evaluate the sphere of influence of slots made on BSS surface with water flowing at 300 °C. Being the influence limited, an alternative solution has been investigated, considering the whole front surface cooled with water at 300 °C. This configuration is effective in reducing the maximum temperature below the limit.

Moreover, this result suggests a design solution for the integration of the BZ water manifolds in WCLL 2017 design. Being the front surface of the BSS to be cooled with water at 300 °C, and considering the BZ coolant system layouts investigated, the inlet manifolds can be integrated in the space between the BP and the BSS.

5 EU DEMO WCLL PHTS AND BoP

5.1 Functions and requirements

In DEMO, the Balance of Plant (BoP) means the complex "chain" of systems devoted to the extraction of the pulsed thermal power generated by the plasma and deposited in BB, Divertor (DIV) and Vacuum Vessel (VV) and its conversion into electricity to be delivered to the external grid [48][49][51]. These systems are Primary Heat Transfer Systems (PHTS) of BB, DIV and VV which are devoted to extract the thermal energy generated by the plasma heating radiated/transported power and neutron deposition, and to transfers it to the Power Conversion System (PCS).

Being the operational sequence of DEMO Power Plant pulsed, BoP design option envisages the use of an Intermediate Heat Transfer System (IHTS) equipped with an Energy Storage System (ESS), which is included in the heat transport scheme between the BB PHTS and the PCS with the aim to buffer energy during the pulse which is returned to the PCS in dwell. This plant solution is needed to avoid the transfer of a pulsed load to PCS itself and to the electrical grid; therefore, it ensures a more continuous production of electricity guarantying system components lifetime.

The WCLL PHTS is developed on the basis of DEMO project requirements [50][51][52]. The design of the major components required for power generation such as generators, reactor coolant pumps, internals, turbine and generator are based on equipment that has successfully operated n power plants. Modifications to these proven designs were based on similar equipment that had successful operating experience in similar conditions. The BB PHTS provides coolant to the In-Vessel interfacing cooling systems (i.e. FW and BZ) during plasma operations, and for the decay heat during normal operation. The PHTS has the function of maintaining the coolant temperatures, pressure and flow rates as required by its interfacing cooling systems. Moreover, it provides the primary confinement for Activation Corrosion Products (ACPSs) and tritium entrained in coolant outside the VV, for this reason the PHTS components shall be located in the Tokamak building.

PCS in DEMO is a complex system where the secondary circuits of the various PHTS systems of the BB, DIV and VV should be integrated into an industrial, reliable and efficient system. The PCS has to be designed to remove the heat from PHTSs during normal and during the dwell time with high efficient conversion of the thermal power to electricity.

5.2 State of the art

One of the key issues connected with the operability of DEMO is that the plasma works in a pulsed way. Therefore, it would be beneficial to transform the intermittent nuclear fusion power output from the reactor into a continuous electrical power output. This is required for two reasons, firstly, a continuous power is more helpful in providing the electrical grid base load, and secondly, the pulsed mode is extremely un-favorable from the Rankine cycle operability, since the turbines could be exposed to severe damage through repeated cyclic stresses caused by start-up and shut-down. Several studies were performed in the past years to face with this problem, focused on the intermediate molten salt heat storage facility integration.

Between 1990-94, in the framework of European Fusion Programme, an extensive, in depth study, called Safety and Environmental Assessment of Fusion Power (SEAFP) [53], was undertaken to consider the safety and environmental aspects of fusion power leading to the publication of the SEAFP report [54] in 1995.

The assessment started with the development of two conceptual power plant designs, termed Model 1 and Model 2. The first model applies Vanadium alloy structures for the components near the plasma, a Lithium ceramic to generate Tritium, and Helium cooling for all reactor components, thus emphasizing the use of low activation materials, the avoidance of chemical reactions between coolant and reactor materials, and improved energy conversion. The latter is based on reduced activation martensitic steel for the structures, a PbLi alloy for Tritium generation, and water cooling throughout. The two models have been chosen to cover a reasonable range of combinations of structural materials, breeder materials and coolants.

Focusing on Model 2, the fusion power from the plasma is 3000 MW and the average NWL 2.1 MW/m^2. The external power absorbed by the plasma (75 MW) and exothermic neutron reactions in the blanket and divertor add to this power. Overall, the cooling system has to remove 3810 MW. The design is based on CANDU technology which meets similar goals. The first wall/blanket/VV cooling system consists of 8 independent loops, each cooling 2 reactor sectors and comprising a single steam generator and double-discharge centrifugal pump. The divertors are cooled by 2 loops which are used for preheating the first wall/blanket/VV steam generators. The total water volume is 410 m^3 (about 360 m^3 in the former 8 loops, about 50 m^3 in the latter 2 loops). The inlet/ outlet temperatures of the 8 loops are 265°C/310°C at a maximum pressure of 130 bar. First wall/blanket cooling are integrated to minimize the number of external connections. The inlet/outlet temperatures of the divertor loops are 223°C/180°C at 130 bar. The maximum pipe diameter is about 0.6 m. Filters and ion exchange are provided to control circulating corrosion products. The steam generator delivers steam at 260°C/ 47 bar for the secondary loop providing a gross conversion efficiency of about 32%. The cooling concept allows for natural coolant circulation in the primary system after a loss of plant service power and use it to ensure emergency decay heat removal until an adequate heat sink is restored. This concept provides cooling when all electrical power to the pumps is lost. The total decay heat drops to 10 MW at most within one day. A diagram of the cooling system is shown in Fig. 5.1.

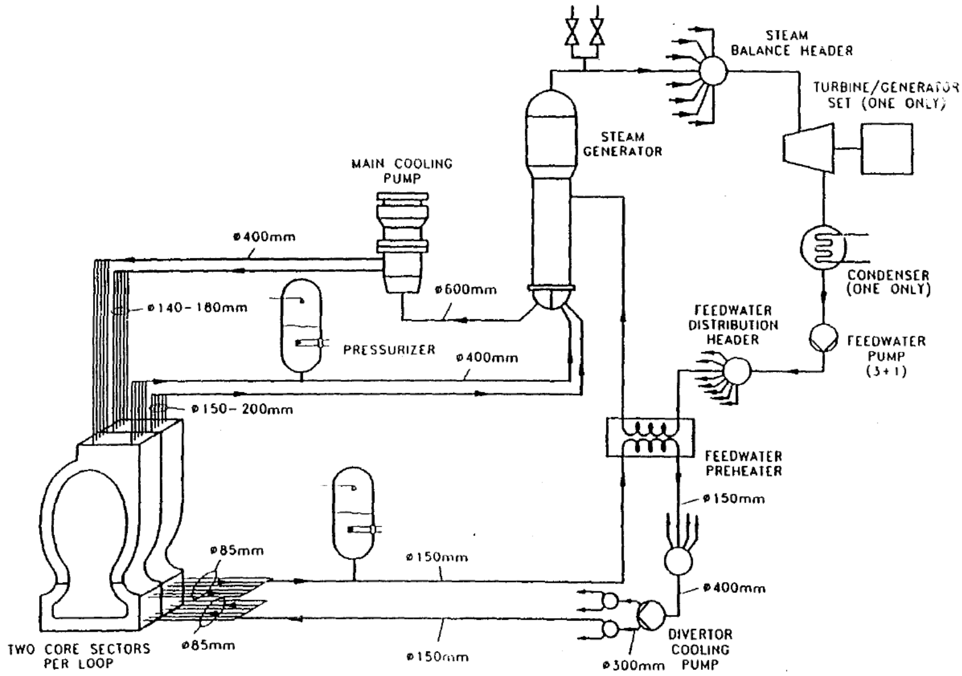

Fig. 5.1 – SEAFP Project, Water Cooling System (Principle) [54].

In 2000, the WCLL reactor concept was studied as part of the European Power Plant Conceptual Studies [17].

The conceptual design relates to a reactor of 1500 MW_e net electrical power power and included the power conversion system and balance of plant. The fusion power is 5000 MW, and it is assumed that the alpha power distributed on the first wall of the blanket is about 23% of the neutron power. The average neutron wall loading is 2.52 MW/m^2 and the average multiplication factor in the blanket is 1.14. The outlet temperature of the blanket cooling loops is set at 325 °C in order to have sufficient margin to saturation. The maximum velocity in the pipes is set at 20 m/s in order to minimize the loop inventory. From geometrical considerations, it is assumed that the energy repartition for the divertor is 66.6% for the outboard region and 33.3% for the inboard region; there are 4000 cooling channels on the outboard vertical targets and 2000 cooling channels on the inboard vertical targets. As the divertor loops operate at lower temperature (140 °C/167 °C) than the blanket cooling loops (285 °C /325 °C) to allow extracting the delivered power, the divertor power is used for preheating the feedwater of the steam generators of the blankets cooling loops. The primary heat transport system comprises six cooling loops for the blankets and two cooling loops for the divertor. The steam generators are based on current PWR technology. For availability reasons, there are two pumps per loop. The adopted parameters (i.e. number of loops, maximum velocity of the coolant) lead to an inventory of 130 m^3 in a blanket loop and 180 m^3 in a divertor loop.

The secondary heat transport system is assumed to be standard PWR technology. Most of the steam from the steam generators goes to the high-pressure turbine (HP) and some to the steam reheater/moisture separator (R/MS). From the HP, some steam is taken to heat the feedwater, in the first stage of the high-pressure heater (HP1*/condensing heat exchanger), and the rest is reheated before going to the low-pressure turbine (LP). The moisture removed from the low-pressure steam in the moisture separator is sent to the feedwater tank (FT). The high-pressure steam used to reheat the low-pressure steam is condensed in the reheater and the condensate is used to provide the last stage of feedwater heating, in high-pressure heater (HP2). From there, it is sent to the FT where it does additional heating. There is only one low-pressure heater, which receives heat from the divertor cooling system (Fig. 3). The other low-pressure heater has to be eliminated due to the low outlet temperature of the divertor cooling loop. A schematic view of the secondary HTS is reported in Fig. 5.2. The efficiency, defined as the ratio between the net power to the grid and the fusion power, is 33.8%.

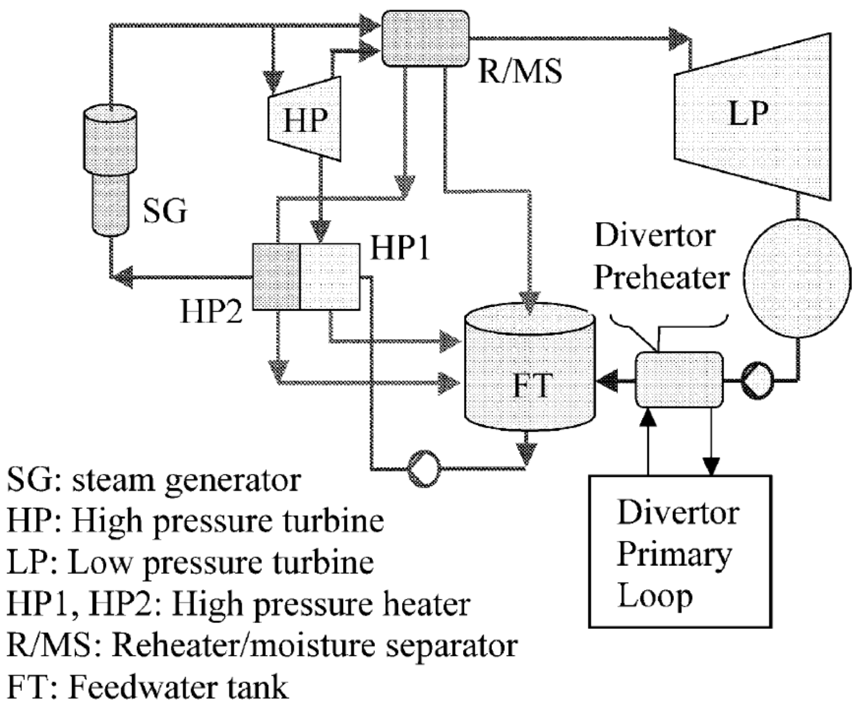

Fig. 5.2 – PPCS WCLL, schematic view of the secondary HTS [17].

In the frame of EFDA programme, in 2013 KIT investigated a design solution for BoP with water as coolant [55][56].

The proposed cycle utilizes heat from two heat sources, the blanket cooling loop and the divertor cooling loop, with 3 stages of low pressure turbine and 2 stages of high pressure turbine. The proposed coolant is the solar salt (60% NaNO3, 40% KNO3), while the initial data for the BoP scheme were obtained from CCFE (Ref. [57]). The efficiency of such a BoP scheme is estimated to be 36.8%. The entering hot salt tank temperature is assumed to be 320.7 °C, then leaving the tank, the salt enters in the steam generator, where steam is produced at 64 bar pressure and 279.8 °C temperature. Cold salt (284.8 °C) exiting from the steam generator still enters additional heat exchanger, where it heats feed water coming to the steam generator from the temperature of 242.9 °C up to 276.8 °C. At this point the cold salt (280.9 °C) flows into the tank. From there, it is pumped back to the water/solar salt heat exchanger where it is heated up. The cycle efficiency decreases from 36.8% down to 29.7%, in case the dwell time is 30 minutes each 2 hours of operation. The calculated heat storage capacity is 50800 ton of solar salt with two equivalent cylindrical tanks of 34 m height and 31.66 m diameter (i.e. ~26700 m^3). The schematic representation of DEMO BoP scheme for water cooled blanket concept with the intermediate heat storage loop is shown in Fig. 5.3.

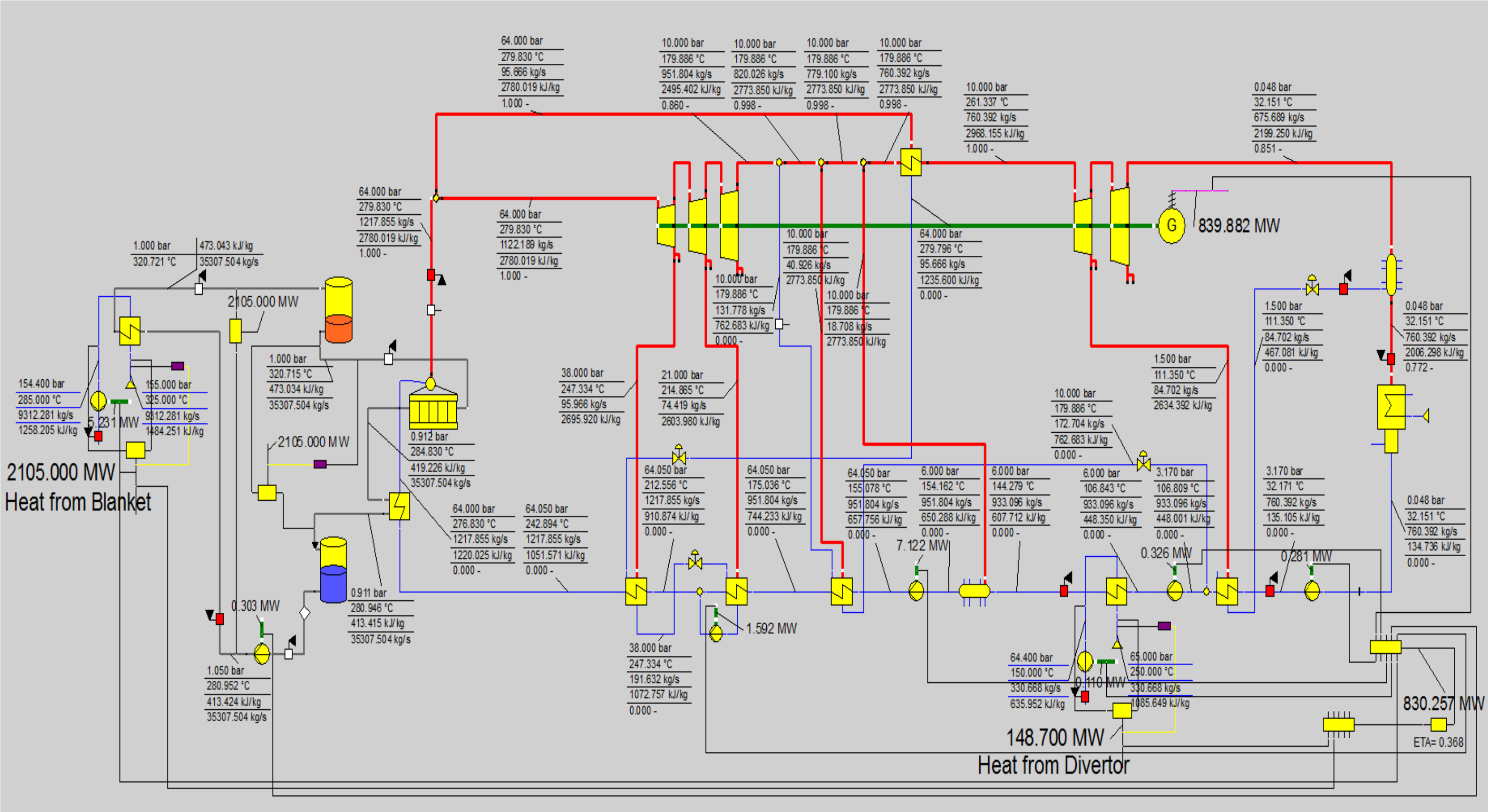

Fig. 5.3 – DEMO BoP scheme for water cooled blanket concept with the integrated intermediate heat storage loop as modeled by KIT

5.3 Conceptual design of DEMO WCLL PHTS and PCS

Since 2014, ENEA and its linked third parties is in charge for the development of the WCLL PHTS and BoP, in the frame of the EUROfusion PPPT WPBoP. Different PHTS have been considered and hereafter summarized:

1. Simplest case, one PHTS directly connected with the PCS, represents the straightforward solution comparable with PWR nuclear power plant technology choice. This solution has the lowest total coolant inventory, relies on the PWR proven technology, but requires the availability of a turbine compatible with the pulsed operation of DEMO. This solution has been disregarded.

2. Alternative solution is the indirect coupling between the PHTS and PCS, where the molten salt intermediate system will be in charge of storing and transferring the energy. This concept implies the largest primary coolant inventory. Indeed, the low heat transfer performances of the molten salt would require a large primary coolant mass inventory and about eight/ten primary to intermediate heat exchangers. This configuration will imply the maximum T mass inventory in the primary system. Possible mitigation would be the segmentation of the PHTS into several systems. This solution was disregarded.

3. Following the preliminary sizing evaluation, the reference solution hereafter discussed is based on two separate PHTS connected with the BZ and the FW coolant systems, respectively. This is consistent with the current WCLL BB design cooling system. The BZ PHTS is larger in terms of energy transferred and relies on a two loops system based on two hot legs and Once Through Steam Generators (OTSGs), four Main Coolant Pumps (MCPs) and cold legs, and one Pressurizer (PRZ). It relates to the PCS, where the superheated steam is delivered to the turbine during the pulse operation. The FW PHTS has lower power and relates to the ESS, in charge of pre-heating the Steam Generator (SG) feed water and of delivering the super-heated steam to the turbine during dwell time. It relies on a two loops system based on two hot legs and water-Molten Salt (MS) Heat Exchangers (HEXs), MCP and cold legs, and one PRZ. Considering the assigned requirement of about 100% of continuous thermal power delivered to the PCS, the hot and cold storage tanks of the ESS system have imposed dimensions. A new thermodynamic cycle was adopted with an inlet temperature of 295 °C and outlet temperature of 328 °C, both in FW and BZ primary systems. This cycle allows to operate in PHTSs at higher temperature, implying a lower ΔT and a greater mass flow rate. The configuration described is the reference configuration studied in 2016 and adopted for the preliminary sizing of primary systems.

4. The 2017 BoP design update will consider the reduction of the dwell time from 30 to 10 minutes, because of optimization of central solenoid recharge time and vacuum pump performance [49]. Thus, according to DEMO recent development [48] a new configuration for ESS has been adopted, which is based on two independent PHTS, with separated functions. Nevertheless, the FW PHTS delivers, through the IHTS, part of the available power to the PCS. This is the reference configuration selected for the analyses performed.

5.3.1 Integration of Breeding Blanket with PbLi and PHTS systems

The WCLL BB sector is linked to the PHTS though the in-vessel piping system which is formed by the feeding and collecting pipes of the two inboard and three outboard segments (Fig. 5.4) [38]. The water coolant pipes are routed through the upper port of DEMO Vacuum Vessel (VV). The following piping lines of BB sector go through the upper port:

- 2 inlet inboard FW feeding pipes (2 segments)
- 2 outlet inboard FW feeding pipes (2 segments)
- 2 inlet inboard BZ feeding pipes (2 segments)
- 2 outlet inboard BZ feeding pipes (2 segments)
- 3 inlet outboard FW feeding pipes (3 segments)
- 3 outlet outboard FW feeding pipes (3 segments)
- 3 inlet outboard BZ feeding pipes (3 segments)
- 3 outlet outboard BZ feeding pipes (3 segments)

The PbLi feeding pipes enters through the lower port, while the outlet pipes exit through the upper port.

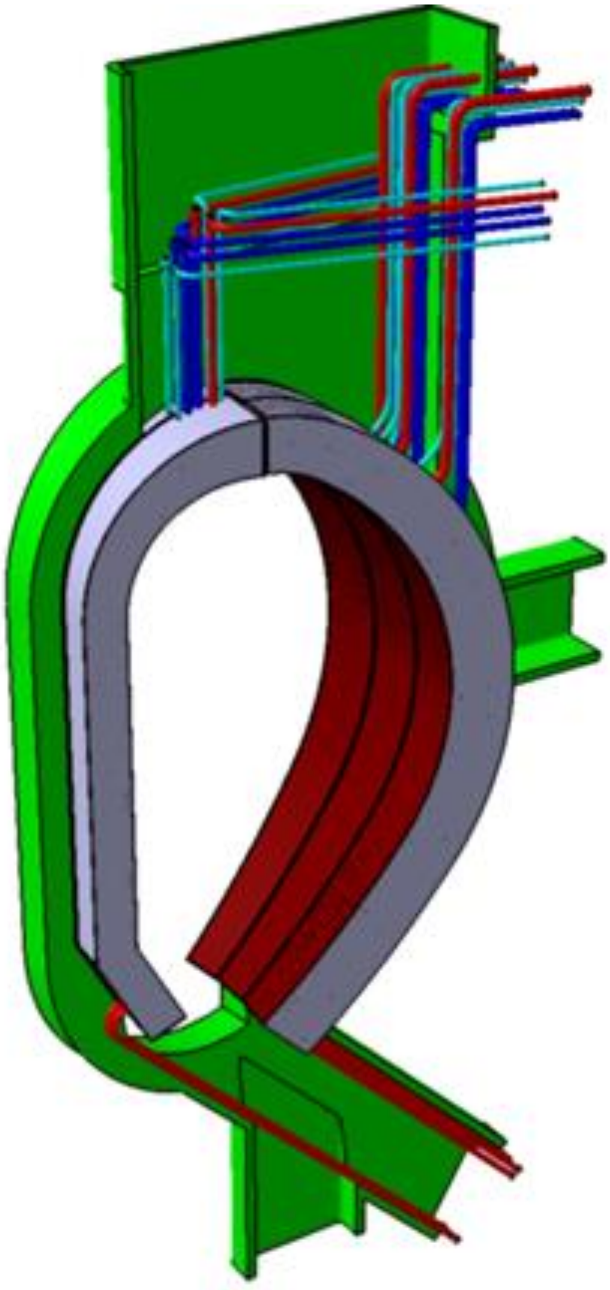

Fig. 5.4 – DEMO WCLL BB sector integration with PbLi and coolant systems.

5.3.2 **Input data**

Power parameters relevant for the PHTS design are reported in Tab. 5.1. The data are referred to DEMO1 and WCLL BB, according with Ref. [60]. The volumetric power densities have been inferred from the results of neutronic analyses performed on the previous PPCS Model A (WCLL) concept [61].

The evaluation of the power data is hereafter summarized:

- The total nuclear heating is 1754.7 MW and it is based on Ref [31]. This value does not include the power deposited in the FW, BZ, manifold structure, and shielding. It should be noted that currently more up-to-dated power data are available from neutronic calculation reported in Ref. [37] and [38];
- The total FW heat flux is calculated on the basis of the average FW heat flux (0.22 MW/m^2) multiplied for the total BB FW surface from Ref [31]. The value is 290.0 MW;
- The power recovered by the First Wall is due to the heat flux (0.5 MW/m^2 in Ref. [60]) and the NWL (177.6 MW). The total is 467.6 MW;
- The total power of the BB available for the thermal balance is: 2044.7 MW. This value differs from the value used for the design Ref. [31]:
- Nuclear power deposited in the manifold zone and shielding is neglected and equal to 10.7 MW and 11.5 MW, Ref. [31].

For computing correctly the neutronic heat produced in the components (accounting for the breeding volume that will be occupied by auxiliaries) the TBR calculated in the breeding blanket is normalized to the reference TBR which is equal to 1.05 [62]. The TBR of WCLL BB conceptual design, obtained from neutronic calculations [37], is 1.14. Considering these assumptions, a new reference the thermal power is obtained and is equal to 1923.4 MW_{th}. The FW and BZ contributions have been scaled considering the new reference total power. The values, compared with previous data in Tab. 5.1, have been considered as reference for the development of the thermal-hydraulic system model (see Sect. 6).

Tab. 5.2 reports the corresponding coolant mass flow rates for the FW and the BZ cooling systems, considering new power and the reference thermodynamic cycle (i.e. 295-328°C), calculated on the basis of RELAP5/Mod3.3 properties [46].

Considering the FW and BZ system, water volume is obtained from WCLL BB CAD 2015. The volume of water coolant is calculated considering the breeder units, the manifolds and the feeding pipes. Hydraulic diameter of feeding pipes is calculated considering a maximum velocity of 7 m/s and the average density of the coolant (697.4 kg/m^3). The feeding pipe tube length considered is 15+15 m (inlet and outlet) plus 10 m to take into account the length for reaching the ports and 10 m for the uncertainty in the knowledge of the geometrical dimensions. Main data are provided in Tab. 5.3.

#	Description	Unit	WCLL 2016 design	WCLL 2017 design
1	Total nuclear heating	***MW***	1754.7	1650.3
2	Total FW heat flux	***MW***	290.0	272.7
3	Neutron Wall Load	***MW***	177.6	167.0
4	*Total FW power*	***MW***	*467.6*	*439.8*
5	*Total BZ power*	***MW***	*1577.1*	*1483.2*
6	Total power	***MW***	2044.7	1923

Tab. 5.1 – DEMO and WCLL BB power balance.

		Power [MW]			**Mass flow rate [kg/s]**		
#	**Description**	**Total**	**FW***	**BZ**	**Total**	**FW**	**BZ**
1	IB segment	11.36	3.066	8.295	58.7	15.84	42.85
2	IB sector	22.72	6.123	16.60	117.4	31.62	85.74
3	Total IB sectors (18)	408.97	110.2	298.7	2113	569.4	1543
4	OB segment	28.04	6.104	21.93	144.8	31.53	113.3
5	OB sector	84.11	18.30	65.80	434.4	94.50	339.9
6	Total OB sectors (18)	1514	329.5	1184	7822	1702	6119
7	***Total reactor***	**1923**	**439.8**	**1483**	**9933**	**2272**	**7661**
*(NWL+HF)							

Tab. 5.2 – WCLL BB power and coolant flow rates (TD 295-328°C).

	Description	MF total	ρ	v	D	L	V	H_2O mass inventory
#	**Unit**	***kg/s***	***kg/m³***	***m/s***	***m***	***m***	***m³***	***kg***
1	IB FW and manifold (1 segment)	--	697.4(1)	7(2)	--	--	0.046	32.08
2	IB BZ and manifold (1 segment)	--	697.4(1)	7(2)	--	--	0.1344	93.73
3	OB FW and manifold (1 segment)	--	697.4(1)	7(2)	--	--	0.061	42.54
4	OB BZ and manifold (1 segment)	--	697.4(1)	7(2)	--	--	0.28	195.27
5	IB FW feeding pipe (1 segment)	**15.84**	697.4(1)	7(2)	0.0643	40	0.130	90.49
6	IB BZ feeding pipe (1 segment)	**42.85**	697.4(1)	7(2)	0.1057	40	0.351	244.8
7	OB FW feeding pipe (1 segment)	**31.53**	697.4(1)	7(2)	0.0907	40	0.258	180.2
8	OB BZ feeding pipe (1 segment)	**113.3**	697.4(1)	7(2)	0.1719	40	0.928	647.3
9	Additional volume due to uncertain geometrical data	--	697.4(1)	--	--	10	19.37	13507
10	DEMO in VV FW cooling system	**2272**		--	--	--	**23.57**	16438
11	DEMO in VV BZ cooling system	**7661**		--	--	--	**82.72**	57690
12	DEMO in VV BB cooling system	**9933**	697.4(1)	--	--	--	106.29	74128

(1) Average density.

(2) Maximum allowed velocity. Local velocity results from design features.

Tab. 5.3 – WCLL BB 2016 In-Vessel inventory.

5.3.3 PHTSs configuration

The operational sequence of DEMO Power Plant is based on nine pulses per each day with a burn time of two hours (power pulse). This means that the total dwell time should be less 40 minutes. Two configurations have been investigated, the first with a dwell time of 30 minutes and the second with a dwell time of 10 minutes (see Sect. 5.3.4). The last is the reference configuration assumed for the WCLL PHTS 2017 conceptual design and for development of the thermal-hydraulic system model. The WCLL PHTS is constituted by two independent primary systems:

- The BZ primary system (BZ PHTS)
- The FW primary system (FW PHTS)

The BZ primary system delivers the power to the PCS, my means of two Once Through Steam Generators (OTSG), and the FW primary system is connected to the Intermediate Heat Storage System (IHTS), which is in charge of accumulating the energy during the power pulse and delivers the heat during the dwell time to the PCS. A 3D CAD model of the PHTS is shown in Fig. 5.5.

The preliminary sizing of the main components was defined taking into account velocity and pressure drops constraints, and it was carried out considering the parameters reported in Tab. 5.1, Tab. 5.2 and Tab. 5.3. The main parameters defined in the preliminary sizing have been used to select the reference configuration and develop a 3D CAD model. The final parameters (i.e. pipes diameters lengths and volumes) are extrapolated from the CAD model and are reported in Tab. 5.7. The pipes diameters and thickness have been defined on the basis of European Standard 10220 [63].

The main components of PHTSs (BZ and FW) are: the sector collectors and distributors, the loop collectors and distributors, the steam generators and heat exchangers, the hot and cold legs, the pressurizers and pumps. One loop per system is foreseen. Main equipments of each loop are symmetrically located with respect the radial-poloidal direction of the tokamak, at about 71 m from each other.

SECTOR COLLECTORS

The sector collectors and distributors are connected to the BZ and FW feeding pipes. In particular, the sector collector is in charge to collect the hot water from the outlet BZ and FW pipes. The sector distributor is in charge to distribute the cold water to inlet pipes. One collector and one distributor per system and per sector is foreseen, and each of them is connected to 2 inboard segments and 3 outboard segments. The pipes diameters have been defined considering a maximum velocity of 12 m/s. Geometrical and hydraulic parameters are summarized in Tab. 5.4.

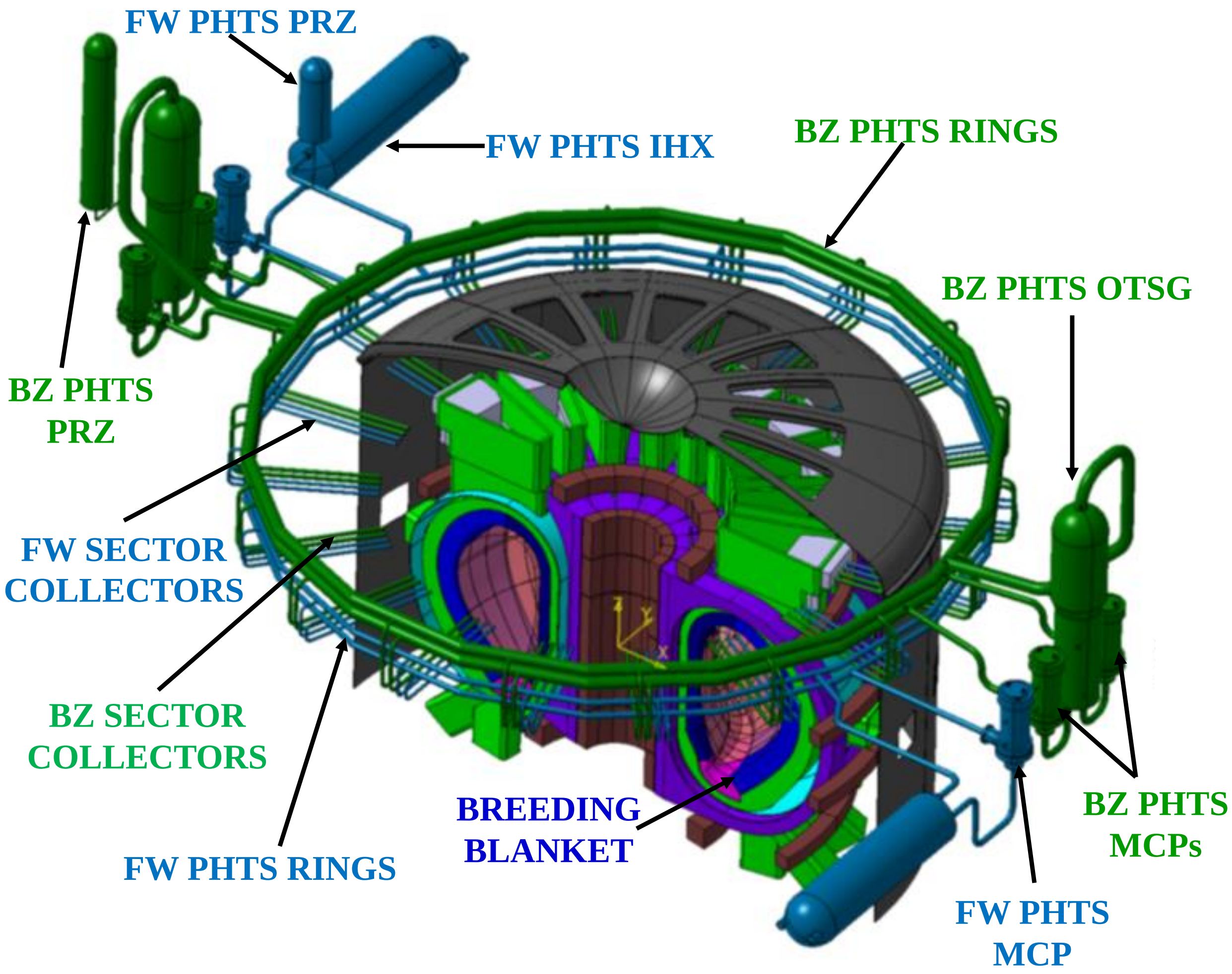

Fig. 5.5 – WCLL PHTS CAD model integrated with tokamak building.

RINGS

The loop collectors and distributors, hereinafter called “rings”, collects and distributes water from (to) the sector collectors to the hot and cold legs. The pipes diameters have been sized assuming that a quarter of the total mass flow rate flows in each quarter of ring and considering a maximum velocity of 12 m/s, to limit pressure drop due to friction factor. The main geometrical parameters are reported in Tab. 5.5.

HOT LEGS/ COLD LEGS

The BZ PHTS foresees one hot leg and two cold legs per loop. Instead, the FW PHTS foresees two hot legs and two cold legs per loop. The pipes diameters have been sized considering as reference velocity 15 m/s. Geometrical and hydraulic parameters are summarized in Tab. 5.6.

	Description	**MF total**	**ρ**	**v**	**D_h**	**L**	**V**	**Coolant mass inventory**
#	**Unit**	***kg/s***	***kg/m^3***	***m/s***	***m***	***m***	***m^3***	***kg***
1	BZ OUT COLLECTOR	425.6	657.76	10.9	0.274	14.6	--	--
2	BZ OUT COLLECTORS (18 sectors)	7761	657.76	--	--	--	15.485	10185
3	BZ IN COLLECTOR	425.6	737.08	9.8	0.274	13.6	--	--
4	BZ IN COLLECTORS (18 sectors)	7661	737.08	--	--	--	14.424	10632
1	FW OUT COLLECTOR	126.2	657.76	11.9	0.143	12.4	--	
2	FW OUT COLLECTORS (18 sectors)	2272	657.76	--	--	--	3.600	2368
3	FW IN COLLECTOR	126.2	737.08	10.6	0.143	11.4	--	--
4	FW IN COLLECTOR (18 sectors)	2272	737.08	--	--	--	3.309	2439

Tab. 5.4 – BZ and FW sector outlet (inlet) collectors.

	Description	MF total	ρ	v	D_h	L	V	Coolant mass inventory
#	Unit	*kg/s*	*kg/m³*	*m/s*	*m*	*m*	*m³*	*kg*
1	BZ OUT RING	1915	657.76	11.8	0.56	--	--	--
2	BZ TOTAL OUT RING	7661	657.76	--	--	143.78	35.41	23293
3	BZ IN RING	1915	737.08	10.5	0.56	--	--	--
4	BZ TOTAL IN RING	7661	737.08	--	--	143.78	35.41	26102
1	FW OUT RING	568	657.76	12.2	0.30	--	--	--
2	FW TOTAL OUT RING	2272	657.76	--	--	143.78	10.14	6667
3	FW IN RING	568	737.08	10.9	0.30	--	--	--
4	FW TOTAL IN RING	2272	737.08	--	--	143.78	10.14	7471

Tab. 5.5 – BZ and FW in and out rings.

	Description	MF total	ρ	v	D_h	L	V	Coolant mass inventory
#	Unit	*kg/s*	*kg/m³*	*m/s*	*m*	*m*	*m³*	*kg*
1	BZ HOT LEG	3831	657.76	13.7	0.734	25.25	--	--
2	BZ TOTAL HOT LEGS (2)	7661	657.76	--	--	--	21.36	14052
3	BZ COLD LEG	1915	737.08	12.7	0.510	7.56	--	--
4	BZ TOTAL COLD LEGS (4)	7661	737.08	--	--	--	6.17	4550
1	FW HOT LEG	1136	657.76	14.8	0.385	11.0	--	--
2	FW TOTAL HOT LEGS (2)	2272	657.76	--	--	--	2.56	1685
3	FW COLD LEG	1136	737.08	10.6	0.385	6.42	--	--
4	FW TOTAL COLD LEGS (2)	2272	737.08	--	--	--	1.49	1101

Tab. 5.6 – Hot leg and cold leg dimensions of BZ and FW PHTS.

		Dim	**D_{ext}**	**Thick**	**Inches**	**D_{int}**	**Section**	**L**	**Qty**	**Vol**
#	**Unit**	**--**	***m***	***m***	**--**	***m***	***m^2***	***m***		***m^3***
1	BZ OUT HEADER RING	DN-650	0.660	0.050	26	0.560	0.2463	143.78	1	35.413
2	BZ IN HEADER RING	DN-650	0.660	0.050	26	0.560	0.2463	143.78	1	35.413
3	BZ COLD LEG	DN-600	0.610	0.050	24	0.510	0.2043	7.556	4	6.174
4	BZ HOT LEG	DN-850	0.864	0.065	34	0.734	0.4231	25.245	2	21.364
5	BZ SG TO PUMP	DN-600	0.610	0.050	24	0.510	0.2043	4.8	4	3.922
6	BZ HL TO PRZ	DN-150	0.168	0.0142	6	0.140	0.0154	4	1	0.061
7	BZ_HOT COLLECTOR	DN-300	0.324	0.025	12	0.274	0.0589	14.6	18	15.485
8	BZ COLD COLLECTOR	DN-300	0.324	0.025	12	0.274	0.0589	13.6	18	14.424
	TOTAL									***132.26***
1	FW OUT HEADER RING	DN-350	0.356	0.028	14	0.300	0.1164	143.78	1	10.136
2	FW IN HEADER RING	DN-350	0.356	0.028	14	0.300	0.1164	143.78	1	10.136
3	FW COLD LEG	DN-450	0.457	0.036	18	0.385	0.1164	6.42	2	1.495
4	FW HOT LEG	DN-450	0.457	0.036	18	0.385	0.1164	11	2	2.561
5	FW HX TO PUMP	DN-450	0.457	0.036	18	0.385	0.1164	10.7	2	2.491
6	FW HL TO PRZ	DN-150	0.1683	0.0142	6	0.140	0.0154	5	1	0.077
7	FW HOT COLLECTOR	DN-150	0.1683	0.0125	6	0.143	0.0161	12.4	18	3.600
8	FW COLD COLLECTOR	DN-150	0.1683	0.0125	6	0.143	0.0161	11.4	18	3.309
	TOTAL									***33.81***

Tab. 5.7 – BZ and FW PHTS nominal diameters, pipe lengths and volumes.

BZ OTSG

The BZ PHTS transfers energy from the BZ of the BB to the PCS during the pulse mode (2 h). for a total power of 1483 MW_{th}. Two OTSGs are heated by the primary water coolant coming from the breeding zone of the breeding blanket. The primary coolant inlet and outlet temperature are 295 °C and 328 °C, respectively, at 15.5 MPa. Thus, the total mass flow rate is 7661 kg/s, calculated on the basis of the RELAP5 water properties [46].

In the WCLL BZ PHTS, the thermal power removed by one OTSG is 742 MW_{th}, the corresponding mass flow rate of the primary system is 3839 kg/s. The OTSG secondary side (water) pressure is assumed 6.41 MPa and the feedwater coolant inlet temperature is 238 °C. The objective is to produce super-heated steam at 299 °C. Therefore, the feedwater mass flow rate is 404 kg/s. The main thermal-hydraulic parameters of primary and secondary side are summarized in Tab. 5.8.

The number of tubes in a OTSG is calculated preserving the water velocity in tubes, assuming in primary side reference velocity of 7 m/s. Geometrical data of SGs tubes are reported in Tab. 5.9. Steam line (secondary side) and downcomer flow areas are calculated considering the reference velocities of steam equal to 30 m/s and 11.5 m/s, respectively.

A RELAP5/mod3.3 model of the OTSG is developed to perform the analyses (see Sect.6.2.2). Scoping analyses are performed to evaluate SG performances, changing the number of tubes, the p/D and the lattice (i.e. square and triangular lattices are considered). For each configuration the main parameters are calculated and reported in Tab. 5.10.

On the basis of the selected configurations further analyses are performed reducing the active tubes length from 15.87 m to 12.99 m and tubes fouling factor from 1.0 to 0.5. Calculations with triangular lattice are also performed, resulting in a greater p/D (1.375), but a smaller riser and vessel diameter. The studied cases are reported in Tab. 5.10.

The selected OTSG is characterized by 7569 tubes, with a length of 12.987 m. A square lattice is considered with a p/D of 1.28. Main geometrical features are reported in Tab. 5.11.

#	Parameter	Unit	DEMO SG
	Primary system		
1	N° SG	--	2
2	SG Power	***MW_{th}***	742
3	Coolant Mass flow/SG	***kg/s***	3830
4	Pressure	***MPa***	15.5
5	Temperature • Inlet • Outlet	***°C***	 328 299
6	Coolant velocity	***m/s***	<7
	Secondary system		
7	Pressure	***MPa***	6.41
8	Temperature • Inlet • Outlet	***°C***	 238 299
9	Feedwater flow/SG	***kg/s***	404

Tab. 5.8 – Primary and secondary systems OTSG TH parameters.

#	Parameter	Unit	DEMO SG
1	Tube Do	***mm***	15.88
2	Thickness	***mm***	0.864
3	Tube Di	***mm***	14.48
4	Tube Area	***mm^2***	157.2

Tab. 5.9 – Primary side OTSG – tubes dimensions

#	Parameter	Unit	Case 1	Case 2	Case 3	Case 4	Case 5
	Primary system – tube side						
1	# of tubes	--	8281	7569	6561	6561	7351
2	p/D	--	1.28	1.28	1.28	1.4	1.28
3	Lattice		Square	Square	Square	Square	Triangular
	Secondary system – shell side						
5	R_{in} riser	***m***	1.052	1.006	0.938	1.101	0.787
6	DC-riser thickness	***m***	0.040	0.040	0.040	0.040	0.040
7	R_{out} riser	***m***	1.092	1.046	0.978	1.141	0.827
8	A_{DC}	***m^2***	1.235	1.235	1.235	1.235	1.235
9	D_i vessel	***m***	2.519	2.440	2.323	2.603	2.076
10	Vessel thickness	***m***	0.23	0.23	0.23	0.23	0.23
11	D_{ext} vessel	***m***	2.979	2.900	2.783	3.063	2.536

Tab. 5.10 – Selected primary and secondary sides OTSG dimensions for the analyses

#	**Parameter**	**Unit**	**Value**
1	SG Power	***MW_{th}***	742
2	Primary side water T_{in}	***°C***	328
3	Primary side water T_{out}	***°C***	295
4	Secondary side water T_{in}	***°C***	238
5	Secondary side water T_{out}	***°C***	299
6	No. of tubes	**--**	7569
7	Tube D_o	***mm***	15.88
8	Thickness	***mm***	0.864
9	Length of tubes	***m***	12.987
10	Lattice	**--**	Square
11	p/D	**--**	1.28
12	Heat transfer area	***m^2***	4903
13	V water tubes	***m^3***	20
14	D_{ext} vessel	***m***	2.9

Tab. 5.11 – BZ PHTS OTSG parameters.

FW PHTS IHX

During the power pulse (2 h) the FW system delivers the power (439.8 MW_{th}) to the IHTS through two water/HITEC HEXs, and the corresponding energy (1759 MJ) is accumulated in the ESS. The overall power transferred through each intermediate heat exchanger is 219.9 MW_{th}. The main thermal-hydraulics parameters are reported in Tab. 5.12.

The reference configuration assumes the temperature cycle 295-328 °C for the primary water coolant system. The secondary fluid considered is the HITEC molten salt (ANNEX A). The thermodynamic cycle of the intermediate system is 280-320 °C. The horizontal IHX is typical liquid-liquid heat exchanger tube and shell with two passes. Pressurized water coolant flows inside U-shaped tubes, in counter current direction with respect the HITEC, which flows shell side.

Considering the reference thermodynamic cycle, the primary side water mass flow rate per IHX is 1136 kg/s, and the secondary side molten salt mass flow rate is 3524 kg/s. The main parameters of the IHX are reported in Tab. 5.12.

The reference pipe dimensions of the primary to intermediate heat exchanger are reported in Tab. 5.13. The heat exchanger tubes have a square lattice configuration. The molten salt velocity in the heat exchanger shall be in the range 0.5 – 2.0 m/s, which is a good compromise between the onset of corrosion issues and the heat transfer performances.
The number of tubes and the water side HTC are plotted as function of the tube diameter in Fig. 5.6. The water coolant velocity in the tubes is assumed lower than 3m/s, in order to keep the MS velocity in the secondary side in the allowed range with reasonable p/D values.

Indeed, Fig. 5.7 reports the molten salt velocity and HTC as function of p/D. The minimum p/D of 1.45 is possible with the water velocity equal to 1.5 m/s, if the molten solar salt velocity is limited to 1m/s. When, larger values of molten solar salt velocity (e.g. 2m/s), the P/D may be further reduced, or larger velocities of coolant water are allowed, which implies a reduced number of tubes. Fig. 5.8 shows that the water side volume and the length of the tubes as function of p/D and water coolant velocity. For each configuration, the molten salt mass velocity is given. When, the molten salt velocity is about 1.80 m/s, the tubes length is reduced below 40 m, and the volume below 50 m^3

Tab. 5.14 reports the parameters relevant for selection as function of velocity and p/D, considering the reference and the alternative thermodynamic cycle. The molten salt velocity shall be increased up to 1.80 m/s, to reduce the total water inventory and the dimensions of the IHX. The main geometrical data of the selected IHX are reported in Tab. 5.15

#	Parameters	Unit	MS Ref. Cycle
1	DEMO FW-PS power	***MW_{th}***	439.8
2	N° IHX	**-**	2
3	IHX Power	***MW_{th}***	219.9
4	Primary side operating temperature range	***°C***	295-328
5	Secondary side operating temperature range	***°C***	280-320
6	Water Mass flow total	***kg/s***	2272
7	Water Mass flow x IHX	***kg/s***	1136
8	Molten salt mass flow total	***kg/s***	7048
9	Molten salt mass flow x IHX	***kg/s***	3524

Tab. 5.12 – WCLL BB FW PHTS main data.

Water side - tube side	Unit	Value
Tube Do	***m***	0.015876
t	***m***	8.640E-04
Tube Di	***m***	0.0141480
Tube Ai	***m^2***	1.572E-04

Tab. 5.13 – Water-molten salt HEX, Ref. MS thermodynamic cycle – tube dimensions.

	v H_2O	v MS	p/D	HTC H_2O	HTC MS	Tube length	H_2O volume	MS TD cycle
#	***m/s***	***m/s***	**--**	***W/m^2K***	***W/m^2K***	***m***	***m^3***	***°C***
1	1.5	1.00	1.40	11964	2475	33.2	72.6	280 – 320
2	**1.5**	**0.90**	**1.45**	**11964**	**2207**	**36.2**	**79.1**	
3	**1.5**	**0.81**	**1.50**	**11964**	**1985**	**39.3**	**85.8**	
4	1.5	0.73	1.55	11964	1798	42.4	92.7	
5	1.5	0.66	1.60	11964	1638	45.7	99.9	
6	2.0	1.07	1.50	15061	2498	42.4	69.5	
7	2.0	0.97	1.55	15061	2263	45.8	75.0	
8	2.0	0.89	1.60	15061	2062	49.3	80.7	
9	2.0	0.81	1.65	15061	1889	52.9	86.6	
10	2.0	0.75	1.70	15061	1739	56.6	92.7	
11	**2.0**	**1.84**	**1.28**	**15061**	**4107**	**28.93**	**47.4**	
12	2.5	1.80	1.37	18004	4007	36.59	48.0	
13	3.0	1.79	1.45	20831	3843	44.19	48.3	

Tab. 5.14 – Water-Molten Salt HEX – IHX parameters relevant to selection.

#	Parameter	Unit	Value

1	IHX Power	MW_{th}	219.9
2	Primary side water T_{in}	*°C*	328
3	Primary side water T_{out}	*°C*	295
4	Secondary side HITEC T_{in}	*°C*	280
5	Secondary side HITEC T_{out}	*°C*	320
6	No. of tubes	--	5211
7	Tube D_o	*mm*	15.88
8	Thickness	*mm*	0.864
9	Length of tubes	*m*	28.9
10	Lattice	--	Square
11	p/D	--	1.28
12	Heat transfer area	m^2	7513
13	V water tubes	m^3	23.7
14	D_{ext} vessel	*m*	3.5

Tab. 5.15 – FW PHTS intermediate heat exchanger parameters.

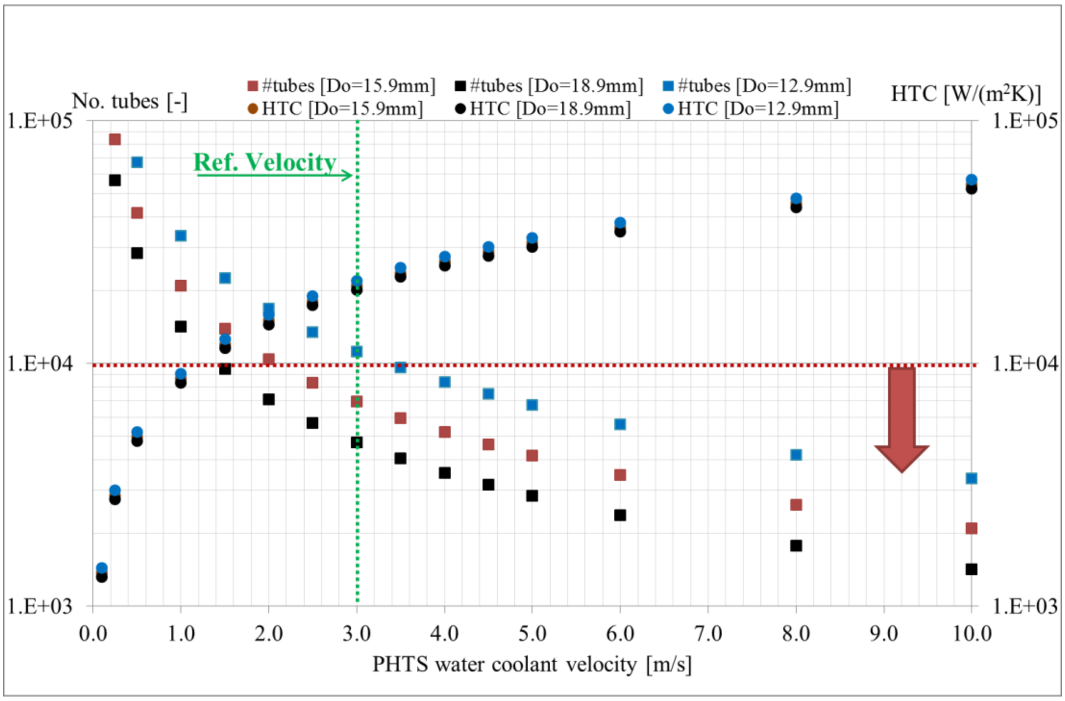

Fig. 5.6 – Water-molten salt HEX, Ref. MS thermodynamic cycle – No. of water tubes and HTC as function of water coolant velocity and tube diameter.

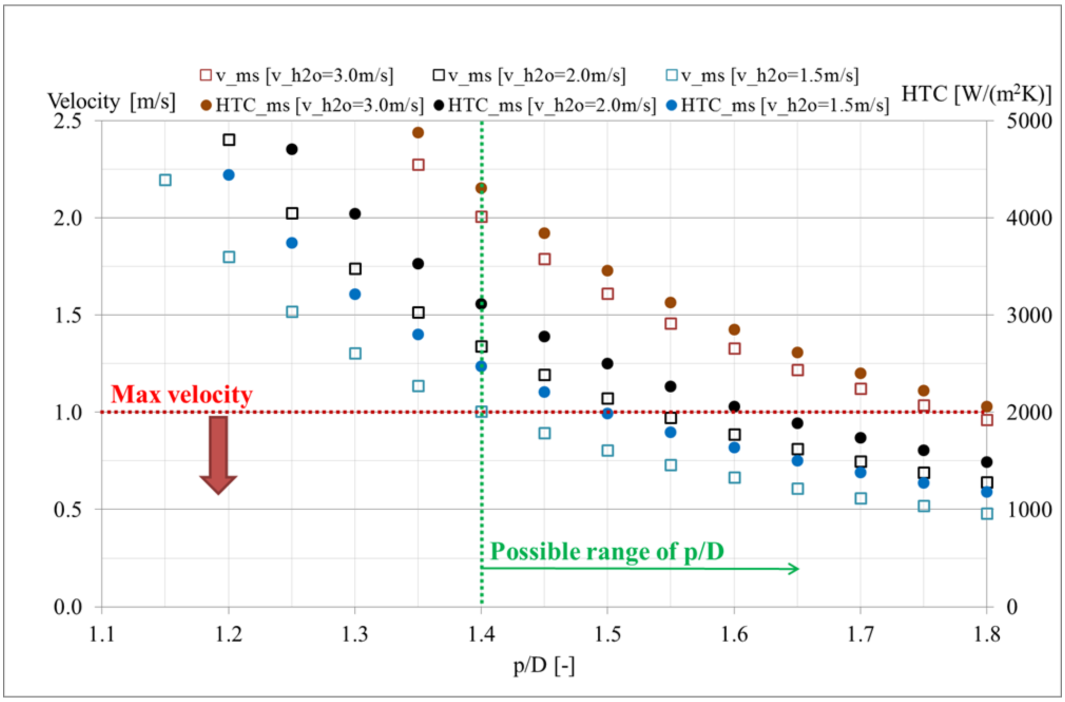

Fig. 5.7 – Water-molten salt HEX, MS velocity and HTC as function of tubes p/D (square lattice).

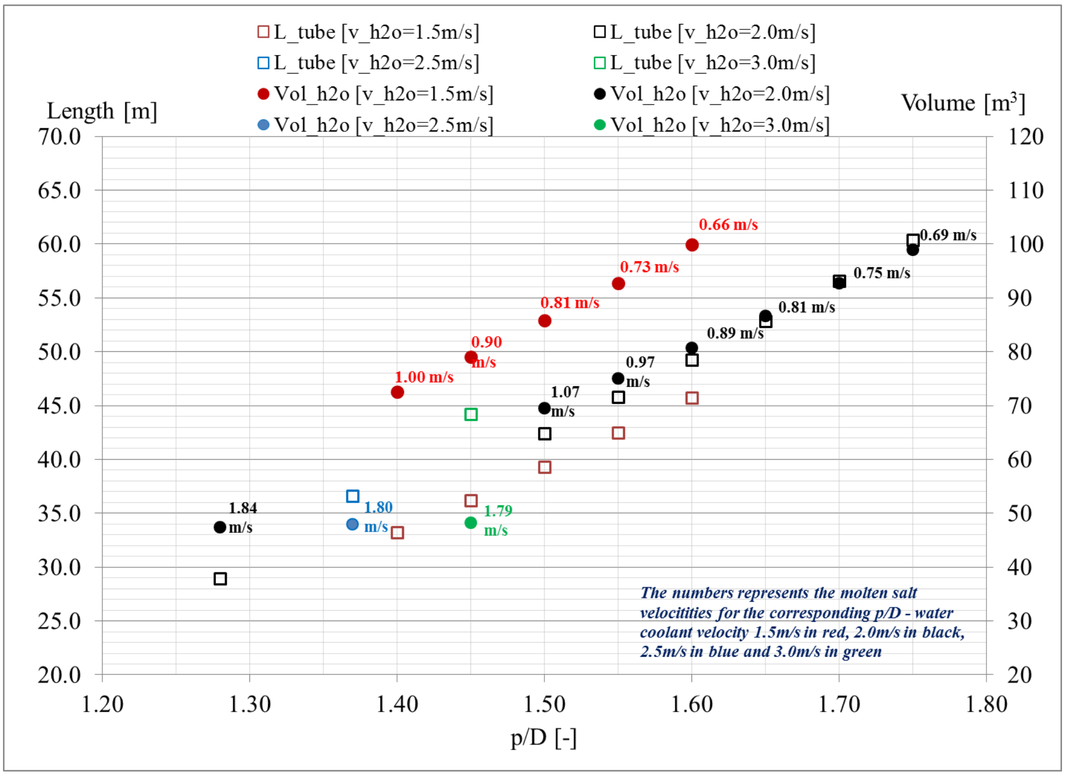

Fig. 5.8 – Water-molten salt HEX, Volume and tube length as function of tubes p/D.

PRESSURIZERS

For each PHTS (BZ and FW) is foreseen a pressurizer. This component has been sized on the base of the PWR [64]. The BZ pressurizer has a water volume of 53 m^3, and the FW pressurizer has a water volume of 25 m^3.

PUMPS

Six pumps are installed in current preliminary PHTS design of DEMO. Four MCPs, two per loop, are installed in the cold legs of the BZ PHTS. The other two MCPs are installed in in the FW PHTS. According with the main data of the PHTS, the pressure drops calculated in the systems (see Tab. 5.17) and a postulated efficiency of 78%, it results that the power of these pumps is 2.294 MW and 1.419 MW, respectively for those installed in the BZ PHTS and in the BZ PHTS. It implies that they can be medium and small PWR pumps.

The main data of the FW PHTS and BZ PHTS are summarized in tables Tab. 5.18, Tab. 5.19, Tab. 5.17. The first two shows that according with the CAD developed the overall volume of both PHTS is 430.6 m^3. The calculated pressure drops are 9.74bar and 9.34 bar for the FW PHTS and BZ PHTS, respectively.

	ρ	**M**	**ΔP**	**Q**	**H**	**η**	**P (Total)**	**P (×MCP)**
Unit	***kg/m³***	***kg/s***	***MPa***	***m³/s***	***m***	**--**	***MW***	***MW***
FW PHTS	737.1	2272	0.974	3.082	99.32	0.78	2.838	1.419
BZ PHTS	737.1	7661	0.934	10.39	95.25	0.78	9.178	2.294

Tab. 5.16 – PHTS MCP power.

BZ PHTS	**ΔP [Pa]**	**FW PHTS**	**ΔP [Pa]**
From BB to SG		*From BB to IHX*	
Out Sector collectors (IB+OB)	1.25e5	Out Sector collectors (IB+OB)	1.73e5
BZ Out Ring (9 sectors)	5.77e4	FW Out Ring (9 sectors)	7.49e4
BZ Hot legs	1.75e5	FW Hot legs	1.40e5
SG	2.12e5	IHX	1.50e5
From SG to BB		*From SG to IHX*	
BZ SG to pump	8.67e4	FW IHX to pump	1.37e5
BZ cold leg (1/4)	1.25e5	FW cold leg (1/4)	8.98e4
BZ In Ring (9 sectors)	4.98e4	FW In Ring (9 sectors)	6.68e4
In Sector collectors (IB+OB)	1.03e5	In Sector collectors (IB+OB)	1.42e5
Total	***9.34 e5***	***Total***	***9.74 e5***

Tab. 5.17 – Reference pressure drop in FW PHTS and BZ PHTS.

\

WCLL BB PHTS main parameters								
Tot. Power [MW_{th}]	FW Power [MW]	$\Delta T_{Blanket}$ [°C]	H [15.5MPa;295°C] [kJ/kg]	H [15.5MPa;328°C] [kJ/kg]	Mass flow [kg/s]	# of systems / loops	ρ [kg/m^3] [15.5MPa;295°C]	ρ [kg/m^3] [15.5MPa;328°C]
1923	439.8	33	1310.0	1503.6	2272	1 / 1	737.08	657.56

FW PHTS						
Loop	Sector Hot / Cold Manifolds	Loop collectors (Hot/Cold)	Hot Legs	Cold Legs	Pump per loop	Heat Exchanger per loop
1	18 / 18	1 / 1	2	2	2	2

Description	#	Pipe DN	Mass flow [kg/s]	Inner. diam. [mm]	Thickness [mm]	Vel. [m/s]	Length [m]	Volume [m^3]	Total Volume [m^3]	**Total Volume [m^3]**
DEMO in VV FW cooling system. 2 IB and 3 OB segments per 18 sectors.	1	--	15.84/ 31.53	--	--	7	40 /40	23.57	23.57	**127.2**
Sector **inlet** collectors (Connecting VV cooling system and loop **collector**)	18	150	126.2	143	12.5	11.9	12.4	0.2	3.6	
Loop collector	1	350	2272	300	28	12.2	143.78	10.14	10.14	
Hot leg	2	450	1136	385	36	14.8	29.3	1.28	2.56	
HEX Water – Molten salt	2	--	1136	--			--	23.7	47.4	
Cold legs	2	450	1136	385	36	10.6	14.8	0.745	1.49	
Loop distributor	1	350	2272	300	28	10.9	143.78	10.14	10.14	
Sector **outlet** collectors (Connecting VV cooling system and loop **distributor**)	18	150	126.2	143	12.5	9.8	11.4	0.183	3.3	
Pressurizer	1	--	--	--	--	--	--	25	25	

Tab. 5.18 – FW PHTS: main data

WCLL BB PHTS main parameters

Tot. Power [MW_{th}]	FW Power [MW]	$\Delta T_{Blanket}$ [°C]	H [15.5MPa;295°C] [kJ/kg]	H [15.5MPa;328°C] [kJ/kg]	Mass flow [kg/s]	# of systems / loops	ρ [kg/m^3] [15.5MPa;295°C]	ρ [kg/m^3] [15.5MPa;328°C]
1923	1483	33	1310	1503.6	7661	01-gen	737.08	657.56

BZ PHTS

Loop	Sector Hot / Cold Manifolds	Loop collectors (Hot/Cold)	Hot Legs	Cold Legs	Pump per loop	Heat Exchanger per loop
1	18 / 18	1 / 1	2	2	2	2

Description	#	Pipe DN	Mass flow [kg/s]	Inner. diam. [mm]	Thickness [mm]	Vel. [m/s]	Length [m]	Volume [m^3]	Total Volume [m^3]	**Total Volume [m^3]**
DEMO in VV BZ cooling system. 2 IB and 3 OB segments per 18 sectors.	1	--	42.85/ 113.3	--	--	7	40 /40	82.72	82.72	
Sector **inlet** collectors (Connecting VV cooling system and loop **collector**)	18	300	425.6	274	25	10.9	14.6	0.860	15.49	
Loop collector	1	650	7761	560	50	11.8	143.78	35.41	35.41	
Hot leg	2	850	3831	734	65	13.7	25.25	10.68	21.36	
OTSG	2	--	3831	--			--	19.7	39.4	
Cold legs	4	600	1915	510	50	12.7	7.556	1.542	6.17	
Loop distributor	1	650	7761	560	50	10.5	143.78	35.41	35.41	
Sector **outlet** collectors (Connecting VV cooling system and loop **distributor**)	18	150	425.6	274	25	9.8	13.6	0.801	14.42	**303.38**
Pressurizer	1	--	--	--	--	--	--	53	53	

Tab. 5.19 – BZ PHTS: main data

5.3.4 ESS configuration

The pipelines connecting the IHX secondary sides to the hot and cold molten salt tanks (e.g. the ESS), the tanks themselves, the steam generator and the pumps constitute the Intermediate Heat Transfer System (IHTS). Considering the operation of DEMO, as well as the design requirement of continuous and near constant electrical power delivered to the grid in both pulse and dwell, the thermal power to be accumulated in the ESS is known and then the dimensions of hot and cold storage tanks of the ESS system are identified.

According with the current specifications [48][49] the dwell time is reduced from 30 minutes to 10 minutes, needed to reduce the large size of molten tank. The preliminary sizing was performed with a dwell time of 30 minutes (ANNEX B), the results achieved are the basis for the development of the ESS with a dwell of 10 minutes.

The preliminary sizing of the ESS with a dwell of 10 minutes is carried out considering that the total thermal power from BB (FW and BZ) is equal to 1923 MW_{th} and the auxiliary systems (DIV and VV) provide a thermal power of 337.3 MW_{th}, used to pre-heat the feedwater of the PCS. It is assumed that the turbine power (1749 MW) during the pulse mode is equal to the turbine power during the dwell mode. The assumptions in terms of powers are summarized in Tab. 5.20.

During the pulse (2 h) the BZ PHTS power (1483 MW_{th}) is delivered to the PCS. The FW PHTS delivers power (439.8 MW) to the ESS. The energy stored during the pulse phase is equal to 1.25×10^{6} MJ which corresponds to a thermal power of 173.9 MW, that is delivered to the PCS during the dwell time. The difference between the FW PHTS power available (439.8 MW_{th}) and the power stored in the ESS is directly delivered to the PCS, and it is equal to 265.9 MW_{th}. The energy is transferred from the ESS to the PCS trough one Helical Steam Generator (HCSG). The hot molten salt flows in shell side and transfers energy to water flowing in the tubes side. The molten salt temperature cycle is 280-320 °C. The feedwater enters in the HCSG with an inlet temperature of 238 °C and exits with an outlet temperature of 299 °C at 6.41 MPa. The HCSG mass flow rate of HITEC is 4375.4 kg/s, and the feedwater mass flow rate, calculated with the enthalpy balance, is 284.1 kg/s.

The heat transfer between the hot molten salt and PCS water is evaluated considering the conduction mechanism through the tube thickness as well as the convection of the liquid water/steam and molten salt streams at the HCSG outer and inner tubes side. The molten salt Heat Transfer Coefficient (HTC) is calculated using the Zukauskas correlation. The water side convective heat transfer is evaluated using RELAP5/Mod3.3 implemented correlation. The HITEC salt velocity is selected accordingly with the geometry in a way that it is in the range between 1 and 1.5 m/s, which is a good compromise between the HTC performances and the pressure drop values and the potential for corrosion issues. he

During the dwell time (10 minutes), the mass flow of molten salt from hot to cold tanks is 33436 kg/s. The ESS contains a mass of molten salt equal to 20062 tons at the beginning of dwell, thus about 11000 m^3 are needed to store this amount of molten salt.

During the dwell time, the ESS delivers power to PCS through 4 HCSGs. The average power available in pulse and dwell time is 2086.4 MW, thus the power of each HCSG is 521.6 MW_{th}.

It wants to be stressed that the HCSG considered for the pulse mode, is one of the four HCSG sized for the dwell time, working at 51 % of the nominal power. The main parameters of the HCSG, in pulse and dwell mode are reported in Tab. 5.21 and Tab. 5.22, respectively.

The main pipes of the IHTS has been preliminary sized, in particular a maximum velocity of 3 m/s is considered for HITEC. One pipe of DN-900 is foreseen from each IHX to the hot tank, and from the cold tank to the IHX. Instead, due to the massive mass HITEC mass flow rate from the HCSG to the cold tank and from the hot tank to the SG two pipes of DN-1050 have been selected (see Tab. 5.24).

#	**VV PHTS**	**Unit**	**Value**
1	Total power from BB	$\boldsymbol{MW_{th}}$	1923
2	BZ power	$\boldsymbol{MW_{th}}$	1483
3	FW power	$\boldsymbol{MW_{th}}$	439.8
4	Auxiliary systems (VV+DIV)	$\boldsymbol{MW_{th}}$	337.3
5	Total power	$\boldsymbol{MW_{th}}$	2260
6	Power to turbine (pulse and dwell)	$\boldsymbol{MW_{th}}$	1749

Tab. 5.20 – Input data for ESS with dwell of 10 minutes.

HCSG PULSE			
#	**Descritpion**	**Unit**	**Value**
1	HCSG nominal power	***MW_{th}***	521.6
2	No. HCSG	**--**	1 (3 off)
3	HCSG operation power	***MW_{th}***	266.2
4	HITEC inlet T	***°C***	320
5	HITEC outlet T	***°C***	280
6	Liquid water inlet T	***°C***	238
7	Steam outlet T	***°C***	299
8	Super-heating	***°C***	19.1
8	Water Mass flow	***kg/s***	145.0
9	Molten salt mass flow	***kg/s***	4266
10	No. of Helical Tubes	**--**	1611

Tab. 5.21 – HCSG pulse mode.

HCSG DWELL			
#	**Descritpion**	***Unit***	**Value**
1	HCSG nominal power	***MWth***	521.6
2	No. HCSG	**--**	4
3	HCSG operation power	***MWth***	521.6
4	HITEC inlet T	***°C***	320
5	HITEC outlet T	***°C***	280
6	Liquid water inlet T	***°C***	238
7	Steam outlet T	***°C***	299
8	Super-heating	***°C***	19.1
8	Water Mass flow	***kg/s***	284.2
9	Molten salt mass flow	***kg/s***	8345
10	No. of Helical Tubes	**--**	1611

Tab. 5.22 – HCSG dwell mode.

#	Descritpion	Unit	Value
1	No. of tubes	--	1611
2	Outlet steam vel limit	***m/s***	36
3	v MS	***m/s***	1.395
4	Tube Do	***m***	0.016
5	t	***m***	0.0008
6	p/D horiz row	--	1.60
7	Vertical row tube pitch	***m***	0.026
8	Di bundle	***m***	1.85
9	De bundle	***m***	3.124
10	Vtot MS	m^3	41.21
11	Vtot water	m^3	17.84
12	Tube length	***m***	68.00
13	Tube heigth	***m***	12.71

Tab. 5.23 – HCSG features.

#	Description	PIPE	OD	THICK	ID	Len	QTY
	In-building	--	***mm***	***mm***	***mm***	***m***	--
1	From IHX 1 to TANK	DN-900	914	8	898	270	1
2	From TANK to IHX 1	DN-900	914	8	898	270	1
3	From IHX 2 to TANK	DN-900	914	8	898	120	1
4	From TANK to IHX 2	DN-900	914	8	898	120	1
	Out-building						
5	From Hot tank to HCSG	DN-1050	1067	8	1051	35	8
6	From HCSG to Cold tank	DN-1050	1067	8	1051	35	8

Tab. 5.24 – IHTS pipes dimensions.

5.3.5 PCS configuration

The thermodynamic cycle hypothesized is derived from the PWR cycles with OTSGs and it is shown in Fig. 5.9. The steam turbine is moved by superheated steam (299 °C at 6.4 MPa) generated into the two OTSGs during the pulse mode and into the four HCSGs during the dwell mode.

The HCSG is part of IHTS and it produces steam mainly during the dwell using the energy from the FW, stored in the hot tank during the pulse phase as sensible heat of the molten salt. Thanks to this double steam sources, that alternatively transfer the BB and FW generated thermal power to PCS, the steam turbine works in a continuous mode with a limited variation of the steam load during the pulse and dwell, being the system able to cope with the power "lost" in dwell caused by the pulsation of the low temperature heat sources (e.g. DIV-PFU, DIV-Cassettes, VV). Consequently, no significant impact on turbine lifetime consumption is expected. Moreover, it is envisaged a reduction of the present large size of molten salt tank, reducing the dwell time (e.g.10 minutes), deriving from the DEMO recent development [48], and adapting the ESS operating system to the new conditions, with an increment of thermal power to the turbine due to the reduction of power needed into the heat storage. This could be possible, thanks to HCSGs work at reduced power during the pulse. An alternative solution could be the elimination of the tank in case of viability of the BOP option with a direct coupling of PHTS to PCS [49].

For an efficiency increment, feedwater preheaters train includes divertor and vacuum vessel Heat Exchangers belonging to correspondent PHTS.

A Gate cycle™ analysis was carried out, mainly focused on the efficiency estimation. The preliminary result is about 37.1% average gross electrical efficiency, considering both pulse and dwell phases. The electrical efficiency is reduced to around 34%, with the consideration of the electrical load (limited to PHTSs, ESS and PCS components for this analysis). An optimized analysis performed with Gate-cycle™ is reported in [67].

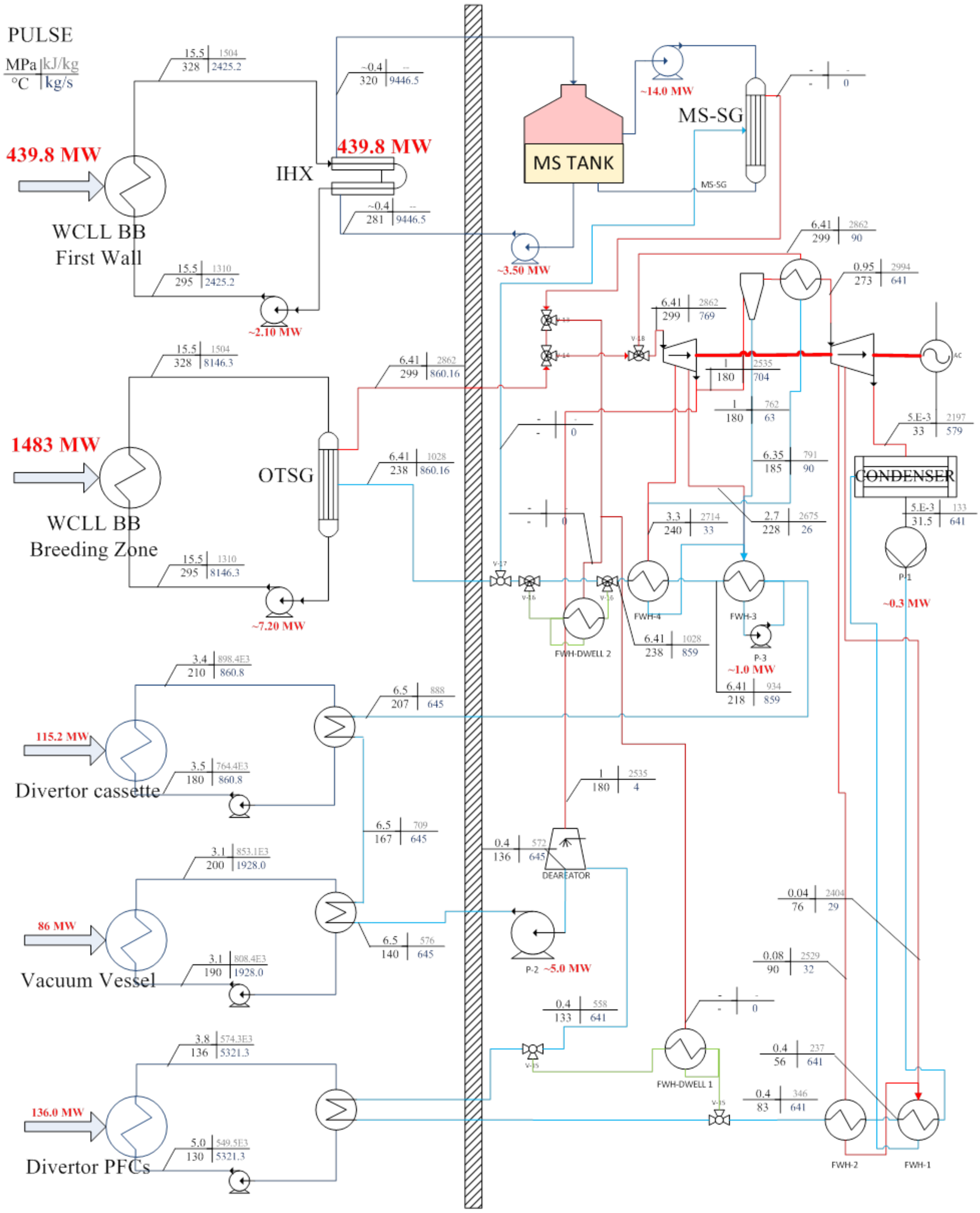

Fig. 5.9 – Preliminary cycle configuration during pulse mode.

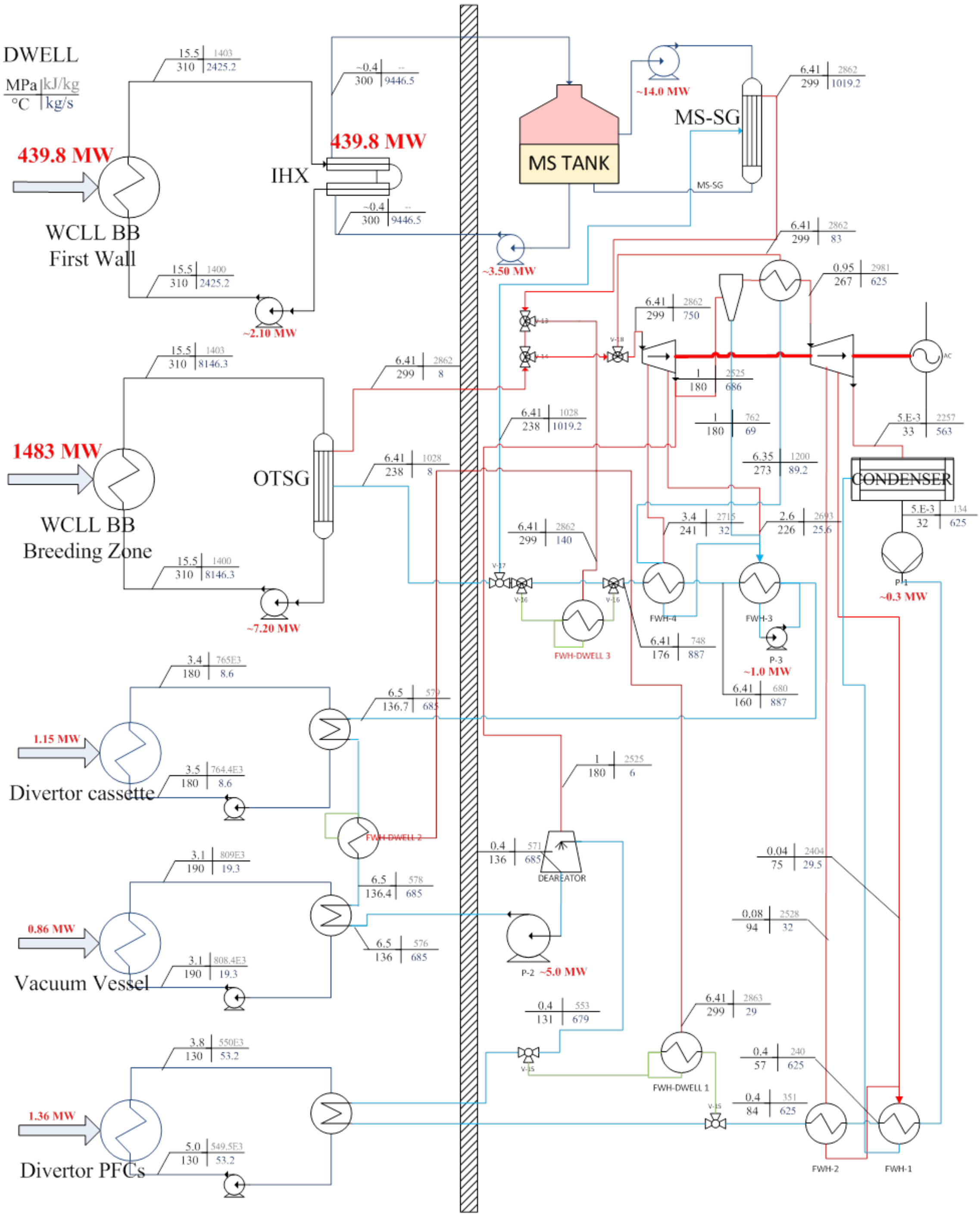

Fig. 5.10 – Preliminary cycle configuration during dwell mode.

6 TH SYSTEM MODEL OF WCLL PHTS

6.1 RELAP5/Mod3.3 code

RELAP5 code [68][69][70] is a thermal-hydraulic code for nuclear system analysis and constitutes the object of continuous assessment in various international institutions. Wide qualification projects and sensitivity and uncertainty analyses of physical models have been performed all over the world, Ref. [72]. A wide literature exists about the code description, capability and application. The light water reactor (LWR) transient analysis code, RELAP5, was developed at Idaho National Engineering Laboratory (INEL) for the U.S. Nuclear Regulatory Commission (NRC). The RELAP5 code has been developed for best estimate simulation of LWR coolant system transients during normal and off normal conditions. The code models the coupled behavior of the reactor coolant system and the core (point kinetic) for simulating accidents in LWR: such as loss of coolant accident (LOCA), anticipated transients without scram (ATWS) and operational transients, such as loss of feed-water (LOFW), loss of offsite power (LOOP) and turbine trip. A generic modeling approach is used. It permits simulating a variety of thermal-hydraulic systems such as turbines, condensers and secondary feed-water (FW) systems. The component models include also pumps, valves, pipes, heat releasing or absorbing structures, reactor point kinetics, electric heaters, jet pumps, etc. In addition, special process models are included for effects such as form loss, flow at an abrupt area change, branching, choked flow (Ramson/Trapp or Henry Fauske models), boron tracking, and non-condensable gas transport. This code is highly generic and can be used for simulation of a wide variety of hydraulic and thermal transients also in non-nuclear systems involving mixtures of steam, water, non-condensable and solute.

Based on one-dimensional, transient, non-homogeneous and non-equilibrium hydrodynamic model for the steam and liquid phases, RELAP5/Mod3 code uses a set of six partial derivative balance equations and can treat a non-condensable component in the steam phase. It is assumed to move with the same velocity and have the same temperature as the vapor phase. Therefore, all properties of the gas phase are mixture properties of the steam/non-condensable mixture [68].

A semi-implicit numeric scheme is used to solve the equations inside control volumes connected by junctions. The fluid scalar properties (pressure, energy, density and void fraction) are the average fluid condition in the volume and are viewed located at the control volume center. The fluid vector properties, i.e. velocities, are located at the junctions and are associated with mass and energy flows between control volumes that are connected in series, using junctions to represents flow paths. The direction associated to the control volume is positive from the inlet to the outlet.

Heat flow paths are also modeled in a one-dimensional direction, using a staggered mesh to calculate temperatures and heat flux vectors. Heat structures and hydrodynamic control volumes are connected through heat flux. These structures are used to simulate pipe walls, heater elements, nuclear fuel pins and heat exchanger surfaces. There are many factors which influences the convective heat transfer coefficient correlation to use (e.g. presence of non-condensable; temperature of the wall; status of the fluid; geometry, etc.). A key factor that effects the magnitude of heat transfer coefficients, besides obvious parameters such as velocity, is the flow field or hydraulic geometry surrounding the surface. The flow field next to the wall influences the velocity profile and turbulence. The user can use pre-defined convection boundary types for available configurations (i.e. tube, parallel plates, vertical bundle with and without cross flow, horizontal bundle, etc.). No coding has been implanted for helical-pipes in vertical structures or bundle with staggered tubes, cross-flow in horizontal structures [72].

The RELAP5/Mod3.3 code does not include all the fluids that are foreseen in the DEMO power plant, such as the PbLi and HITEC. Thus, in order to develop a dynamic model of the Primary Heat Transfer System and of the Energy Storage System, an extended version of RELAP5/Mod3.3 code has been set-up [58] with the implementation of the PbLi and HITEC fluid proprieties, as well as relevant heat transfer correlations.: i.e. Sieder-Tate, Zukauskas, Seban-Shimazaki and Ushakov.

The implementation of the material properties is realized modifying the source files of the thermal hydraulic system code RELAP5/Mod3.3, generating the executable files with Intel Fortran Compiler for LINUX operative system.

The RELAP5 code requires the complete description of liquid and steam phase material properties, using correlations. For both PbLi and HITEC fluid, the following properties have been implemented: the specific volume, the internal energy, the entropy, the thermal expansion coefficient, and the adiabatic compression coefficient of liquid and vapor phase, and the saturation curve as function of pressure and temperature. The thermodynamic properties of the PbLi and HITEC material have been determined from the available thermophysical properties.
As for the code default fluid, the pressure drops coefficients can be set-up by the user, even if there are restrictions in the transition between laminar and turbulent regime.

Moreover, a complete description of main phenomena required the implementation of heat transfer correlations [58]. The heat transfer correlation of HITEC molten salt fluid is the Sieder Tate correlation. The Zukauskas correlation was implemented to simulate the cross-flow heat transfer in helical tubes [58]. As regard PbLi, the Seban-Shimazaki Mikityuk, and Ushakov correlations were implemented, the last describes the heat transfer in tubes bundle.

Improvements will be needed to simulate the two-phase flow in the primary side of helical steam generators, to take into account the increase of the heat exchange due to the centrifugal force.

6.2 DEMO nodalization

A description of the RELAP5/Mod3.3 nodalization [46] is summarized below distinguishing:

- The FW primary system, which includes the in-vessel and ex-vessel components of the primary side and the secondary side which is constituted by the molten salt intermediate system.
- The BZ primary system, which includes the in-vessel components and the ex-vessel components of the primary side and the secondary side.

The RELAP5/Mod3.3 input deck adopted for simulating the FW and BZ PHTS is a nodalization carried out with a “sliced approach”. This nodalization scheme is suitable for a better code response. Main attention is focused to the accurate geometric nodalization: the elevations of the various parts of the plant are maintained in the nodalization; more detailed nodalization has been implemented in regions where a higher accuracy of the prediction is necessary (i.e. breeding blanket segment). K-loss coefficient in junction is evaluated or estimated on the basis of geometries.
The roughness is set 3.2e-5 m in all components apart from the IHX tubes where is 4.0e-6 m.

6.2.1 FW PHTS nodalization

The RELAP5/Mod3.3 thermal-hydraulic model of the FW PHTS represents the in-vessel components and ex vessel components of the primary system and the molten salt intermediate system, which represent the secondary side. The complete list of components is reported in Tab. 6.1.

The in-vessel components are the FW channels, the manifolds, and the collectors. The FW channels and manifolds are modeled with an equivalent PIPE component of 75 axial volumes, representing the inlet and outlet of the two inboard and three outboard segments. One pipe per sector is considered. The total length is 54.42 m, and the equivalent area is calculated for each region to represent the real geometry. A BRANCH component is used to model the cold distributor and the hot collector, which link the in-vessel and ex-vessel components.
The ex-vessel components are the sectors, the main hot and cold rings, the hot and cold legs, the IHX and the two pumps.

The sectors collectors are modeled with a PIPE component. One inlet sector collector and one outlet sector collector are modeled for each DEMO sector for a total of 18 pipes. Each pipe is connected through a MULTIPLE JUNCTION component to the cold ring and to the hot ring, respectively.

The hot ring is modeled with two PIPES component, each representing half of the ring. The model of the hot ring has proportion 1:1 with the real geometry, the total length is 71.89 m and the area is equal to 0.07049 m^2. The two pipes are linked with a BRANCH component, which connects the hot ring to the two hot legs. Each hot leg is modeled with a PIPE component with geometry 1:1 and it is linked through a BRANCH component to the IHX.

The primary side of the IHX is modeled with an equivalent PIPE, which is characterized by a total length of 28.9 m, the flow area is the equivalent area of 5211 tubes and is equal to 0.8192 m^2, the hydraulic diameter is 0.014148 m. The inlet plenum and the outlet plenum are modeled with a BRANCH component. The outlet plenum is linked to the pump with a PIPE component.

The pump is modeled with a PUMP component. The main characteristics are reported in Tab. 6.2. The pump of each loop is linked to the cold leg, modeled with a PIPE component and linked through a BRANCH to the main cold ring, which is modeled with two PIPE components connected with two BRANCH components. Each pipe of the cold ring is representative with a 1:1 geometry, with a total length of 71.89 m and area equal to 0.07049 m^2.

The pressurizer, linked to hot leg of the loop 1, is modeled with a PIPE component, which represents the housing, with a total height of 9.85 m and volume of 25 m^3. The surge line is modeled with a BRANCH, a PIPE and a SINGLE JUNCTION. The spray system is modeled with a TIME DEPENDENT VOLUME and a TIME DEPENDENT JUNCTION to set the boundary conditions. The porv and relief systems are modeled with a valve (MOTOR VALVE) and a TIME DEPENDENT VOLUME.

The secondary side of the IHX, which foresees the HITEC molten salt as secondary fluid, is modeled with a TIME DEPENDENT VOLUME and a TIME DEPENDENT JUNCTION, to set the inlet and outlet boundary conditions, and a PIPE component which represents the shell of the IHX, it is characterized by an area of 1.201 m^2. The molten salt flows in the IHX in counter-current direction. The heat exchange with the primary system is modeled with a thermal structure.

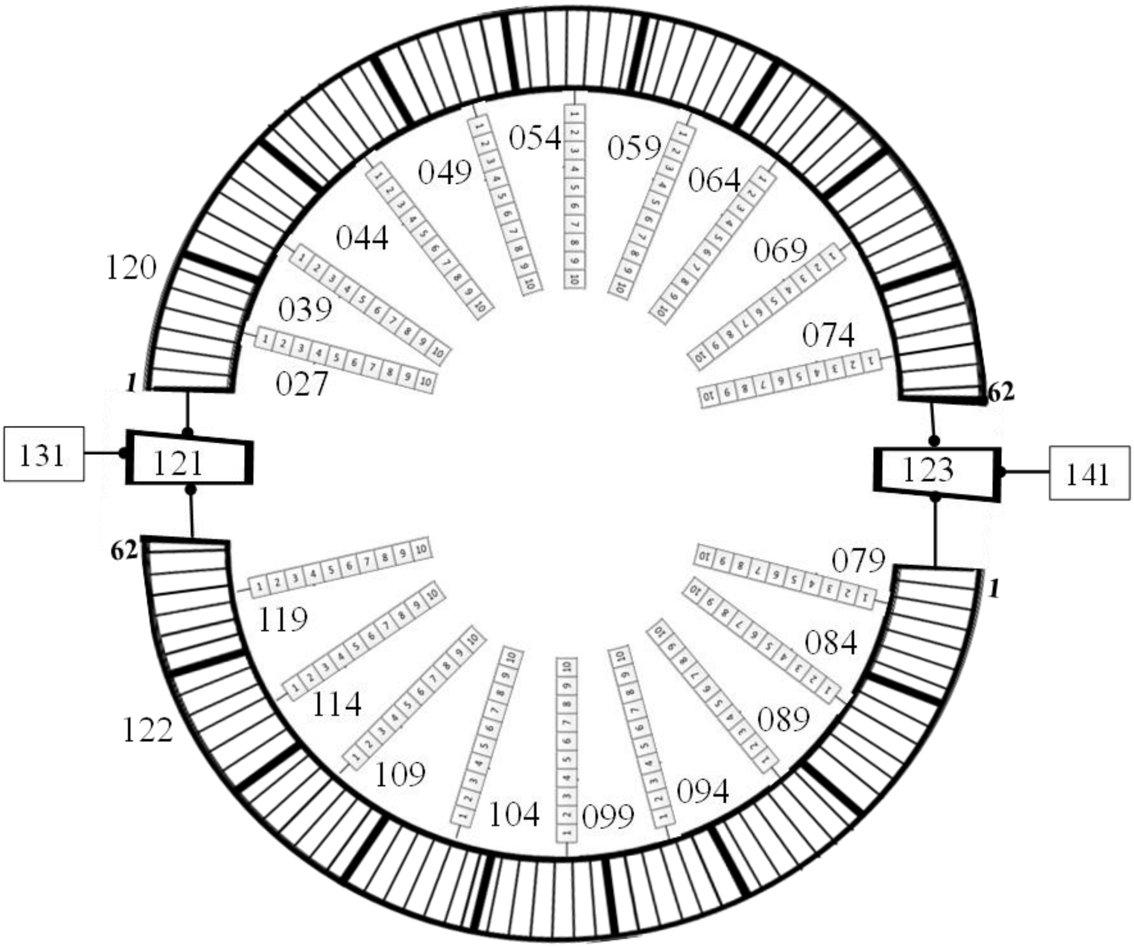

Fig. 6.1 – FW PHTS nodalization by RELAP5/Mod3.3: hot ring and hot sectors.

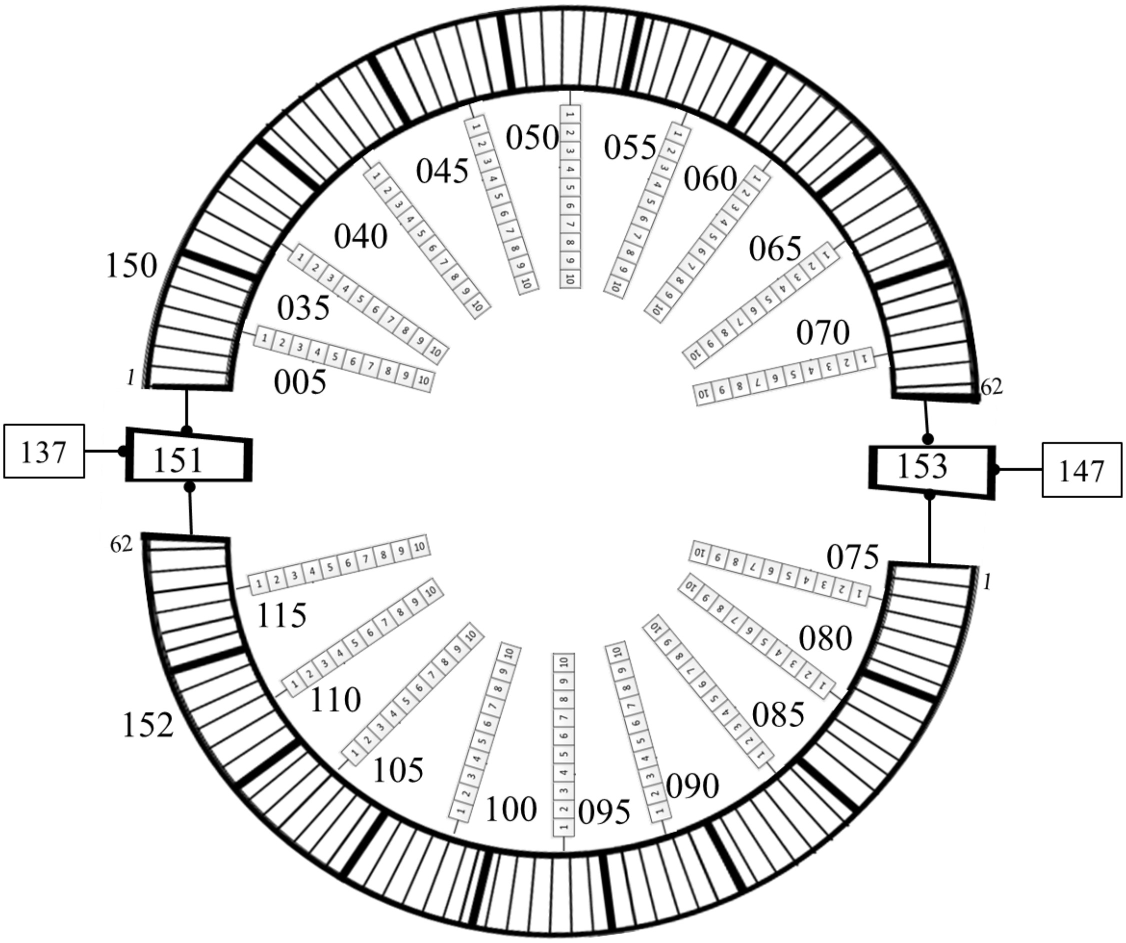

Fig. 6.2 – FW PHTS nodalization by RELAP5/Mod3.3: cold ring and cold sectors.

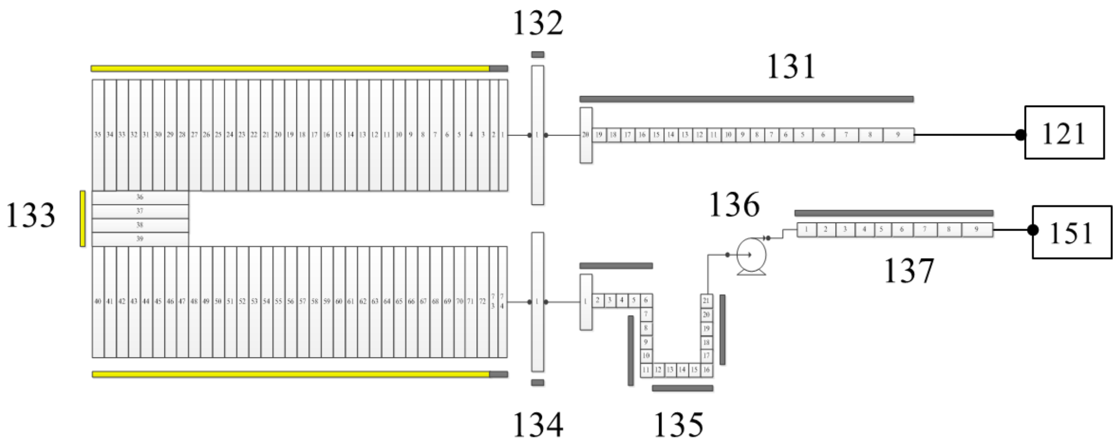

Fig. 6.3 – FW PHTS nodalization by RELAP5/Mod3.3: IHX tubes side, hot and cold legs.

#	RELAP Component	RELAP Component Type	FW PHTS Region
FW IN-VV COMPONENTS AND SECTORS			
1	001	MTPJUN	FW PHTS main COLD ring to FW sectors connections and to HOT ring
2	005- 115	PIPE	FW BB sector (1-18) - inlet
3	006 - 116	BRANCH	FW BB sector (1-18) cold distributor
4	007- 117	PIPE	FW BB sector (1-18) - in/out-board in/out manifolds + FW tubes
5	026- 118	BRANCH	FW BB sector (1-18) - hot collector
6	027 - 119	PIPE	FW BB sector (1-18) - outlet
FW HOT RING			
7	120	PIPE	FW Hot Ring loop Part 1
8	121	BRANCH	FW Hot Ring FW loop Part 1 connection with HL1
9	122	PIPE	FW Hot Ring loop Part 2
10	123	BRANCH	FW Hot Ring loop Part 2 connection with HL2
FW LOOP 1			
11	131	PIPE	FW Hot Leg 1
12	132	BRANCH	FW IHX 1 inlet plenum Part 1
13	133	PIPE	FW IHX 1
14	134	BRANCH	FW IHX 1 outlet plenum Part 2
15	135	PIPE	FW loop seal 1
16	136	PUMP	PUMP 1
17	137	PIPE	FW cold leg 1
FW LOOP 2			
18	141	PIPE	FW Hot Leg 2
19	142	BRANCH	FW IHX 2 inlet plenum Part 1
20	143	PIPE	FW IHX 2
21	144	BRANCH	FW IHX 2 outlet plenum Part 2
22	145	PIPE	FW loop seal 2
23	146	PUMP	PUMP 2
24	147	PIPE	FW cold leg 2
COLD RING			
25	150	PIPE	FW Cold Ring loop Part 1
26	151	BRANCH	FW Cold Ring loop Part 1 connection with CL1
27	152	PIPE	FW Cold Ring loop Part 2
28	153	BRANCH	FW Cold Ring loop Part 2 connection with CL2

FW PRZ CONNECTED TO HL-1			
29	155	PIPE	PRZ housing
30	156	BRANCH	PRZ surge line 1
31	157	PIPE	PRZ surge line 2
32	158	SNGLJUN	PRZ surge line jun
33	160	TMDPVOL	SPRAY system
34	161	TMDPJUN	SPRAY system
35	162	VALVE	PORV system
36	163	TMDPVOL	PORV system
37	164	VALVE	RELIEF system
38	165	TMDPVOL	RELIEF system
FW IHTS			
39	610	TMDPVOL	IHX 1 MS side - MS cold side
40	611	TMDPJUN	IHX 1 MS side - MS cold side
41	612	BRANCH	IHX 1 MS side - MS hot side
42	615	PIPE	shell IHX 1 - MS side
43	616	BRANCH	IHX 1 MS side - MS hot side
44	617	TMDPVOL	IHX 1 MS side - MS hot side
45	620	TMDPVOL	IHX 2 MS side - MS cold side
46	621	TMDPJUN	IHX 2 MS side - MS cold side
47	622	BRANCH	IHX 2 MS side - MS hot side
48	625	PIPE	shell IHX 2 - MS side
49	626	BRANCH	IHX 2 MS side - MS hot side
50	627	TMDPVOL	IHX 2 MS side - MS hot side

Tab. 6.1 – FW PHTS RELAP5/Mod3.3 nodalization.

PARAMETER	**UNIT**	**RELAP5/Mod3.3 FW PHTS**
Speed	***rad/s***	100
Head	***m***	184.83
Flow	***kg/s***	1135.8
Torque	***Nm***	22966

Tab. 6.2 – FW PHTS nodalization by RELAP5/Mod3.3: pump parameters.

6.2.2 **BZ PHTS nodalization**

The RELAP5/Mod3.3 thermal-hydraulic model of the BZ PHTS represents the in-vessel and ex vessel components of the primary system and the secondary side. The complete list of components is reported in Tab. 6.3.

The in-vessel components are the BZ tubes, the manifolds, and the collectors. The BZ tubes and manifolds are modeled with an equivalent PIPE component of 75 axial volumes, representing the inlet and outlet of the two inboard and three outboard segments. One pipe per sector is considered. The total length is 54.42 m, and the equivalent area is calculated for each region to represent the real geometry. A BRANCH component is used to model the cold distributor and the hot collector, which link the in-vessel and ex-vessel components.

The ex-vessel components are the sectors, the main hot and cold rings, the hot and cold legs, the OTSG and the four pumps.

The sectors collectors are modeled with a PIPE component. One inlet sector collector and one outlet sector collector are modeled for each DEMO sector for a total of 18 pipes. Each pipe is connected through a MULTIPLE JUNCTION component to the cold ring and to the hot ring, respectively.

The hot ring is modeled with two PIPES component, each representing half of the ring. The model of the hot ring has proportion 1:1 with the real geometry, the total length is 71.89 m and the area is equal to 0.2463 m^2. The two pipes are linked with a BRANCH component, which connects the hot ring to the two hot legs. Each hot leg is modeled with a PIPE component with 1:1 geometry and it is linked through a BRANCH component to the IHX.

The primary side of the OTSG is modeled with an equivalent PIPE, which is characterized by a total length of 12.987 m, the flow area is the equivalent area of 7569 tubes and it is equal to 1.1899 m^2, the hydraulic diameter is 0.014148 m. The inlet plenum and the outlet plenum are modeled with a BRANCH component. The outlet plenum is linked to the pump with a PIPE component.

The pump is modeled with a PUMP component. The main characteristics are reported in Tab. 6.2. The pump of each loop is linked to two cold legs, modeled with a PIPE component and linked through a BRANCH to the main cold ring, which is modeled with two PIPE components connected with two BRANCH components. Each pipe of the cold ring is representative with 1:1 geometry, with a total length of 71.89 m and area equal to 0.2463 m^2.

The pressurizer, linked to hot leg of the loop 1, is modeled with a PIPE component, which represents the housing, with a total height of 9.85 m and volume of 53 m^3. The surge line is modeled with a BRANCH, a PIPE and a SINGLE JUNCTION. The spray system is modeled with a TIME DEPENDENT VOLUME and a TIME DEPENDENT JUNCTION to set the boundary conditions. The porv and relief systems are modeled with a valve (MOTOR VALVE) and a TIME DEPENDENT VOLUME.

The inlet and outlet boundary conditions of the secondary side are set up with a TIME DEPENDENT VOLUME and a TIME DEPENDENT JUNCTION. The riser is modelled with BRANCH and PIPE components, with flow area 1.68 m^2. The heat exchange between primary and secondary side is modeled with a thermal structure.

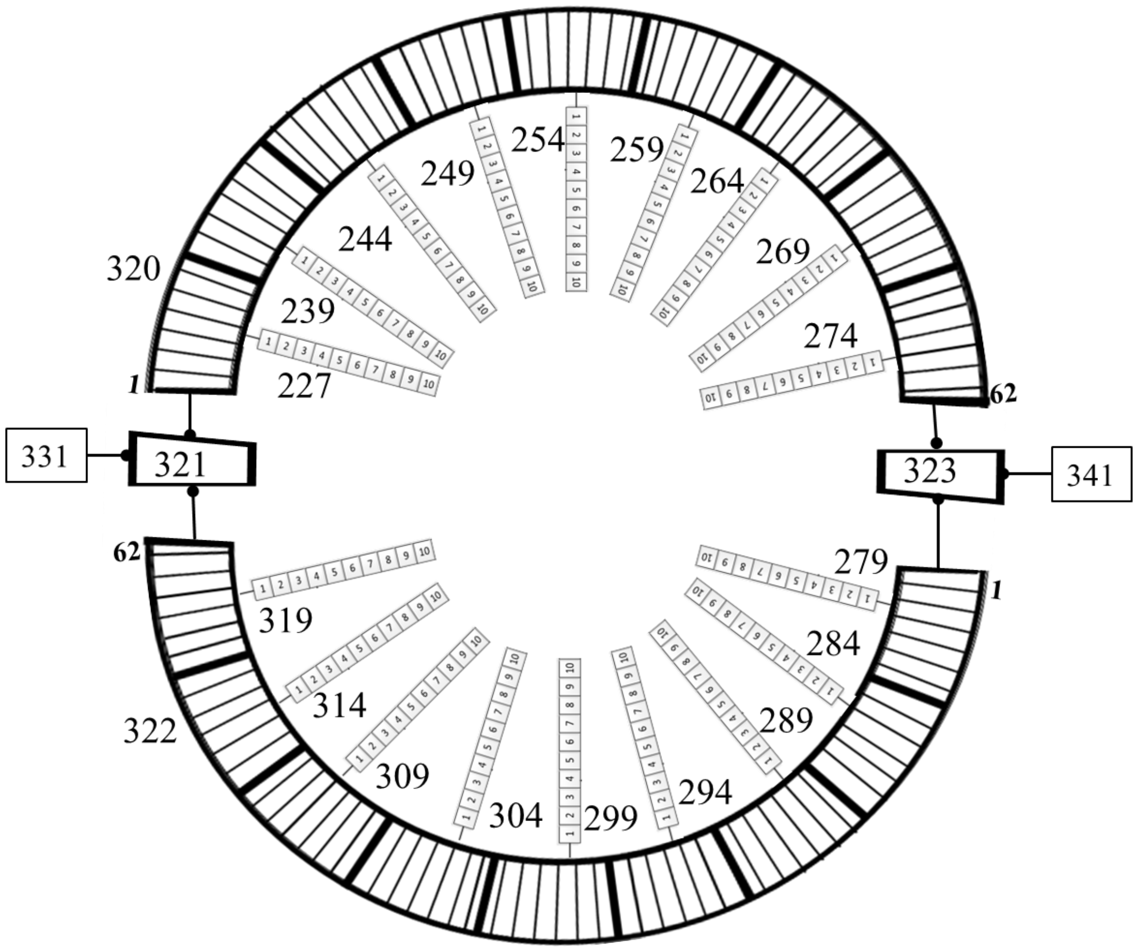

Fig. 6.4 – BZ PHTS nodalization by RELAP5/Mod3.3: hot ring and hot sectors.

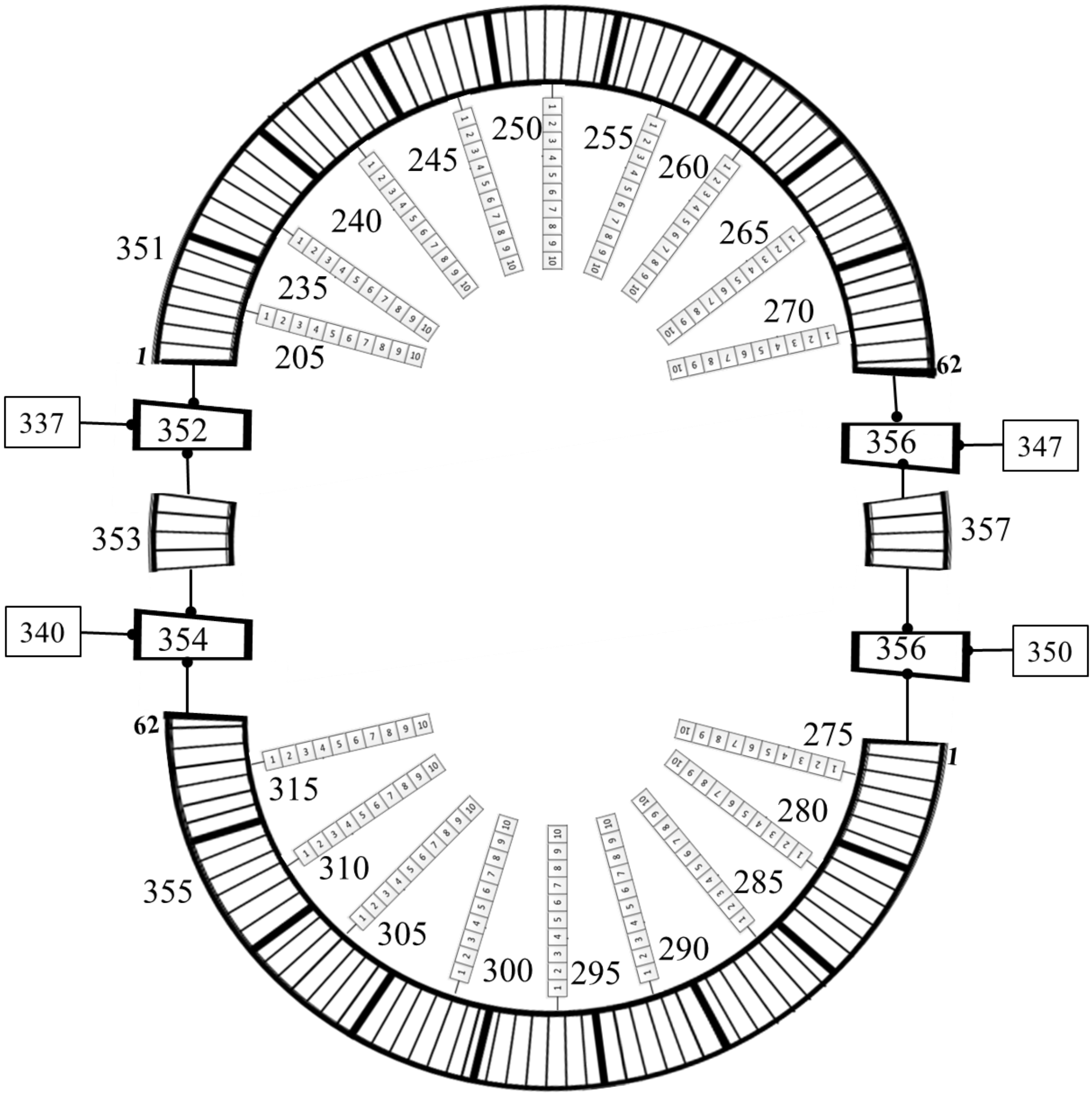

Fig. 6.5 – BZ PHTS nodalization by RELAP5/Mod3.3: cold ring and cold sectors.

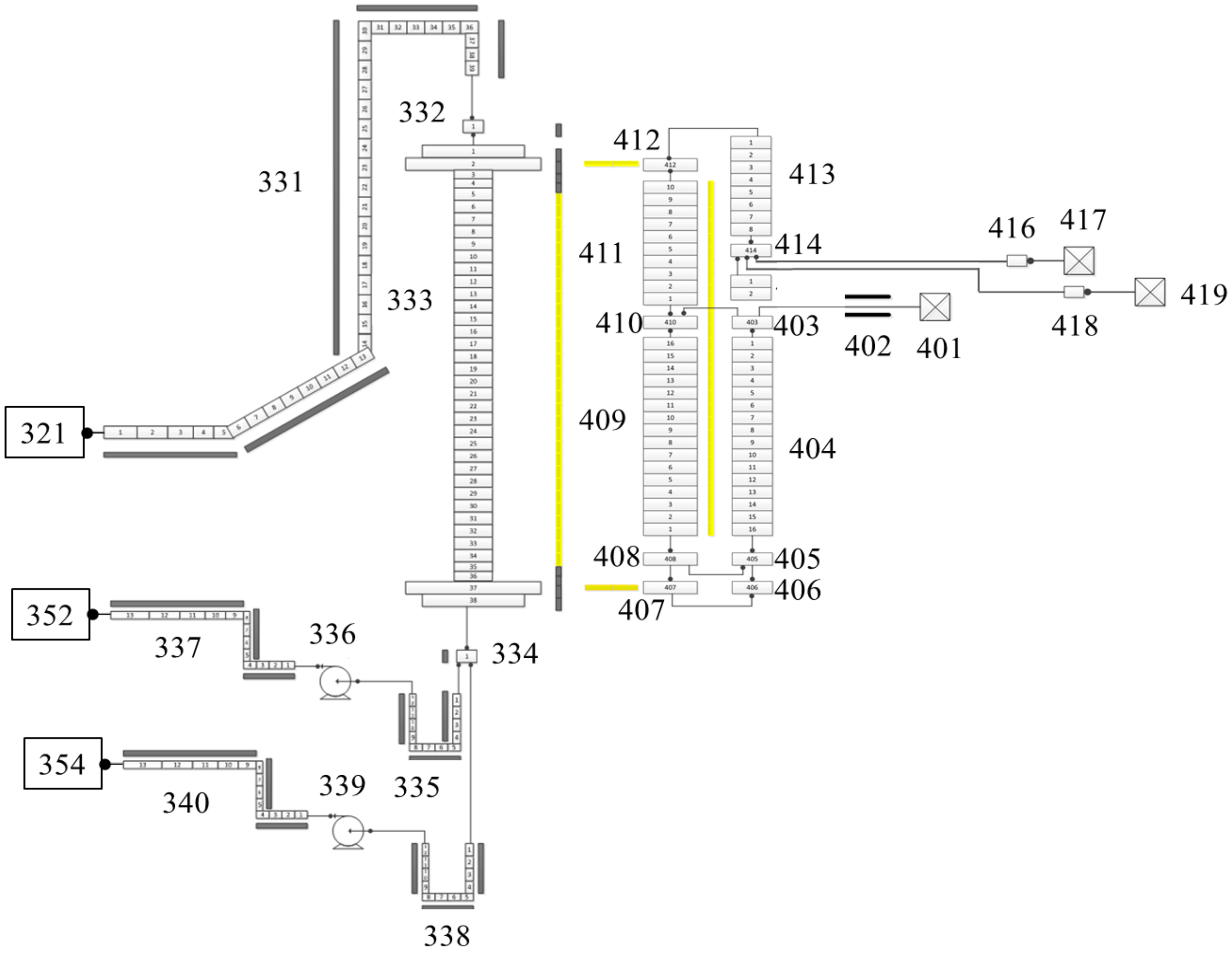

Fig. 6.6 – RELAP5/Mod3.3 BZ PHTS nodalization.

#	RELAP Component	RELAP Component Type	BZ PHTS Region
BZ IN-VV COMPONENTS AND SECTORS			
1	201	MTPJUN	BZ PHTS main COLD ring to FW sectors connections and to HOT ring
2	205 - 315	PIPE	BZ BB sector (1-18) - inlet
3	206 - 316	BRANCH	BZ BB sector (1-18) cold distributor
4	207 - 317	PIPE	BZ BB sector (1-18) - in/out-board in/out manifolds + FW tubes
5	226- 318	BRANCH	BZ BB sector (1-18) - hot collector
6	227 - 319	PIPE	BZ BB sector (1-18) - outlet
BZ HOT RING			
7	320	PIPE	BZ Hot Ring loop Part 1
8	321	BRANCH	BZ Hot Ring loop Part 1 connection with HL1
9	322	PIPE	BZ Hot Ring loop Part 2
10	323	BRANCH	Hot Ring BZ loop Part 2 connection with HL2
BZ LOOP 1			
11	331	PIPE	BZ Hot Leg 1
12	332	BRANCH	BZ IHX 1 inlet plenum Part 1
13	333	PIPE	BZ IHX 1
14	334	BRANCH	BZ IHX 1 outlet plenum Part 2
15	335	PIPE	BZ loop seal 1
16	336	PUMP	PUMP 1
17	337	PIPE	BZ cold leg 1
18	338	PIPE	BZ loop seal 1.2
19	339	PUMP	PUMP 1.2
20	340	PIPE	BZ cold leg 1.2
BZ LOOP 2			
21	341	PIPE	BZ Hot Leg 2
22	342	BRANCH	BZ SG 2 inlet plenum Part 1
23	343	PIPE	BZ SG 2
24	344	BRANCH	BZ SG 2 outlet plenum Part 2
25	345	PIPE	BZ loop seal 2
26	346	PUMP	PUMP 2
27	347	PIPE	BZ cold leg 2
28	348	PIPE	BZ loop seal 2.2
29	349	PUMP	PUMP 2.2
30	350	PIPE	BZ cold leg 2.2
BZ COLD RING			
31	351	PIPE	BZ Cold Ring loop Part 1
32	352	BRANCH	BZ Cold Ring loop 1 Part 1 connection with CL1 loop 1

33	353	PIPE	BZ Cold Ring loop Part 2
34	354	BRANCH	BZ Cold Ring loop Part 2 connection with CL2 loop 1
35	355	PIPE	BZ Cold Ring loop Part 3
36	356	BRANCH	BZ Cold Ring loop Part 3 connection with CL1 loop 2
37	357	PIPE	BZ Cold Ring loop Part 4
38	358	BRANCH	BZ Cold Ring loop Part 4 connection with CL2 loop 2
BZ PRZ CONNECTED TO HL-1			
39	360	PIPE	PRZ housing
40	361	BRANCH	PRZ surge line 1
41	362	PIPE	PRZ surge line 2
42	363	SNGLJUN	PRZ surge line junction
43	364	TMDPVOL	SPRAY system
44	365	TMDPJUN	SPRAY system
45	369	VALVE	PORV system
46	370	TMDPVOL	PORV system
47	371	VALVE	RELIEF system
48	372	TMDPVOL	RELIEF system
BZ OTSG			
49	401	TMDPVOL	OTSG 1 Feedwater cold side
50	402	TMDPJUN	OTSG 1 Feedwater cold side
51	403	BRANCH	OTSG 1 Feedwater cold side
52	404	PIPE	OTSG 1 down comer bottom
53	405	BRANCH	OTSG 1 bottom down comer
54	406	BRANCH	OTSG 1 bottom down comer
55	407	BRANCH	OTSG 1 Riser bottom
56	408	BRANCH	OTSG 1 Riser bottom
57	409	PIPE	OTSG 1 riser
58	410	BRANCH	OTSG 1 riser middle
59	411	PIPE	OTSG 1 riser upper part
60	412	BRANCH	OTSG 1 riser top
61	413	PIPE	OTSG 1 down comer top
62	414	BRANCH	OTSG 1 down comer middle
63	415	PIPE	OTSG 1 down comer middle
64	416	BRANCH	OTSG 1 Steam line 1
65	417	TMDPVOL	OTSG 1 Steam line 1
66	418	BRANCH	OTSG 1 Steam line 2
67	419	TMDPVOL	OTSG 1 Steam line 2
68	431	TMDPVOL	OTSG 2 Feedwater cold side
69	432	TMDPJUN	OTSG 2 Feedwater cold side
70	433	BRANCH	OTSG 2 Feedwater cold side
71	434	PIPE	OTSG 2 down comer bottom
72	435	BRANCH	OTSG 2 bottom down comer

73	436	BRANCH	OTSG 2 bottom down comer
74	437	BRANCH	OTSG 2 Riser bottom
75	438	BRANCH	OTSG 2 Riser bottom
76	439	PIPE	OTSG 2 riser
77	440	BRANCH	OTSG 2 riser middle
78	441	PIPE	OTSG 2 riser upper part
79	442	BRANCH	OTSG 2 riser top
80	443	PIPE	OTSG 2 down comer top
81	444	BRANCH	OTSG 2 down comer middle
82	445	PIPE	OTSG 2 down comer middle
83	446	BRANCH	OTSG 2 Steam line 1
84	447	TMDPVOL	OTSG 2 Steam line 1
85	448	BRANCH	OTSG 2 Steam line 2
86	449	TMDPVOL	OTSG 2 Steam line 2

Tab. 6.3 – BZ PHTS nodalization by RELAP5/Mod3.3.

PARAMETER	**UNIT**	**RELAP5/Mod3.3 FW PHTS**
Speed	***rad/s***	100
Head	***m***	184.83
Flow	***kg/s***	3830.5
Torque	***Nm***	22966

Tab. 6.4 – FW PHTS nodalization by RELAP5/Mod3.3: pump parameters.

6.3 Nodalization and sizing verifications

A preliminary evaluation has been carried out to determine the applicability of the code in predicting selected phenomena, which are relevant for future simulations. In view of this, the code performances have been checked and compared with theoretical calculations. In particular, the pressure drops in the primary systems (FW and BZ) and the heat exchange performances in the OTSG and in the IHX have been verified.

The pressure drops of the primary systems have been evaluated and compared with the calculated pressure drops. The results are reported in Fig. 6.7 and Fig. 6.8 for the FW PHTS and the BZ PHTS, respectively. Minor differences are observed in the hot legs and heat exchangers (i.e. OTSG and IHX).

The performances of the primary systems heat exchangers and steam generators have been carried out evaluating the response of the components to different operating conditions. The geometrical features of the OTSG have been also verified through scoping calculations.

As regard the IHX of the FW PHTS sensitivity analyses are performed evaluating the influence of the fouling factor (from 1 to 0.5) in the primary side tubes. The decrease of the temperature difference demonstrated the worsening of the heat exchange due to the increase of the fouling. Moreover, the IHX performances have been evaluated considering an increase of FW power and of the pump velocity. The increase of power (i.e. 5% and 10% of nominal value), determines the increase outlet temperature, and thus of the temperature difference, in primary and secondary side. Finally, sensitivities are carried out changing the pump velocity, decreasing the nominal of 5% and increasing from 5% to 20%. Minor influence is noted in both primary and secondary side of the heat exchanger.

As regard the OTSG, scoping analyses are performed to evaluate performances, changing the number of tubes, the p/D and the lattice (i.e. square and triangular lattices are considered). Moreover, sensitivity analyses were performed changing the tubes length (from 15.87 to 12.99 m) and tubes fouling factor from 1.0 to 0.5. Calculations with triangular lattice are also performed, resulting in a greater p/D (1.375), but a smaller riser and vessel diameter. The results of the preliminary verifications are reported in Tab. 6.6

The selected OTSG (RUN #11 in Tab. 6.6) is characterized by 7569 tubes, with a length of 12.987 m. A square lattice is considered with a p/D of 1.28.

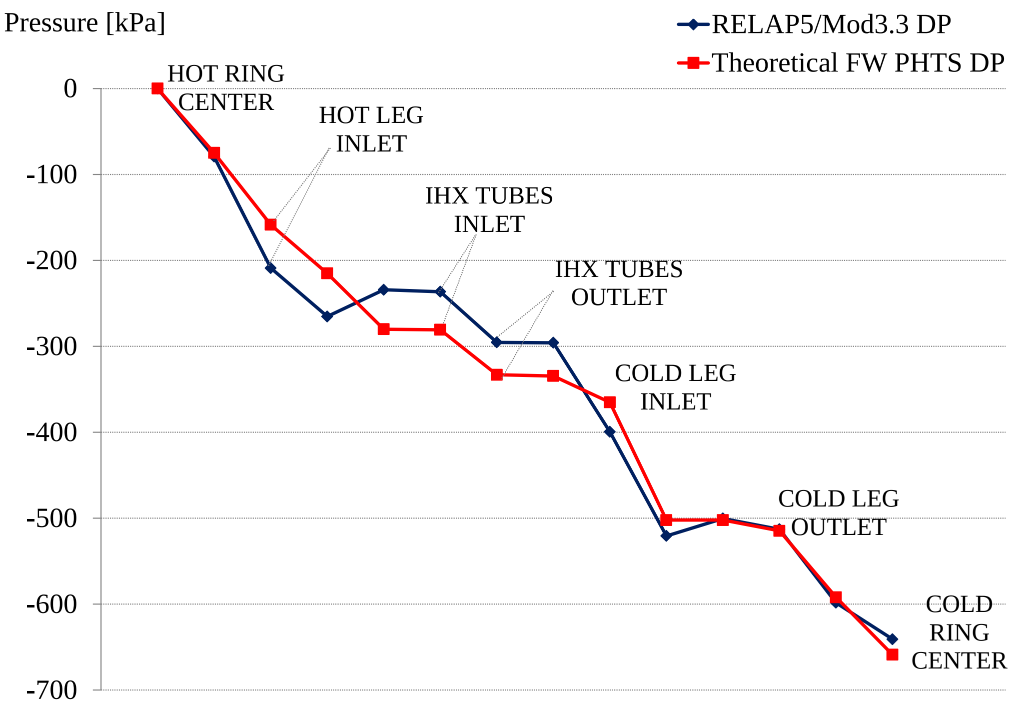

Fig. 6.7 – FW PHTS pressure drops versus length.

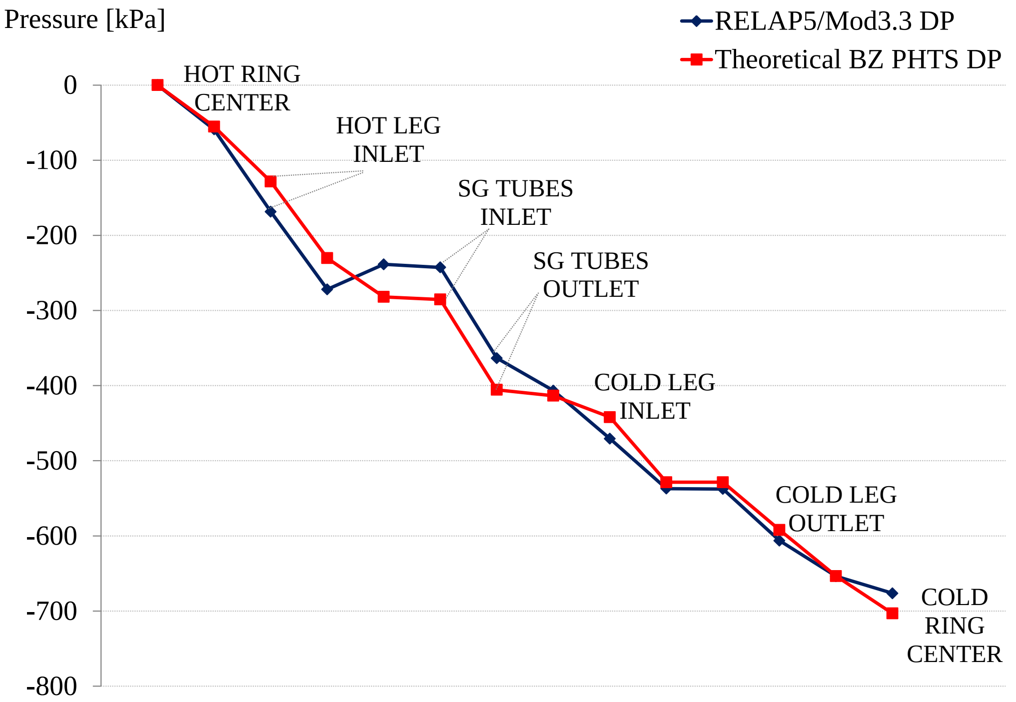

Fig. 6.8 – BZ PHTS pressure drops versus length.

#	ID	k	*FF	FW Power	Pump velocity	IHX1 Power	IHX2 Power	H_2O T_{in}	H_2O T_{out}	ΔT	MS T_{in}	MS T_{out}	ΔT
		--	**--**	***kW***	***rad/s***	***kW***	***kW***	***K***	***K***	***K***	***K***	***K***	***K***
Ref.		--	--	2.199E+05	--	*2.199E+05*	*2.199E+05*	601.15	568.15	33.0	553.15	593.15	40.0
1	DEMO_WCLL_r00g	1	1	2.199E+05	100	2.230E+05	2.318E+05	600.78	569.53	31.25	553.19	593.75	40.56
2	DEMO_WCLL_r00g1	**0.5**	1	2.199E+05	100	2.236E+05	2.298E+05	600.34	570.50	29.84	553.19	593.86	40.67
3	DEMO_WCLL_r00g2	0.5	**0.8**	2.199E+05	100	2.234E+05	2.297E+05	601.97	572.32	29.65	553.19	593.83	40.64
4	DEMO_WCLL_r00g3	0.5	**0.5**	2.199E+05	100	2.231E+05	2.292E+05	607.06	577.84	29.22	553.19	593.77	40.58
5	DEMO_WCLL_r00g5	0.5	1	**2.298E+05**	100	2.323E+05	2.388E+05	602.06	571.25	30.81	553.19	590.37	42.25
6	DEMO_WCLL_r00f1	0.5	1	**2.439E+05**	100	2.447E+05	2.516E+05	604.48	572.34	32.14	553.19	595.44	44.51
7	DEMO_WCLL_r00g6	0.5	1	2.199E+05	**95**	2.221E+05	2.284E+05	600.04	570.38	29.66	553.19	597.70	40.40
8	DEMO_WCLL_r00g7	0.5	1	2.199E+05	**105**	2.251E+05	2.313E+05	600.64	570.62	30.02	553.19	593.59	40.94
9	DEMO_WCLL_r00g8	0.5	1	2.199E+05	**110**	2.265E+05	2.328E+05	600.94	570.74	30.20	553.19	594.13	40.94
10	DEMO_WCLL_r00g9	0.5	1	2.199E+07	**120**	2.295E+05	2.357E+05	601.33	570.98	30.35	553.19	594.40	41.20

*FF=Fouling Factor

Tab. 6.5 – Scoping calculations by RELAP5/Mod33: IHX sensitivities.

RUN #	ID	T CL	v tube out	No. tubes	P/D	Lattice*	Active Tube length	Tsl	v bundle outlet	v DC out	v SL out	W	FF**
		°C	***m/s***	***--***	***--***	***--***	***m***	***°C***	***m/s***	***m/s***	***m/s***	***MW***	***--***
Ref.		*295.0*	--	--	--	--	*15.881*	*299.0*	--	--	--	*788.6*	
1	OTSGdemo_r01	293.2	4.2	8281	1.280	S	15.873	322.0	7.8	13.3	35.0	826.0	1.1
2	OTSGdemo_r02	292.9	4.2	8281	1.280	S	15.873	325.3	7.6	12.8	33.4	831.2	1.5
3	OTSGdemo_r03	293.5	4.2	8281	1.280	S	14.430	315.7	7.5	12.9	33.8	817.5	1.0
4	OTSGdemo_r04	294.3	4.2	8281	1.280	S	12.987	305.2	6.8	11.8	30.8	801.6	1.0
5	OTSGdemo_r05	293.8	4.2	8281	1.280	S	15.873	312.7	7.3	12.4	32.5	813.1	0.8
6	OTSGdemo_r06	293.4	4.2	8281	1.280	S	15.873	320.0	7.5	12.8	33.4	823.8	1.0
7	OTSGdemo_r07	293.4	4.6	7569	1.280	S	15.873	318.5	7.7	11.9	31.5	821.7	1.0
8	OTSGdemo_r08	293.7	4.6	7569	1.280	S	14.430	312.2	7.6	11.9	31.0	812.5	1.0
9	OTSGdemo_r09	295.1	4.3	8281	1.280	S	15.873	294.2	6.6	11.4	29.8	783.5	0.5
10	OTSGdemo_r10	293.7	4.6	7569	1.400	S	15.873	313.5	6.1	12.5	32.5	814.3	1.0
11	**OTSGdemo_r11**	**294.5**	**4.6**	**7569**	**1.280**	**S**	**12.987**	**302.4**	**7.5**	**11.8**	**30.8**	**797.2**	**1.0**
12	OTSGdemo_r12	293.7	5.3	6561	1.280	S	15.873	314.4	9.5	12.9	33.7	815.5	1.0
13	OTSGdemo_r13	293.4	4.8	7351	1.375	T	15.873	318.8	8.6	12.9	33.9	822.1	1.0
14	OTSGdemo_r15	294.9	4.6	7569	1.280	S	12.987	297.5	7.5	11.8	30.7	788.5	0.9
*S= square lattice; T = triangular lattice **FF=Fouling Factor													

Tab. 6.6 – Scoping calculations by RELAP5/Mod33: OTSG results.

7 CONCLUSIONS AND PERSPECTIVES

The Ph.D. work, conducted at ENEA C.R. Brasimone, was carried out in the framework of the European Power Plant and Physics Technological Programme, under the coordination of the EUROfusion Consortium, and it was co-funded by an EUROfusion Engineering Grant.

The aim of this Ph.D. thesis work was the development of the conceptual design of the Water Cooled Lithium Lead breeding blanket and its Primary Heat Transfer System, as well as their integration, demonstrating the compatibility with the DEMO requirements. The activity focused on the thermal-hydraulic design, the sizing and analyses of the Breeding Blanket system and of the main components of the Primary Heat Transfer System, Energy Storage System and Power Conversion System. This was pursued through engineering approaches and the application of numerical tools, such as thermal-hydraulic system codes and CFD codes.

The research activity has led to the development of a complete conceptual design of WCLL breeding blanket, integrated with the PHTS. Moreover, the configuration and main components of the PHTS, the IHTS/ESS, necessary due to the pulsed operation of DEMO, and the PCS are defined. The milestones achieved are hereafter discussed before the future perspectives.

<u>Thermal-hydraulic design and analyses of WCLL BB</u>

The activity had the objective of investigating thermal and fluid-dynamic behavior of the WCLL breeding blanket.

Detailed analyses of elementary breeding unit were carried out, based on the conceptual designs developed from 2015 to 2017. Thus, a complete three-dimensional finite volume model of the breeding blanket was set-up, using ANSYS CFX 15.0 code. The model includes solid and fluid domains, and represents, in detail, an elementary cell of the blanket (i.e. breeding unit). Moreover, CFD analyses of the PbLi manifolds and thermal analyses of the BSS were performed.

The design studies and the analyses brought to the feedbacks hereafter listed:

- The MMS configuration presents drawbacks, such as the PbLi fill and drain procedures during start-up and shut-down and the He removal during operation, and thermal and thermo-mechanical stresses at caps edges of the modules. Thus, the SMS approach was adopted.

- The CFD analyses of PbLi manifolds demonstrated the needed of simplifying the PbLi manifold, to enhance the feasibility of the WCLL design.
- The maximum temperature of PbLi domain is 412 °C, the hot region is localized near the FW, as it is the region with higher power density. The maximum temperature in Eurofer stiffeners is 408 °C. The cooling water enters at 285 °C and exits at 322 °C and 328 °C in FW and BZ systems, respectively.
- The FW system extracts 5% of heat deposited in the BZ system. This phenomenon is related to the equatorial region and cannot be extrapolated to the others breeding blanket cell in poloidal direction.
- The thermal field of the BZ domains (i.e. PbLi and stiffeners) is characterized by an asymmetry in toroidal direction, due to the coolant system layout. To improve the temperature symmetry alternative configurations were investigated during 2017.
- The thermal analyses performed on outboard and inboard segment BSS demonstrated that the outboard BSS temperature is 306 °C (maximum allowed temperature of the material is 550 °C). Thus, refrigeration of outboard segment is not needed. On the contrary, the BSS of the inboard segment is affected by a power density which requires a cooling. For this reason, it was decided to integrate the water manifolds of the FW and BZ systems.
- CFD analyses performed in 2017 have been performed with the main objectives of enhancing cooling performances, ensuring the toroidal symmetry of the thermal field and simplifying the design. Several configurations have been investigated.
- The coolant system layouts studied are constituted by a simple configuration in which the cooling pipes are assembled between the vertical stiffeners. This design choice is pursued to enhance the design manufacturing. Two configurations have been selected as promising, in which the overall tubes length is considerably reduced.
    - The first configuration is constituted by twelve U-shaped tubes. This is the simplest solution, with reduced overall tube lengths.
    - The second configuration foresees six HC tubes. The main advantage of this configuration is that the overall length of pipes is reduced preserving the cooling surface of the tubes in front of the FW, where the volumetric power density is higher.

  Thanks to the reduction of the number of tubes the coolant velocity is increased up to 5 m/s, and thus the HTC inner side is maximized.
- The maximum temperature of PbLi domain is 435 °C, the hot region is localized at the top of the breeding unit near the FW, where the higher power density is concentrated. The maximum temperature in Eurofer stiffeners is 433 °C. The cooling water enters at 295 °C and exits at 327.8 °C and 328.8 °C in FW and BZ systems, respectively.

<u>WCLL BB and PHTS integration and thermal-hydraulic design and analyses of PHTS and BoP</u>

This activity had the objective of integrating the WCLL blanket system with the Primary Heat Transfer System, in a complete Balance of Plant. The main achievements are:

- The PHTS of DEMO WCLL BB were defined. The selected configuration relies on two separate PHTSs: the BZ primary system and the FW primary system. The reference thermodynamic cycle the two PHTSs foresees water at 15.5 MPa, and 295-328 °C of inlet and outlet temperature, respectively.
- The main components of PHTS (e.g. SG, HX, pumps) were preliminary sized and rely on existing technologies. During pulse time (2 h) the BZ PHTS delivers power (1483 MW_{th}) to the PCS through two OTSGs. The selected OTSG is characterized by 7569 tubes, with a length of 12.987 m. The FW PHTS delivers the power (439.8 MW_{th}) to the IHTS through two water/HITEC heat exchangers. The selected IHX is characterized by 5211 tubes, with a length of 28.9 m. The pump power is 2.294 MW and 1.419 MW, respectively for those installed in the BZ PHTS and in the FW PHTS.
- The energy stored during the pulse phase is equal to 1.25×10^6 MJ which corresponds to a thermal power of 173.9 MW, that is delivered to the PCS during the dwell time. During the dwell time, the ESS delivers power to PCS through 4 HCSGs. The average power available in pulse and dwell time is 2086.4 MW, thus the power of each HCSG is 521.6 MW_{th}. The ESS tanks mass inventory is about 40062 tons.
- An extended version of RELAP5/Mod3.3 code has been set-up with the implementation of the PbLi and HITEC fluid properties, as well as relevant heat transfer correlations. The heat transfer correlations implemented for HITEC molten salt are Sieder-Tate and Zukauskas correlations, the last permit to simulate the heat transfer in cross-flow of helical tubes. The heat transfer correlations implemented in the code for the PbLi fluid are the Seban-Shimazaki, Mikityuk and Ushakov, the last is used to simulate the heat transfer in tubes bundle.
- A thermal-hydraulic system model of the PHTSs and steam generators has been developed using RELAP5/Mod3.3 code. The model includes the in-vessel and ex vessel components of the primary side and the secondary side of the FW PHTS and BZ PHTS. The results of the pressure drop along the primary systems resulted consistent with the theoretical evaluation done in the design phase. Moreover, the performance of the SGs and IHXs have been studied and resulted in agreement with the design data.
- The configuration selected present an average electrical power of 659.7 MW. A preliminary Gate-cycle™ analyses demonstrated that the average gross electrical efficiency is about 37.1%, considering both pulse and dwell phases, and the net electrical efficiency of 34%.

Future perspectives

The research activity has provided a preliminary conceptual design of WCLL BB and its PHTS, ESS and CPV for DEMO. Further analyses are needed to enhance and to optimize the selected design choices. These analyses will continue in the framework of the EUROfusion activities during the forthcoming years, e.g.

- Detailed CFD analyses of FW and BZ coolant manifolds to calculate the heat transfer between the hot and cold manifolds;
- CFD analyses of the FW cooling system, to evaluate the cooling performances in different poloidal positions, on the basis of detailed heat loads (data delivered in July 2017);
- Optimization of the mass flow rate distributions in the FW and BZ systems, at different poloidal positions;
- Application of the RELAP5/Mod3.3 system thermal-hydraulic model to identify pros and cons of the WCLL BB PHTS, IHX and BoP design and to perform dynamic analyses focused on operational transients.

ANNEX A: Material properties

Eurofer

The structural material of WCLL breeding blanket is a Reduced Activation ferritic/Martensitic steel (RAFM) developed and produced in Europe (designated Eurofer). The physical and mechanical properties are those given in [73] and listed for different temperature in Tab. A 1.

T [°C]	**α_m [$10^{-6}K^{-1}$]**	**E [Gpa]**	**ρ [kgm^{-3}]**	**C_p [$Jkg^{-1}K^{-1}$]**	**λ [$Wm^{-1}K^{-1}$]**	**W [10^{-6}ohm m]**	**$S_{y,min}$ [MPa]**	**$S_{u,min}$ [MPa]**
20		217	7750	448	28.3	0.50	516	637
100	10.7	212	7728	486	29.2	0.60	480	595
200	11.0	207	7699	522	30.7	0.74	457	555
250		205		537		0.80	449	537
300	11.2	203	7666	551	30.2	0.87	442	517
350		200		566		0.93	431	495
400	11.7	197	7633	584	29.3	1.00	416	468
450		194		612		1.07	393	434
500	12.0	189	7596	655	29.5	1.13	360	392
550		184		721		1.20	316	340
600	12.3	178	7558	801	31.2	1.7	257	277
650		170				1.33	181	200
700	12.5	161					87	107

T: temperature; α_m: Ave. coef. of therm expansion; E: Young's module; ρ: density; C_p: specific heat; λ: thermal conductivity; W: electrical resistivity; $S_{y,min}$: minimum yeld strength; $S_{u,min}$: ultimate tensile strength.

Tab. A 1 – Thermo-physical properties of Eurofer [73].

Water

The coolant is water at typical PWR conditions. The thermo-dynamic properties used are those in reference [46]. The properties relevant for calculations are reported in

P [MPa]	T [K]	T [°C]	V [m3/kg]	rho [kg/m3]	H [J/kg]
15.50	558.0	285.0	1.32E-03	755.97	1.258E+06
15.50	563.0	290.0	1.34E-03	746.77	1.284E+06
15.50	**568.0**	**295.0**	**1.36E-03**	**737.08**	**1.310E+06**
15.50	593.0	320.0	1.47E-03	680.60	1.452E+06
15.50	598.0	325.0	1.50E-03	666.84	1.484E+06
15.50	**601.0**	**328.0**	**1.52E-03**	**657.76**	**1.50E+06**
15.50	603.0	330.0	1.53E-03	651.85	1.517E+06
6.41	572.15	299	0.033029	30.3	2862000
6.41	511.15	238	0.00122	819.7	1028500

Tab. A 2 – Thermo-dynamic properties of water.

PbLi

The breeder/neutron multiplier is the alloy Lithium Lead (PbLi). The thermo-physical properties of the PbLi material implemented for the simulations are referenced in [40]. Some values of the most useful properties, calculated at some relevant temperatures, are provided in Tab. A 3. The PbLi dynamic viscosity is defined by the following equation:

$$\mu_{PbLi} = 1.87 \cdot 10^{-4} \cdot e^{\frac{11640}{T \cdot R}} \; [Pa \cdot s]$$

T [°C]	α_m [10^{-6}K^{-1}]	ρ [kgm^{-3}]	C_p [Jkg^{-1}K^{-1}]	λ [Wm^{-1}K^{-1}]	W [10^{-6}ohm m]
20	116.8	10172	192	7.69	114.8
300	121	9839	190	13.18	127
350	122	9779	189	14.16	129
400	122.5	9720	189	15.14	131
450	123	9661	188	16.12	133
500	124	9601	188	17.1	135.2
550	125	9542	187	18.08	137
600	126	9482	187	19.06	140
650	126	9423	187	20.04	142
700	127	9363	186	21.02	143.7
T: temperature; α_m: Ave. coef. of therm expansion; ρ: density; C_p: specific heat; λ: thermal conductivity; W: electrical resistivity.					

Tab. A 3 – Thermo-physical properties of PbLi [40].

HITEC

The molten salt HITEC is a salt mixture [75][76]:

- 7% of $NaNO_3$, molecular weight 84.995 g/mol
- 40% of $NaNO_2$ molecular weight 69.000 g/mol
- 53 % of KNO_3 molecular weight 101.103 g/mol

Molecular weight of mixture 87.134g/mol.

The operative range of HITEC salt is 415 K – 811K, with a melting point of 415.15 K, and it characterized by a latent heat of fusion of 83736 J/kg [75]. In the range of interest, the specific heat at constant pressure is equal to 1560 J/kgK.
The HITEC density has been evaluated considering the following correlation [75]:

$$\rho = 2080 - 0.7324 \cdot (T - 273.15)\ (K)$$

The dynamic viscosity is obtained from the following equation:

$$\mu = 2.1554 \cdot 10^{-4} \cdot e^{\left(\frac{1006.4131}{T-273.15)+83.7755}\right)}$$

The thermal conductivity is calculated with the following equation:

$$\lambda = 0.4465 + 0.1788 \cdot 10^{-3} \cdot (T - 273.15) - 1.1486 \cdot 10^{-6} \cdot (T - 273.15)^2$$

ANNEX B: Preliminary sizing of ESS with dwell 30’

The Energy Storage System (ESS) is constituted by pipelines connecting the IHX secondary sides, the hot and cold tanks, the steam generator and the pumps. Considering the operation of DEMO, as well as the assigned requirement of about 100% of continuous thermal power delivered to the PCS the hot and cold storage tanks of the ESS system have imposed dimensions. These dimensions appear too large. Re-sizing may be achieved reducing the dwell time or reducing the requirement of thermal power that shall be delivered to the PCS.

The preliminary sizing of HCSG was performed with Solar Salt [58]. During the pulse (2 h) the mass flow of Solar Salt from cold to hot tanks is 7757 kg/s. During the dwell time, the mass flow of molten salt from hot to cold tanks is 31028 kg/s. The ESS contains a mass of molten salt equal to 55851 tons at the beginning of dwell, thus 30219 m^3 are needed to store this amount of molten salt.

During dwell time (0.5 h), the hot molten salt is delivered to 4 HCSG. The total thermal power available during dwell time is 1870MW_{th}. The hot molten salt flows in shell side and transfers energy to water flowing in the tubes side. The molten salt TD cycle is 280-320 °C. The feed-water enters in the HCSG with an inlet temperature of 238 °C, and exits with an outlet temperature of 299 °C at 6.41 MPa).

The sizing of the HCSG has been done considering the Solar Salt as ESS reference coolant. Considering one HCSG the mass flow rate of Solar Salt is 7757.1 kg/s, and the water mass flow rate, calculated with the enthalpy balance is 255 kg/s. The main boundary conditions are reported in Tab B 1.

The heat transfer between the intermediate ESS and the CPS is evaluated considering the conduction through the tubes thickness as well as the convection in the liquid water / steam and Solar Salt sides. The molten salt HTC is calculated using the Zukauskas correlation. The water side convective heat transfer is evaluated using RELAP5/Mod3.3. Four different configurations have been identified. They differ for the number of tubes and other geometrical parameters. Tab B 2 – HC-SG parameters relevant for selection. presents for each case the parameters relevant for selection. The number of tubes is determined by the choices of the tube inner diameter and the maximum steam velocity. The MS salt velocity is selected accordingly with the geometry in a way that is in the range between 1 and 1.5 kg/s, which is a good compromise between the HTC performances and the pressure drop values and the potential for corrosion issues.

The water volume of one HCSG is calculated between 16 and 24 m^3, whereas the tube length is between 60 and 90 m. The selected configuration is identified with Case C.

#	MS water IHX - PCS SG	Unit	Value
1	DEMO FW power	GW_{th}	1.870
2	N° HCSG	-	4
3	HCSG Power	GW_{th}	0.468
4	Solar Salt T_{in}	*°C*	320
5	Solar Salt T_{out}	*°C*	280
6	Liquid water T_{in}	*°C*	238
7	Steam T_{out}	*°C*	299
8	Water Mass flow total	*kg/s*	1019.9
9	Water Mass flow x SG	*kg/s*	255.0
10	Solar salt mass flow total	*kg/s*	31028.5
11	Solar salt mass flow x SG	*kg/s*	7757.1

Tab B 1 – HCSG main boundary conditions.

#	Description	Unit	Case A	Case B	Case C	Case D
1	N° tubes	--	**1191**	**1116**	**1446**	**1782**
2	Steam out velocity (limit)	*m/s*	33.0	36.0	36.0	30.0
3	MS velocity	*m/s*	1.043	1.484	1.435	1.176
4	Tube D_o	*m*	0.0185	0.0180	0.0160	0.0160
5	t	*m*	0.0008	0.0008	0.0008	0.0008
6	p/D horiz row	--	2.00	1.80	1.60	1.60
7	Vertical row tube pitch	*m*	0.024	0.022	0.022	0.022
8	D_i bundle	*m*	1.50	1.15	1.85	1.85
9	D_e bundle	*m*	3.091	2.619	3.021	3.226
10	V_{tot} MS	m^3	67.69	43.36	37.18	40.03
11	V_{tot} water	m^3	24.04	19.32	16.02	17.41
12	Tube length	*m*	90.00	82.00	68.00	60.00

Tab B 2 – HC-SG parameters relevant for selection.

Bibliography

[1] F. Romanelli, et al., *Fusion Electricity – A Roadmap to the Realization of Fusion Energy*, EFDA Report, ISBN 978-3-00-040720-8T, 2012.

[2] https://www.euro-fusion.org

[3] S. M. Weston, *Fusion An Introduction to Physics and Technology of Magnetic Confinement Fusion*, Physics Textbook, Wiley-VCH Verlag GmbH &Co., 2010

[4] *Status report on fusion research*, International Fusion research Council (IFRC), Nuclear Fusion, Volume 45, Number 10A, 21 September 2005

[5] A.R. Raffray, M. Akiba, V. Chuyanov, L. Giancarli, S. Malang, *Breeding blanket concepts for fusion and material requirements*, Journal of Nuclear Materials, Volume 307-311/21-30, (2002)

[6] L. Giancarli, M. Ferrari, M.A. Futterer, S. Malang, *Candidate blanket concepts for a European fusion power plant study*, Fusion Engineering and Design, Volume 49-50/445-456, (2000)

[7] G. Federici, et al., *Overview of the design approach and prioritization of R&D activities towards an EU DEMO*, Fusion Eng. Des. 109–111 (2016) 1464–1474.

[8] L.V. Boccaccini et al., *Objectives and status of EUROfusion DEMO blanket studies*, Fusion Eng. Des. 109-11, (2016), 1199-1206.

[9] Helmut Hurzlmeier, Botond Meszaros, *EU DEMO1 2015 - DEMO_TOKAMAK_COMPLEX*, 2M9AJJ, 08 May 2015.

[10] Ronald Wenninger, Gianfranco Federici, *DEMO1 Reference Design - 2015 April ("EU DEMO1 2015")*, 2LBJRY.

[11] A. Del Nevo, E. Martelli, M. Eboli, *First Summary of specific design requirement for WCLL BB*, EUROfusion Internal Deliverable, WPBB-D-311-01, February 2015

[12] A. Del Nevo, E. Martelli, *Revised summary of WCLL blanket requirements*, EUROfusion Internal Deliverable, WPBB-311-T007-D002, March 2016

[13] A. Del Nevo, E. Martelli, *Update of the WCLL System Requirements and Interface*, EUROfusion Internal Deliverable, WPBB-DEL-BB-3.1.1-T008-D001, July 2017

[14] L. Giancarli, M. Dalle Donne, W. Dietz, *Status of the European breeding blanket technology*, Fus. Eng. Des., 36 (1997), 69-79

[15] D. Maisonnier, et al., *The European power plant conceptual study*, Fus. Eng. Des., 75-79 (2005) 1173-1179.

[16] Y. Chen, U. Fisher P. Pereslavtsev, F. Wasastjerna, *The EU Power Plant Conceptual Sudy – Neutronic Design Analyses for Near Term and Advanced Reactor Models*, Forschungszentrum Karlsruhe GmbH, Karlsruhe, 2003.

[17] P. Sardain, et al., *Power plant conceptual study – WCLL concept*, Fus. Eng. Des., 69 (2003) 769-774.

[18] Aubert J, Aiello G, Jonquères N, Li Puma A, Morin A, Rampal G. *Development of the water cooled lithium lead blanket for DEMO*. Fusion Eng. Des., 89 (2014), 1386–1391.

[19] A. Del Nevo, E. Martelli, M. Eboli, *Summary of key parameters for the design of the PHTS and related BoP for the WCLL*, EUROfusion Internal Deliverable, WPBB-D-311-04, July 2014.

[20] A. Del Nevo, E. Martelli, M. Eboli, *Summary of key parameters for the design of the Blanket RH System,* EUROfusion Internal Deliverable, WPBB-D-311-03, July 2014.

[21] A. Del Nevo, E. Martelli, M. Eboli, *Safety relevant aspects identified for the WCLL BB*, EUROfusion Internal Deliverable, WPBB-D-311-02, August 2014

[22] A. Del Nevo, E. Martelli, M. Eboli, *First Summary of specific design requirement for WCLL BB*, EUROfusion Internal Deliverable, WPBB-D-311-01, February 2015

[23] A. Del Nevo, E. Martelli, *Update of the WCLL System Requirements and Interface*, EUROfusion Internal Deliverable, WPBB-DEL-BB-3.1.1-T008-D001, July 2017

[24] A. Del Nevo, E Martelli, M. Eboli, G. Di Gironimo, R. Mozzillo, A. Lanzotti, P. A. Di Maio, P. Arena, G. Bongiovì, R. Giammusso, F. Moro, D. Flammini, R. Villari, W. Ambrosini, S. Paci, *CAD, Neutronic, Thermo-hydraulics & Thermo-mechanical analyses - Contribution to DDD2014, EUROfusion project deliverable,* WPBB-BB-321-T001-D001, March 2015

[25] A. Del Nevo, M. Eboli, E. Martelli, *Report to define the limits related to the adoption of a WCLL BB coupled with a Heat Storage Facility*, EUROfusion Internal Deliverable, WPBOP-3.1.3-01-01, March 2015

[26] A. Del Nevo, E. Martelli, M. Eboli, *Operational parameters for WCLL release 2014*, EUROfusion Internal Deliverable, WPBB-D-313-01, March 2015.

[27] A. Del Nevo, E. Martelli, M. Eboli, *Magnetic material amount and distribution in WCLL blanket zone*, EUROfusion WPBB-D-311-05, March 2015.

[28] A. Del Nevo, M. Eboli, E. Martelli, *Report to define the limits related to the adoption of a WCLL BB coupled with a Heat Storage Facility*, EUROfusion WPBOP-D-3.1.3-01, March 2015.

[29] A. Del Nevo, E Martelli, M. Eboli, *Design Description Document (DDD) 2014 for WCLL*, EUROfusion Project Deliverable, WPBB-D-312-01-A, June 2015

[30] A. Del Nevo E. Martelli, P. Arena, G. Bongiovì, G. Caruso, G. Di Gironimo, P.A. Di Maio, I. Di Piazza, N. Forgione, R. Forte, M. Frullini, R. Giammusso, F. Giannetti, A. Giovinazzi, D. Giulietti, G. Mariano, R. Mozzillo, A. Naviglio, S. Paci, M. L. Richiusa, A. Tassone, R. Villari, *WCLL Design Report 2015*, EUROfusion Internal Deliverable, WPBB-321-T002-D001, March 2016

[31] A. Del Nevo, E. Martelli, *Design Description Document 2015 for WCLL (update of DDD 2014)*, EUROfusion Internal Deliverable, WPBB-3.1.2-T004-D001, July 2016

[32] R. Mozzillo, A. Del Nevo, E. Martelli, G. Di Gironimo, *Rationale and method for design of DEMO WCLL breeding blanket poloidal segmentation*, Fusion Eng. Des., 124 (2017), 664-668, http://dx.doi.org/10.1016/j.fusengdes.2017.01.039.

[33] P.A. Di Maio, P. Arena, G. Bongiovì, P. Chiovaro, A. Del Nevo, M.L. Richiusa, *On the thermo-mechanical behavior of DEMO water-cooled lithium lead equatorial outboard blanket module*, Fusion Eng. Des., 124 (2017), 725-729, http://dx.doi.org/10.1016/j.fusengdes.2017.05.051.

[34] P. A. Di Maio, et Al., *On the optimization of the first wall of the DEMO WCLL outboard breeding blanket equatorial module*, Fusion Eng. Des. 109-111 (2016) 335–341

[35] A. Del Nevo et al., *WCLL breeding blanket design and integration for DEMO 2015: status and perspectives*, Fusion Eng. Des., 124 (2017), 682-686, http://dx.doi.org/10.1016/j.fusengdes.2017.03.020.

[36] E. Martelli, G. Caruso, F. Giannetti, A. Giovinazzi, A. Del Nevo, *CFD analysis of WCLL BB PbLi manifold*, Fusion Eng. Des., 124 (2017), 1015-1018, http://dx.doi.org/10.1016/j.fusengdes.2017.04.108

[37] E. Martelli, A. Del Nevo, P. Arena, G. Bongiovì, G. Caruso, G. Di Gironimo, P.A. Di Maio, N. Forgione, M. Eboli, F. Giannetti, D. Giulietti, G. Mariano, F. Moro, R. Mozzillo, S. Paci, A. Tassone, R. Villari, *WCLL design report 2016*, EUROfusion Internal Deliverable, WPBB-3.2.1-T003, March 2017

[38] A. Del Nevo, E. Martelli, *Integration for WCLL – DDD 2016 for WCLL (update of DDD 2015)*, EUROfusion Internal Deliverable, WPBB-3.1.2-T005-D001, July 2017

[39] E. Martelli, G. Caruso, F. Giannetti, A. Del Nevo, *Thermo-hydraulic analysis of EU DEMO WCLL breeding blanket*, Fusion Engineering and Design (under review).

[40] E. Mas de les Valls et al., Lead-Lithium eutectic material database for nuclear fusion technology, Journal of Nuclear Materials 376 (2008) 353-357.

[41] S. Smolentsev, et. al., Numerical study of corrosion of ferritic/martensitic steels in the flowing PbLi with and without a magnetic field, Journal of Nuclear Materials 432 (2013) 294-304.

[42] E. Martelli, et al, *Advancements in DEMO WCLL breeding blanket design and integration*. Int. J. Energy Res., (2017), doi: 10.1002/er.3750.

[43] F. Moro, A. Del Nevo, D. Flammini, E. Martelli, R. Mozzillo, S. Noce, R. Villari, *Neutronic analyses in support of the WCLL DEMO design development*, Proceeding of ISFNT13, Kyoto September 2017.

[44] A. Tassone et al., *Recent progress in the WCLL breeding blanket design for the DEMO fusion reactor*, IEEE Transactions on Plasma Science, July 2017 (accepted).

[45] ANSYS CFX 15.0 User’s Guide, November 2013.

[46] ISL Inc, *RELAP5/MOD3.3 Code Manual Volume I: Code Structure, System Models, and Solution Methods*, Nuclear Safety Analysis Division, July 2003

[47] A. Spagnuolo, *CFX analysis and development of multy-physics coupling methodology*, EUROfusion Internal Deliverable, July 2017.

[48] G. Federici et al., *DEMO Design Activity in Europe: Progress and Updates*, Proceeding of ISFNT13, Kyoto September 2017.

[49] L. Barucca, S. Ciattaglia, M. Chantant, A. Del Nevo, W. Hering, E. Martelli, I. Moscato, *Status of EU DEMO Heat Transport and Power Conversion Systems*, Proceeding of ISFNT13, Kyoto September 2017.

[50] M. Coleman, J. Anthony, *DEMO Power Plant Requirements Document*, (2MG7RD v. 2.1), December 2015.

[51] M.Chantant, *PHTS System Requirements Document*, EFDA_D_2MDCLJ v1.2, EUROfusion WP-BOP-2.1.1 v1.2, 12 Aug 2016.

[52] F. Giannetti, *DEMO BoP SRD and support to WCLL BB BoP preliminary design*, EUROfusion Internal Deliverable, WPBoP-2.2-T003, April 2017.

[53] I. Cook, G. Marbach, L. Di Pace, C. Girard, P. Rocco, N.P. Taylor, *Results conclusions and implications of the SEAFP-programme*, Fusion Engineering and Design 51-52 (2000) 409/417.

[54] J Raeder, I Cook, F H Morgenstern, E Salpietro, R Bünde, E Ebert: Safety and Environmental Assessment of Fusion Power (SEAFP): *Report of the SEAFP Project*. European Commission DGXII, Fusion Programme, EURFUBRU XII-217/95, Brussels, June 1995.

[55] E. Bubelis, *Conceptual design definition for an intermediate cooling loop configuration and coolant*, EUROfusion deliverable WP BOP-3.1.4.-01-01, 12 November 2014.

[56] A. Del Nevo, D. Rozzia, M. Eboli, E. Martelli, M. Utili, *Investigation in support of the conceptual design of the energy storage system for WCLL BB*, EUROfusion Internal Deliverable WPBOP-3.1.3-01, April 2016.

[57] H. Latham et al., *Definition of steam based power conversion system for fusion DEMO reactor*, Report for TA WP13-DAS08, 18 December 2013.

[58] E. Martelli, A. Del Nevo, F. Giannetti, M. Polidori, *DEMO BoP – WCLL PHTS and PCS preliminary design*, EUROfusion Internal DeliverableWPBOP-2.2-T003, April 2017.

[59] E. Martelli, F. Giannetti, G. Caruso, A. Tarallo, M. Polidori, L. Barucca, A. Del Nevo, *Study of WCLL Breeding Blanket and Primary Heat Transfer System Integration*, Proceeding of ISFNT13, Kyoto September 2017.

[60] A. Spagnuolo, *Estimate of average load on the First Wall* – 2016, EFDA_D_2MV2DW v1.0, EUROfusion, 03 Aug 2016.

[61] B. Sieglin, *Heat Flux Impact to Target and First Wall in Plasmas with Mitigated ELMs.*, European Fusion Physics Workshop, Split, 2014.

[62] A. Spagnuolo, EFDA_D_2MLE3X v1.2 - Input_data_by_BB-BOP_for_SAE-VVPSS_2017, EUROfusion internal document, August 2017.

[63] European Standard EN10220, CEN, December 2002.

[64] M. Di Prinzio, Sizing of Pressurizer for water cooled primary circuit, https://idm.euro-fusion.org/?uid=2N8WPD&version=v1.0, August 2017.

[65] A. Tarallo, G. Di Gironimo, *Pre-conceptual 3D CAD implementation of PHTS, ESS and PCS design for water-cooled blanket concept*, EUROfusion Internal deliverable, WPBOP-2.1.2-01,

[66] US-NRC, OECD-NEA, Pressurized water reactor main steam line break (MSLB) benchmark - Volume I: Final Specifications, NEA/NSC/DOC (99)8, April 1999.

[67] L. Malinowski, M. Lewandowska, F. Giannetti, *Analysis of the secondary circuit of the DEMO fusion power plant using GateCycle*, Fusion Eng. and Des., 124 (2017), 1237-1240, http://dx.doi.org/10.1016/j.fusengdes.2017.03.026.

[68] INFORMATION SYSTEMS LABORATORIES, RELAP5/Mod3.3 code manual volume I: code structure, system models, and solution methods, July 2003.

[69] INFORMATION SYSTEMS LABORATORIES, RELAP5/Mod3.3 code manual volume II: user’s guide and input requirements, January 2003.

[70] INFORMATION SYSTEMS LABORATORIES, RELAP5/Mod3.3 code manual volume II: appendix A input requirements, June 2004.

[71] INFORMATION SYSTEMS LABORATORIES, RELAP5/Mod3.3 code manual volume VII: summaries and reviews of independent code assessment reports, December 2001.

[72] INFORMATION SYSTEMS LABORATORIES, RELAP5/Mod3.3 code manual volume IV: models and correlations, December 2001.

[73] Tavassoli, Fusion Demo Interim Structural Design Criteria (DISDC)/Appendix A Material Design Limit Data/A3. S18E Eurofer Steel, EFDA TASKTW4-TTMS-005-D01, CEA Report DMN/DIR/NT/2004-02/A, December 2004.

[74] A. Venturini, D. Martelli, *Literature review of PbLi alloys properties*, ENEA Internal Deliverable LM-D-R-262, April 2017.

[75] Coastal Chemical Co., L.L.C. –HITEC® Heat Transfer Salt technical brochure.

[76] M.S. Sohal. M. A. Ebner, P. Sabharwall, P. Sharpe, Engineering database of liquid salt thermophysical and thermochemical properties, INL/EXT-10-18297 1.0, 2013.